UNIVERSITÄTSKLINIKUM HAMBURG-EPPENDORF

Institut für Neuroimmunologie und Multiple Sklerose

Prof. Dr. Manuel A. Friese

Stimulation and inhibition of protein-protein interactions to modulate autophagic pathways

Dissertation

zur Erlangung des Doktorgrades PhD
an der Medizinischen Fakultät der Universität Hamburg.

vorgelegt von:

Daniel Küver
aus Hamburg

Hamburg 2022

Angenommen von der
Medizinischen Fakultät der Universität Hamburg am: **16.05.2022**

Veröffentlicht mit Genehmigung der
Medizinischen Fakultät der Universität Hamburg.

Prüfungsausschuss, der Vorsitzende: **Prof. Dr. Manuel Friese**

Prüfungsausschuss, zweiter Gutachter: **Prof. Dr. Markus Glatzel**

Content

List of Tables

List of Figures

1 Introduction

1.1 Neurodegenerative diseases

Based on the 2019 world population prospects from the United Nations, there will be a two-fold increase of people aged over 60 years until the year 2050. During the same period, it is expected that the amount of the oldest part of the population, people aged over 80 years, will increase by a factor of three (**Figure 1**)[1]. Due to the fact that age is the main risk factor for many neurodegenerative diseases (ND), the incidence of neurodegenerative diseases increases by prolonged lifespan and demographic shift of the population[2].

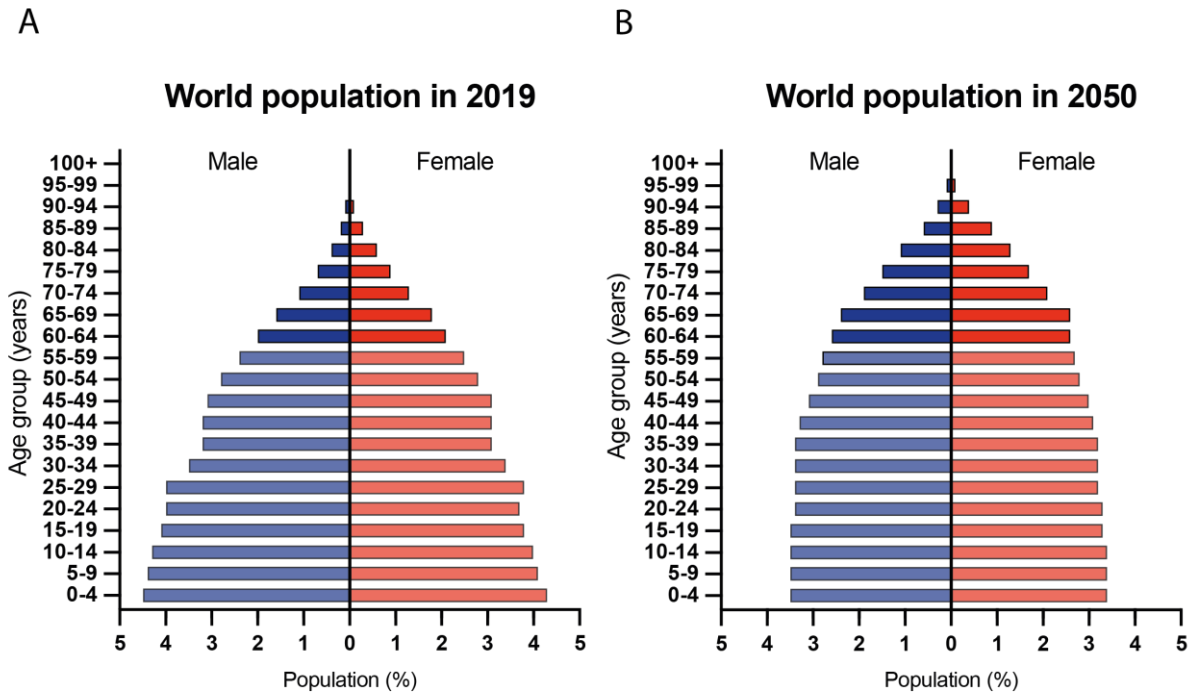

Figure 1 I Age structure of the world's population in 2019 and 2050.
The 2019 world's population prospect of the United Nations predict a twofold increase of people aged over 60 years between 2019 and 2050. People aged over 80 years are expected to increase threefold. Data taken from United Nations[1].

Neurodegenerative diseases are a group of disorders which manifest mainly in the aging population and can affect the peripheral nervous system as well as the central nervous system (CNS)[3]. A characteristic for neurodegenerative diseases is the progressive degeneration of the neuronal structure and function, which is based on the gradual loss of specific neurons and their connections in certain brain areas and neural pathways[4]. The onset of ND is mainly insidious and starts usually between the age of 50-75 years, leading to gradual loss of physical capabilities and massive behavioral,

physical and cognitive impairments[5]. Cytoskeletal changes as well as cytoplasmic, interstitial or intranuclear protein deposits lead to a manifestation of characteristic morphological changes and symptoms (**Figure 2**).

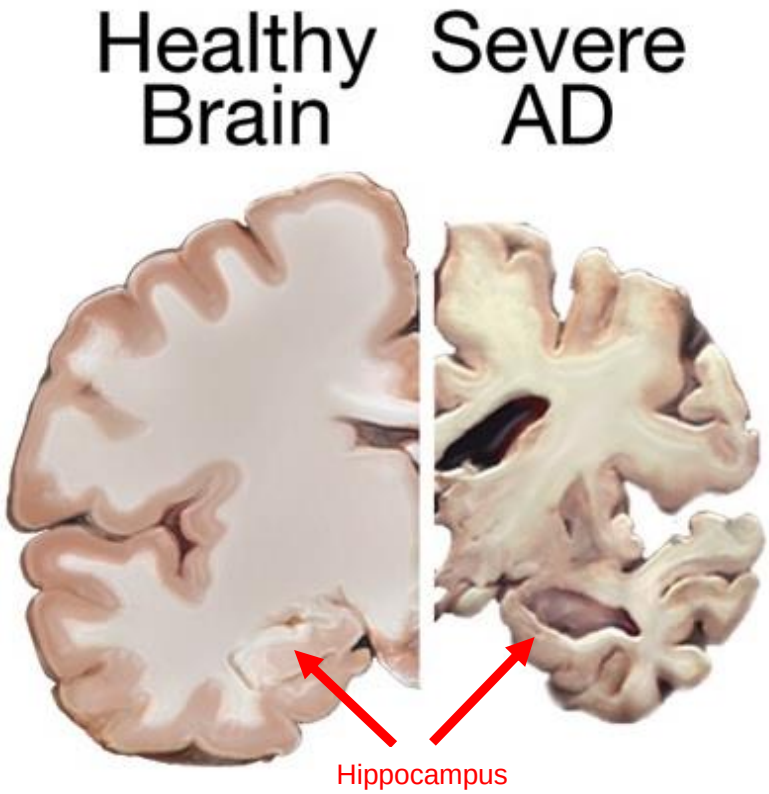

Figure 2 I Comparison of healthy brain with Alzheimer's brain.

Coronal sections of a healthy brain (left) and Alzheimer's brain (right) showing enlargement of the ventricles and hippocampal atrophy (arrow). Figure adapted from Alzheimer's Association[6].

Many ND share this common pathogenic mechanism of misfolded proteins and its aggregation, which causes disruptions in cell function leading to neuronal dysfunction and death[7]. Impairments in nucleocytoplasmic transport, mitochondrial dysfunction and autophagy dysregulation are common characteristics of neurodegeneration[8].
Beside cardiovascular events and the loss of vital cerebral functions, affected people mainly die as a result of secondary infections[9]. Currently, only few treatments exist for ND, with most targeting symptoms instead of the underlying disease pathology[10]. Due to the fact, that ND are still considered as incurable, there remains a critical need for new innovative treatment approaches targeting these devastating diseases.

1.1.1 The role of protein aggregates in neurodegenerative diseases

One hallmark of many neurodegenerative diseases such as Alzheimer's disease (AD), Huntington's disease (HD) and Parkinson disease (PD) is the presence of disease-specific misfolded and aggregated proteins (among others: Tau, amyloid β, α-synuclein and huntingtin) (**Figure 3**)[7,11]. It has been shown, that the aggregation and deposition of misfolded proteins leads to proteinopathies of the central nervous system (CNS)[12]. So far, there are many known proteinopathies, from which the amyloidosis forms the most prevalent form in neurodegeneration. In amyloidosis, misfolded proteins undergo a gradual conversion from soluble proteins to insoluble species. Here, the misfolded proteins form intermolecular β-sheet rich intermediate species like soluble small oligomers or protofibrils, which further assemble into pore like annular and tubular structures (fibrils). These fibrils further grow exponentially to aggregates by association with monomers[13]. Accumulating filamentous structures deposit in the cytosol and nucleus of affected brain cells or in the extracellular space[7].

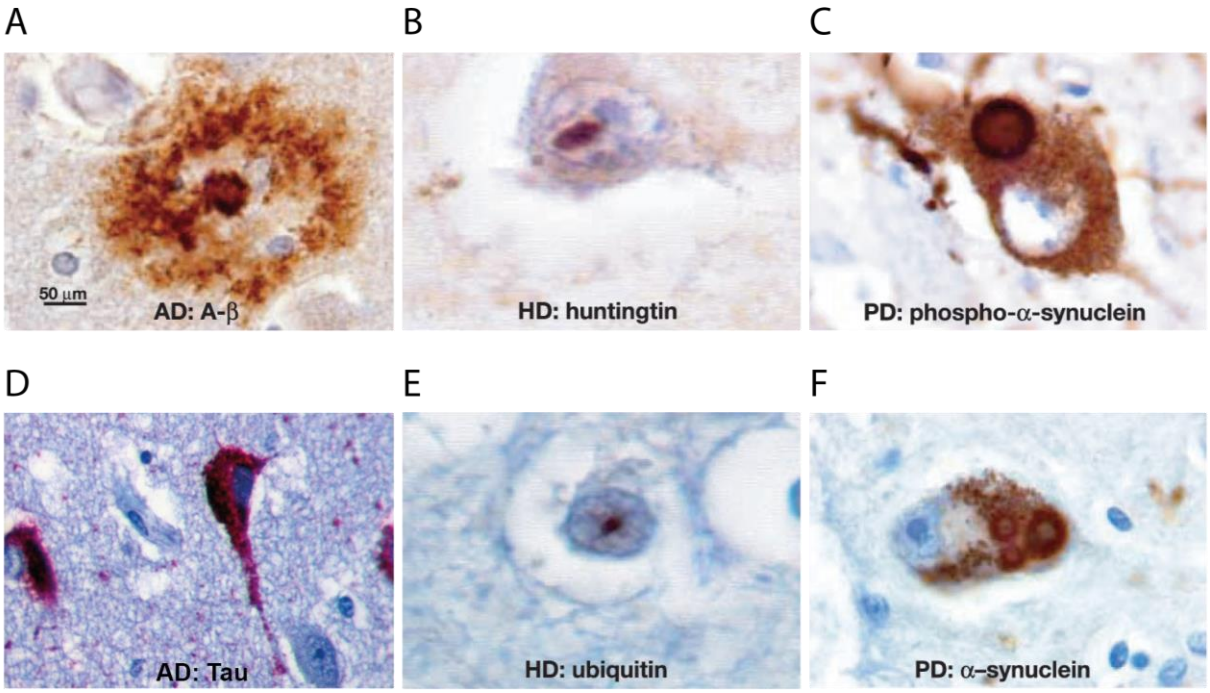

Figure 3 I Characteristics of abnormal protein deposits in neurodegenerative diseases.
Intracellular and extracellular protein deposits in neurodegenerative diseases. (**A**) AD, neuritic plaque of cerebral cortex stained for Aβ, (**B**) HD, intracellular inclusion of cerebral cortex stained for huntingtin, (**C**) PD, Lewy body of substantia nigra stained for phosphorylated α-synuclein, (**D**) AD, neurofibrillary tangle of hippocampus stained for Tau, (**E**) HD, intranuclear inclusion of cerebral cortex stained for ubiquitin, (**F**) PD, Lewy body of substantia nigra stained for α-synuclein. Figure adapted from Ross et al.[11].

Proteins and peptides participate in almost every process within cells. In order to fulfil its critical role for biological functions, proteins need to fold into its native three-dimensional structure[14]. However, due to genetic and environmental factors such as oxidative stress or post-translational modifications, proteins and peptides can misfold. In this case the cellular protein quality control including molecular chaperones, the ubiquitin proteasome system (UPS) as well as the autophagy system can adapt to this protein damage by inducing stress responses[14]. Molecular chaperones play a key role in correcting protein folding into its native state whereas the UPS and autophagy system lead to the degradation of misfolded proteins (**Figure 4**)[12]. If the generation of misfolded proteins exceeds the cell's capacity of refolding and degrading, protein aggregates can accumulate.

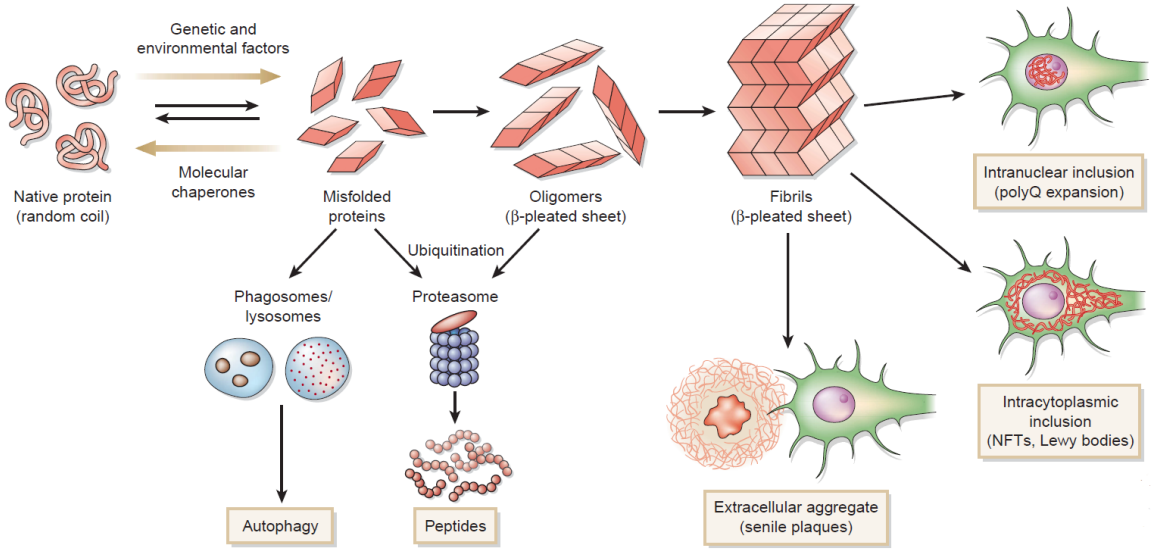

Figure 4 I Schematic overview of protein misfolding and aggregation.
Genetic and environmental factors leading to protein misfolding. Protein aggregates are formed over several intermediate states such as oligomerized misfolded proteins and fibrils. Cellular quality controls including chaperones, the ubiquitin proteasome system (UPS) and autophagy can limit the accumulation of misfolded proteins by refolding or degradation. Figure taken from Forman *et al.*[12].

Protein aggregates have been described to be cytotoxic when accumulated over a certain period[15]. In many neurodegenerative diseases, the accumulation of abnormal protein aggregates leads to a progressive loss of structure and function of neurons inducing neuronal death by loss-of-function and gain-of-function mechanisms[16-17]. There is an ongoing debate on the exact species along the aggregation pathway, whether it is oligomers, proto-fibrils or mature fibrils driving disease progression. Based on the fact that mature filamentous aggregates are found in areas undergoing neurodegeneration, insoluble protein aggregates are believed to be detrimental[19]. In

this traditional perspective, protein aggregates may create physical obstacles for important cellular processes such as protein trafficking or axonal transport. Furthermore, based on its inherent “stickyness” protein aggregates might also sequester critical proteins including its soluble counterparts leading to loss of function toxicity[19]. In Alzheimer’s disease, the most frequent neurodegenerative disorder[20], the microtubule associated protein Tau aggregates (**Figure 3D**) and contributes to neurodegeneration. As Tau stabilizes microtubules, its loss of function perturbs microtubule stability and axonal transport[21].

Most recently, increasing evidence suggests that pre-fibrillary species are cytotoxic as well as leading to the hypothesis that soluble oligomers rather than insoluble protein aggregates drive neurodegeneration. However, the theory of toxicity of mature protein aggregates has not been refuted so far. Due to the fact that soluble oligomers and insoluble aggregates exist in an equilibrium, both species are interconnected in neurodegenerative pathology[22].

1.1.2 Treatment approaches

All currently approved treatments for neurodegenerative diseases (ND) merely alleviate disease-associated symptoms without reversing or slowing down disease progress[23]. For that reason, there is an urgent need for the discovery and development of disease-modifying drugs, which in turn requires more advanced understanding of the molecular basis of pathogenesis, and progression of neurodegenerative diseases. So far, various approaches for targeting neurodegenerative diseases have been developed, from which some of them are described in more detail below.

1.1.2.1 Upregulation of autophagic activity

Based on the fact that many genetic mutations which regulate autophagy are linked to NDs, it has been suggested that induction of autophagy can be used as a therapeutic strategy for most NDs[24]. However, excessive upregulation of autophagy can be detrimental to maintain cellular homeostasis and could lead to unwanted side effects. The main autophagy inducing agents can be classified into mTOR-dependent and mTOR-independent[25]. The first mTOR dependent autophagy inducer has been Rapamycin, which inhibits the kinase activity of mTOR by allosteric binding[25]. Rapamycin has been shown to reduce neuronal death and to improve

neurodegenerative disease symptoms by inducing autophagic activity[26-27]. However, Rapamycin showed limited absorption, which is why several Rapamycin derivatives such as Temsirolimus, Everolimus and Ridaforolimus have been developed. In addition to Rapamycin and its derivatives, the natural compound Curcumin has been described to have a therapeutic effect on neurodegenerative diseases in *in vitro* and *in vivo* models by inhibiting the PI3K/Akt/mTOR pathway[27-28]. Furthermore, Curcumin has also shown to enhance the expression of autophagy related proteins such as Beclin1, Atg5 or Atg16L1 resulting in an increase of autophagic activity[28].

Due to the fact, that mTOR is also described to have autophagy independent functions, mTOR-dependent inducers could result in non-specific side effects[29]. The approach of developing mTOR independent autophagy inducers circumvents these mTOR-related side effects. One example of a mTOR-independent agent is the disaccharide Trehalose. This has been shown to induce autophagy by activation of AMPK and the transcription factor TFEB, which in turn promotes the clearance of protein aggregates[30-31]. Furthermore, some mood stabilizing compounds such as Verapamil, Loperamide or Clonidine have been shown to induce the degradation of protein aggregates via autophagy. These compounds induce autophagy by decreasing levels of inositol phosphate 3 (IP3), an inhibitor of autophagosome formation[32].

Apart from inducing autophagy, another approach is to enhance the global protein quality control in order to correct or eliminate misfolded proteins. Targeting molecular chaperones has been shown to reduce aggregation and toxicity of various aggregation prone proteins by inducing chaperone machineries refolding misfolded proteins[33].

1.1.2.2 Inhibition of protein aggregation

The interference with the aggregation of aggregation prone proteins is a promising disease-modifying approach for the treatment of neurodegenerative diseases. Compounds which prevent the formation of protein aggregates may contribute to neuroprotection by reducing the protein aggregate burden. Early aggregation inhibiting compounds were aromatic planar molecules that inhibit the formation of aggregates by interfering with the stacking of planar β-sheet surfaces of misfolded proteins[34]. In 2018, Pujols et al. developed a compound inhibiting the aggregation of α-synuclein, the main component of Lewy bodies found in PD. The lead compound SynuClean-D was found to inhibit the aggregation of α-synuclein *in vitro* as well as *in vivo*[35]. However, inhibition of protein aggregation does not solve the problem of the accumulation of the disease

related soluble precursors, such as monomers and small oligomers, as this has no influence on its synthesis and clearance. Since the 1990s, many aggregation inhibiting and modulating compounds have been developed[36] from which only one aggregation modulator for Tau (TRx0237) is currently in clinical trials[37] and is expected to be completed in June 2022.

1.1.2.3 Targeted degradation of pathological proteins

Currently, chemical inhibitors, agonists and antagonists are widely used for treatment of various diseases. However, misfolded proteins often show unusual PPIs independently of their intrinsic functions, causing dysfunction in specific compartments such as mitochondria and nucleus leading to neuronal cell death. Due to this toxic gain of function of misfolded proteins, the conventional drug discovery approaches aiming for the modulation (such as inhibition) of intrinsic function of proteins cannot be applied to neurodegenerative diseases[38]. Due to this lack of ligand binding sites for the classical inhibitor approach, misfolded proteins in neurodegenerative diseases are considered as “undruggable“[39].

Apart from the approach to induce the whole protein degradation machinery, the idea of targeted degradation is to selectively degrade disease-causing proteins by small molecule compounds[40]. Such an approach of a compound induced protein degradation is the molecular glue, which facilitates the interaction of a target protein and an E3 ubiquitin ligase, inducing the degradation via the ubiquitin proteasomal pathway. The most well-studied molecular glue is Thalidomide which has been described in 2010 to bind to the E3-ligase Cereblon[41] driving the degradation of a range of neo-substrates such as the lymphoid transcription factors Ikaros and Aiolos[41].

A similar approach of inducing the protein-protein interaction between a target protein and an E3-ligase is the concept of the proteolysis targeting chimera (PROTAC). PROTACS are heterobifunctional compounds composed of a ligand for the target protein and an E3-ligase recruiting ligand. PROTACS utilize the ubiquitin proteasomal system (UPS) for target degradation. In UPS, the E3 ligase repeatedly labels protein substrates with ubiquitin, which are recognized by large proteasome complexes hydrolyzing the target protein. Once the ternary complex between target protein, PROTAC and the E3 ligase is formed ubiquitin is conjugated to lysine residues on the surface of the target protein for its subsequent degradation by the proteasome. Due to the mode of action of PROTACs to bind target proteins to trigger its catalytic

degradation, it can theoretically target the 80% of the proteome, which is currently referred as “undruggable”[38]. Since there are more than 600 E3 ligases in the human genome, whose expression differs in different tissues, PROTACs harnessing specific E3 ligases show high tissue specificity[40]. Additionally, to its high tissue specificity, PROTACs also show high substrate specificity, as the warheads against a target protein are developed to be highly selective. It has been shown, that PROTACs work catalytically and can be recycled after one target protein was ubiquitinated, thus working in a sub-stoichiometric manner[39]. This leads to a longer and stronger biological effect of PROTACS, which allows treatment at very low concentrations[39].

Pioneers in the development of PROTACs are Crews and co-workers, who developed first these hybrid molecules inducing the interaction of a target protein and an E3-ligase for treatment of Cancer[42]. The first attempt of PROTAC development for treatment of NDs was performed in 2016 by Chu *et al*., who developed a peptide based PROTAC targeting the Tau protein[43]. However, these PROTACs are peptide based and show cell penetration issues[44]. In 2019, Arvinas Inc. reported to have discovered a small-molecular PROTAC that potentially degrades pathogenic Tau[45]. It is notable, that this small molecule based PROTAC is able to cross the blood brain barrier and can be administered peripherally.

Among its various advantages, PROTACs have some limitations as PROTAC mediated degradation dependent on proteasomes, which have limited ability to degrade large structures such as aggregates or organelles[46]. Furthermore PROTACs suffer from a relative high molecular mass (>600 Da) and show to be less compliant with Lipinski´s rule of five describing optimal drug like properties[47]. Additionally, the linker design in PROTAC development has proven to be critical, as for best performance the target proteins need to be in optimal orientation to the ubiquitin conjugating E2/E3 ligase to be effectively ubiquitinated. This makes PROTAC design much labor intensive[48].

Next to the PROTAC approach, further development in the field of bi-functional molecules for degradation of target proteins via the autophagic pathway has been made. In 2019, Li *et al*. identified several molecular glues, which induce the interaction between polyQ-expanded Huntingtin (HTT) and the autophagosomal membrane protein LC3[49]. Using these molecular glues, levels of mutant HTT could be reduced in an autophagy dependent manner. Furthermore the identified compounds were also able to reduce HD-relevant phenotypes in mice and *Drosophila*[49]. However,

identification and development of molecular glues have been demonstrated as challenging, as the compound needs to bind to a target protein while concomitantly eliciting a molecular glue effect with an E3-ligase[50].

Most recently, approaches harnessing the autophagy machinery for targeted protein degradation have been developed as novel treatments for NDs. The so called autophagy tethering chimera (ATTEC) or autophagy targeting chimera (AUTAC) link the target protein to the phagophore membrane for its subsequent degradation[51-52].

The approaches of ATTEC and AUTACs harnessing the autophagy pathway for target degradation, expand the range of substrates for targeted degradation towards aggregated proteins, non-proteinous biomolecules and organelles[52]. This is a clear advantage of autophagy harnessing approaches over PROTACs, as the scope of PROTACS is limited to soluble intracellular proteins[53]. However, the mode of action of the ATTEC and AUTAC approaches have some limitations. The AUTAC approach does not link the target proteins directly to the autophagic pathway, as its mode of action is dependent on the K63 linked ubiquitination of target proteins[52]. As the ATTEC approach is basically a molecular glue connecting target proteins with LC3[51], compound identification and development is complicated.

1.1.2.4 Therapeutic antibodies targeting disease related proteins

A hallmark of AD is the extracellular accumulation of Aβ and intracellular neurofibrillary tangles predominantly consisting of Tau protein. However, due to the prion-like spreading of Tau through the extracellular space, antibody based approaches to reduce extracellular Aβ-plaques and hence the trans-synaptic spreading of Tau are promising[54]. So far, several studies have shown that active and passive immunization for Tau in mice reduces pathology and motor deficits[55-56]. This principle may also be applied to other neurodegenerative diseases such as PD where α-synuclein has been described to spread pathologically as the disease progresses[57]. One major drawback of the therapeutic antibody approach is the fact that in general it is believed that antibodies cannot penetrate cells effectively. For that reason, only extracellular proteins can be targeted[58]. However, aggregated Tau targeting human monoclonal antibodies (mAb) such as Gosuranemab, Tilavonemmab and Semorinemab are currently in Phase II trials[59]. Patients treated with high doses of Aducanumab in a phase III trial, showed a 23% decrease of cognitive decline and a 27% decrease on the AD assessment scale subscale 13 (ADAS-Cog-13)[59]. Aducanumab, a mAb

targeting extracellular accumulated Aβ has been approved by the U.S. food and drug administration (FDA) [59] for treating Alzheimer's disease patients. However, there is still controversial discussion about efficacy and safety leading to the rejection of Aducanumab as treatment for Alzheimer's disease by the European Medicines Agency[60].

1.1.2.5 Antisense oligonucleotides (ASO) to reduce production of pathogenic proteins

ASOs are synthetic single stranded strings of nucleic acids that consist of only 8-50 bases. Through complementary binding of the ASO to a defined part of pre-messenger ribonucleic acid (mRNA) or mature mRNA, the expression of a gene can be modulated. A limitation of ASOs for its clinical use is their susceptibility for degradation by cellular nucleases. However, chemical modifications such as sulfur to oxygen substitutions and modifications of the sugar ribose moiety has been shown to improve target RNA binding and therapeutic utility[61]. An advantage of ASOs is its high target selectivity. As ASOs bind to pre-mRNA, introns and exons can be targeted, allowing a unique target sequence for ASOs. However, similar to viral-mediated siRNAs, ASO treatment requires repeated administration for maintaining a therapeutic effect.

Lowering the production of disease associated proteins is a promising approach with potential benefits for many neurodegenerative diseases. In 2016, two ASOs were approved by the US food and drug administration (FDA) which showed high potential in treatment of Duchenne muscular dystrophy and spinal muscular atrophy. ASOs for the treatment of neurodegenerative disease have also been developed. ASOs targeting the polyQ-expanded HTT showed a 50-80% decrease of mRNA in mouse brains. However, the ASO treatment was not reducing the mutant HTT alone but also wtHTT levels were reduced[62]. Recently, two ASO-based HTT lowering approaches from Roche as well as. Wave Therapeutic´s has failed clinical phase III and phase I/II trials[63]. Further ASOs selectively targeting mutant HTT by targeting specific single nucleotide polymorphisms (SNPs) in addition to CAG expansion, showed promising reduction of mutated HTT in pre-clinical models of Huntington's disease[64]. Furthermore, ASO-based therapies are also of interest for the treatment of other neurodegenerative diseases similar to Huntington diseases such as Alzheimer's disease or Parkinson's disease with Tau and α-Synuclein as pathologic proteins.

Currently, Ionis Pharmaceuticals Inc. is conducting a phase II trial of intrathecally administered Tau targeting ASOs in patients with a mild form of Alzheimer's disease[65].

1.2 Autophagy

Almost 60 years ago, in 1963 Christian de Duve introduced the term autophagy from the Greek words αυτό (self) and φαγία (eating) describing a process for the degradation and recycling of cellular components[66]. For a very long time, autophagy was solely considered as a stress induced cellular response to nutrient deprivation. However, research of the last two decades revealed the multifaceted role of autophagy in almost all mammalian cells to ensure homeostasis and as protein quality control.

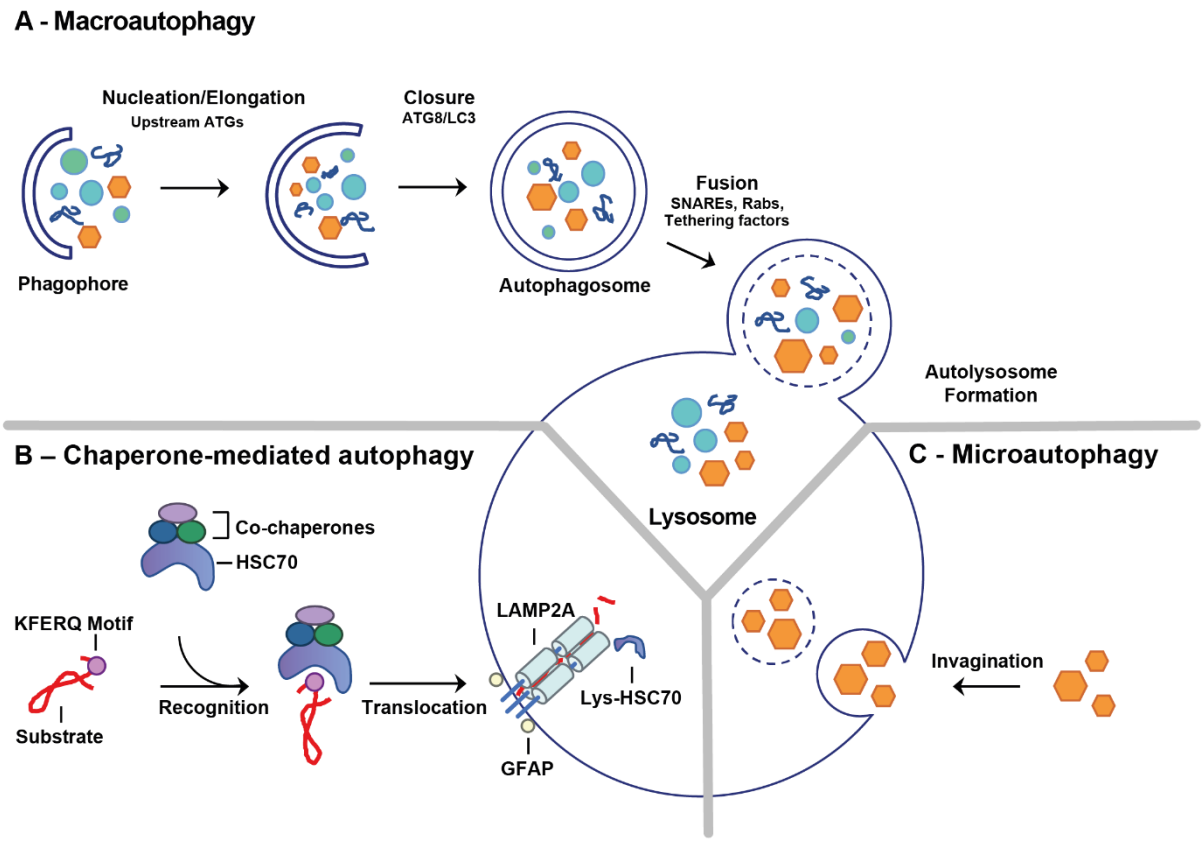

Figure 5 I Different types of autophagy.
Autophagy can be classified into three types according to the way of cargo delivery to the lysosome. (**A**) Macroautophagy describes the most common form consisting of different sequential steps leading to formation of autophagosomes, which fuses with lysosomes for cargo degradation. (**B**) Chaperone mediated autophagy contributes to cellular homeostasis by degrading the KFERQ sequence containing proteins. (**C**) Microautophagy degraded cytosolic proteins by direct sequestration into the lysosome. Figure adapted from Tomaipitinca et al.[69].

Autophagy can target cytoplasmic components as well as larger structures such as damaged mitochondria and peroxisomes[67]. Additionally, autophagy plays a crucial role

in cellular processes such as aging, inflammation and homeostasis. Impairments of autophagy have been associated with many pathological conditions including cancer, infectious diseases, diabetes, cardiovascular diseases as well as neurodegenerative disorders[68]. So far, there are three types of autophagy, which are classified according to the way in which the cargo is recruited to the lysosome. Chaperone mediated autophagy (CMA), does not require the formation of vesicles as the target proteins are directly transferred into the lumen of the lysosome[70] (**Figure 5B**). The CMA selectively degrades individual and soluble cytosolic proteins containing a specific pentapeptide motif (KFERQ)[71]. Chaperones such as the heat shock cognate protein 70 (HSP70) recognizes and binds to the KFERQ motif and recruits the target protein to the lysosome. Here, the chaperone-protein complex is recognized by the lysosomal receptor lysosome associated membrane protein 2A (LAMP2A). With the help of other intra lysosomal chaperones, the target structure is transferred into the lysosome for its subsequent degradation.

Dysregulation of CMA has been associated with several neurodegenerative diseases such as Alzheimer's disease, Parkinson's disease as well as Huntington's disease, as dysregulation causes abnormal levels of disease-linked protein within the cell[5,72].

Microautophagy describes a non-selective process, which degrades cytoplasmic material (**Figure 5C**). Here, proteins and small constituents are directly embedded by invagination of the lysosomal membrane for its subsequent degradation by hydrolytic enzymes[70].

Macroautophagy in turn can degrade target proteins in a selective as well as non-selective manner (**Figure 5A**). The non-selective process is mainly used by the cells for the turnover of cytoplasmic material under stress conditions, such as nutrient deprivation. Here, proteins are randomly sequestered by the autophagosome and degraded by the lysosome. The selective process of macroautophagy targets specific structures such as protein aggregates, or organelles for instance damaged mitochondria and peroxisomes[67]. The molecular mechanisms of macroautophagy are described below.

1.2.1 Molecular mechanisms of macroautophagy

Autophagy is a highly conserved degradation and recycling process in eukaryotic cells, whereby dispensable and potentially dangerous material is degraded in the lysosome[73]. The best studied form of autophagy, macroautophagy, utilizes double-

membrane vesicles, autophagosomes, to deliver cytoplasmic contents to the lysosome for degradation. In general, the autophagy process can be divided into the following sequential steps: Initiation, autophagosome formation, fusion and cargo degradation (**Figure 6**).

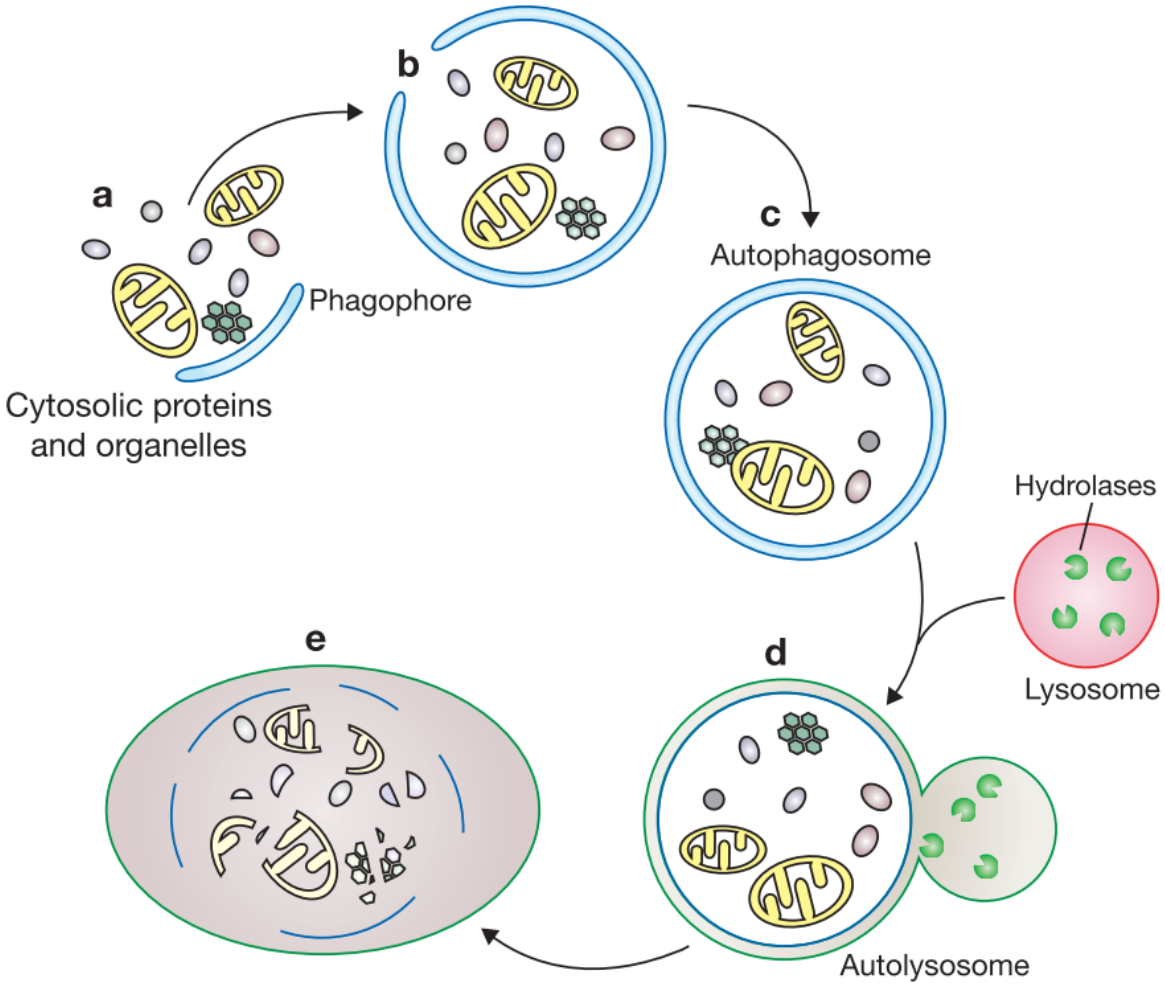

Figure 6 I Schematic overview of the autophagy process.
(**A, B**) Cytosolic material such as proteins or organelles are sequestered by the expanding phagophore. After closing, the double-membrane autophagosome is formed (**C**) and subsequently fuses with a lysosome forming the autolysosome (**D**). After fusion, the contents are degraded by exposure to the lysosomal hydrolases (**E**). Figure obtained from Xie *et al.*[74].

1.2.2 Initiation of autophagy

On top of the autophagy initiation cascade is the Unc-51- like kinase 1 (ULK1) which exists in a large complex with Atg13, Atg101 and focal adhesion kinase family interacting protein of 200 kDa (FIP200). The activity of the ULK1:Atg13:FIP200 complex (ULK1 kinase complex) is negatively regulated by the two major mammalian nutritional and energetic sensor proteins mammalian target of rapamycin (mTOR) and protein kinase-A (PKA) which mediate the initiation by phosphorylation and activation

of ULK1 and Atg13[75]. Under nutrient rich conditions, ULK1 and Atg13 are phosphorylated and inhibited by mTOR complex 1 (mTORC1). Furthermore, ULK1 is also inhibited by the activity of the protein kinase-A (PKA) and autophosphorylation[76]. However, upon nutrient deprivation, mTORC1 dissociates from the ULK1 complex leading to activation of ULK1 activity. ULK1 in turn undergoes autophosphorylation, which induces its kinase activity leading to phosphorylation of Atg13 and FIP200. Furthermore, upon activation, ULK1 binds to AMPK, which further phosphorylates ULK1, causing the activated ULK1 complex to localize to the omegasome. This endoplasmic reticulum (ER) subdomain rich in phosphatidylinositol 3 phosphate (PI3P) initiates autophagosome formation[77-78].

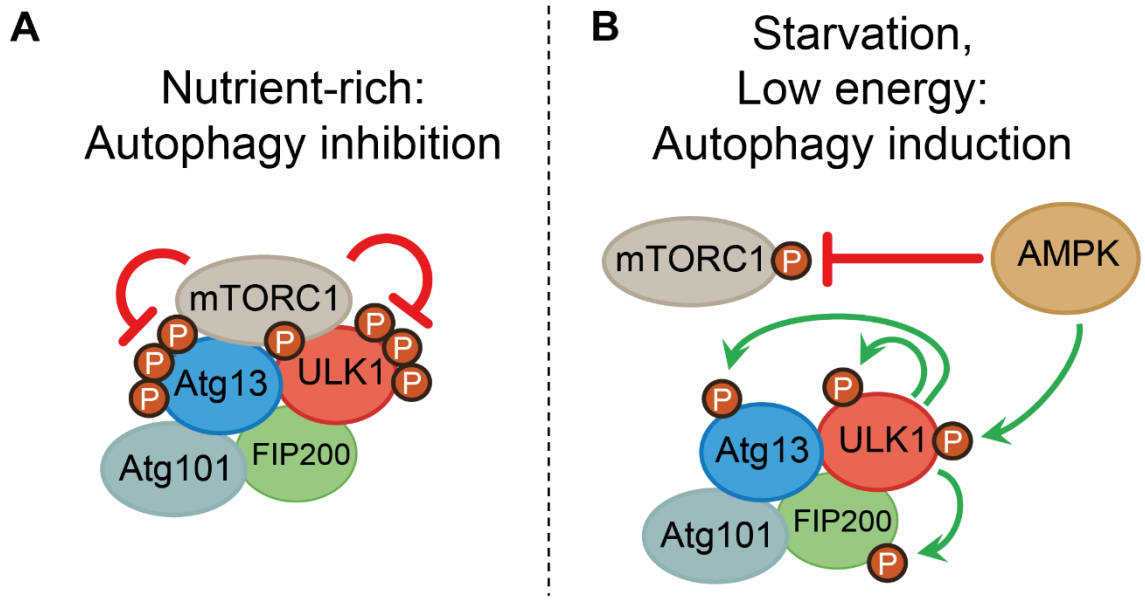

Figure 7 I ULK1 phosphorylation dependent induction of autophagy.
Schematic overview of autophagy induction via ULK1 phosphorylation. (**A**) Under nutrient rich conditions, ULK1 and Atg13 are phosphorylated and inhibited by mTORC1 leading to autophagy inhibition. (**B**) Under nutrient deprivation, mTORC1 dissociates from ULK1 and leads to phosphorylation of Atg13 and FIP200 by ULK1. ULK1 now binds to AMPK leading to further phosphorylation and autophagy induction. Figure adapted from Zhao *et al.*[76] and Alers *et al.*[79].

1.2.3 Autophagosome formation

Following the autophagy induction, autophagosome precursor formation stats with the assemblage of Atg1/ULK1 complexes forming a scaffold for the recruitment of other Atg proteins[80]. Multiple ULK complexes appear at the ER subdomain supported by the interaction of FIP200 with the ER transmembrane proteins VAPA and VAPB. The Atg9 containing vesicles then localize to the autophagosome formation site binding to the ULK complex in a PI3K complex I –dependent manner[80]. The Atg9 vesicles serve as

source of membranes for formation of autophagosome precursors. Atg8-family proteins such as microtubule-associated light chain 3 (LC3) isoforms and GABA receptor-associated proteins (GABARAPs) get lipidated by the Atg16/Atg16L1 complex interaction with the E2 enzyme Atg3 and are inserted to the Atg9 vesicles. The Atg8 family proteins are likely to exert function on autophagosome precursor formation by tethering Atg9 vesicles to facilitate its homotypic fusion[80]. However, how this process takes place is still under investigation. Membrane elongation and autophagosome formation are triggered by PI3P which was activated by vacuolar protein sorting 15 and 34 (VPS15 and VPS34).

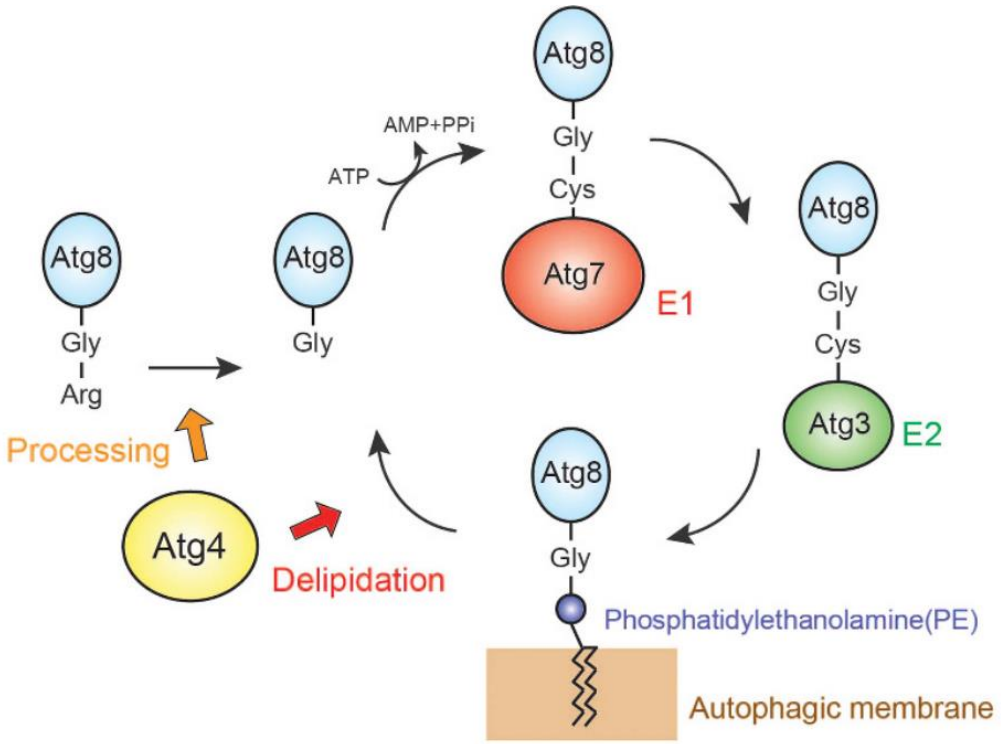

Figure 8 I The Atg8 conjugation system.
For insertion into the autophagosomal membrane, Atg8 family members such as LC3 and GABARAP need to undergo phosphatidylethanolamine conjugation. Figure adapted from Maruyama *et al.* [81].

During autophagosome elongation and maturation, Atg8 family members are inserted into the emerging autophagosomal membrane. For that purpose, the Atg8 proteins have to undergo a PE conjugation (**Figure 8**). Here, the cysteine protease Atg4 cleaves the C-terminal end of Atg8 family members to release a C-terminal glycine residue[81]. The Atg8 is then adenylated in an ATP-dependent manner by the E1 enzyme Atg7 allowing the subsequent formation of an Atg8-Atg3 dimer. The E2 enzyme Atg3 conjugates the phosphatidylethanolamine to the Atg8. For the final conjugation step,

the E3-like Atg12-Atg5-Atg16 complex is required[81]. The conjugated Atg8-PE is then inserted into the autophagic membrane.

1.2.4 Autophagosome lysosome fusion

After complete closure of the autophagosome, ATG4 releases the outer membrane LC3 from phosphatidylethanolamine (PE) by cutting the amide bond between LC3 and PE[82]. For degradation of the autophagosomal content, the autophagosome needs to fuse with the lysosome. Therefore, the autophagosome and lysosome move bidirectional along microtubules to the perinuclear region where the fusion of the autolysosome takes place[83]. The movement of the autophagosomes has been shown to be mediated by dynein whereas the lysosome movement is mediated by kinesins[84]. The fusion process between autophagosome and lysosome requires the coordination of soluble N-ethylmaleimide-sensitive factor attachment protein receptors (SNARES), small GTPases, tethering factors and other proteins.

A key process during autophagosome lysosome fusion is the SNARE complex mediated fusion. The autophagosomal STX17 and lysosomal VAMP8 membrane proteins interact by mediation of SNAP29[68]. As of late, the interaction between autophagosomal YKT6 and lysosomal STX7 has been shown to play a role in the fusion event independently of the STX17-VAMP8 pathway[85]. To promote the fusion process, further regulators such as small GTPases like RAB7A, RAB33B and RAB2A and tethering factors such as the homotypic fusion and protein sorting (HOPS) complex are involved[84]. The HOPS complex is recruited to the lysosome by activity of the RAB7A effector pleckstrin homology and RUN domain containing M1 (PLEKHM1). Here, the HOPS complex controls the fusion event by interaction with STX17 and the assembly of the SNARE complex[84]. The SNARE complex between STX17, VAMP8 and SNAP29 is further stabilized by the RAB7A effector protein pic P-granules autophagy protein 5 homolog (EPG5) which binds to LC3. Additionally, Atg14 has been reported to bind to the STX17-SNAP29 complex to facilitate its interaction with VAMP8 to promote autophagosome lysosome fusion[68].

1.2.5 Cargo degradation

After successful fusion of the autophagosome with the lysosome to form the autolysosome, the inner autophagosomal membrane (IAM) is disrupted and the

sequestered material is degraded by acidic hydrolases[86]. In yeast, the disruption of the IAM is facilitated by the phospholipase Atg15, however the mammalian homologue is so far unidentified but might function similarly to Atg15[86]. After disruption of the IAM, lysosomal enzymes gain access to the autophagic substrates. Currently, about 60 lysosomal hydrolases have been described to degrade sequestered material such as proteins, aggregates and organelles[67]. The majority of the lysosomal enzymes have an acidic pH optimum, which make the function dependent on efficient acidification of the autolysosome[67]. The destiny of the catabolites generated by the degradation of autophagic substrates is so far poorly understood. However, it is highly accepted that they are transported into the cytosol through various transporters of the lysosomal membrane for recycling by the cell[87].

1.2.6 Methods to monitor autophagic flux

Autophagy plays a crucial role in physiological conditions along with pathological conditions such as cancer, infectious diseases, diabetes, cardiovascular diseases as well as neurodegenerative disorders[68]. This leads to a high interest in methods to accurately monitor autophagic activity.

As defined by Klionsky *et al.* "autophagic flux refers to the entire process of autophagy, which encompasses the inclusion (or exclusion) of cargo within the autophagosome, the delivery of cargo to lysosomes (via fusion of the latter with autophagosomes or amphisomes) and its subsequent breakdown and release of the resulting macro-molecules back into the cytosol"[88]. So far, most methods for monitoring autophagic flux rely on autophagic cargo degradation or the autophagosome lysosome fusion event[89]. The reason for focusing on these steps is that it can be discriminated between the number of autophagosomes and the degradative activity. Common methods for determining autophagic flux are the monitoring of autophagy markers such as LC3 or fluorescent probes like RFP-GFP-LC3, which are described in more detail below.

1.2.7 Monitoring autophagic flux by Western Blot or TR-FRET for LC3-II and p62

As autophagosomal LC3 is one of the most studied autophagosome markers, playing a key role in initiation and formation of autophagosomes[90], its turnover is a common approach to measure autophagic flux in mammalian cells. Based on the fact that LC3 needs to undergo structural modifications from pro-LC3 to LC3-II to be inserted into

the autophagosomal membrane (**Figure 8**), the amount of LC3-II reflects the number of autophagosomes and autophagy-related structures[89] (**Figure 9**).

For measuring the turnover of autophagic markers, several methods such as western blotting or TR-FRET assays have been developed[90]. In response to starvation, the number of autophagosomes increases and according to the rise in number of autophagosomes, also the amount of LC3-II increases. As standard, the levels of LC3-II are measured in presence and absence of lysosomal inhibitors such as Bafilomycin or Chloroquine in order to determine whether autophagic flux is enhanced or inhibited[91].

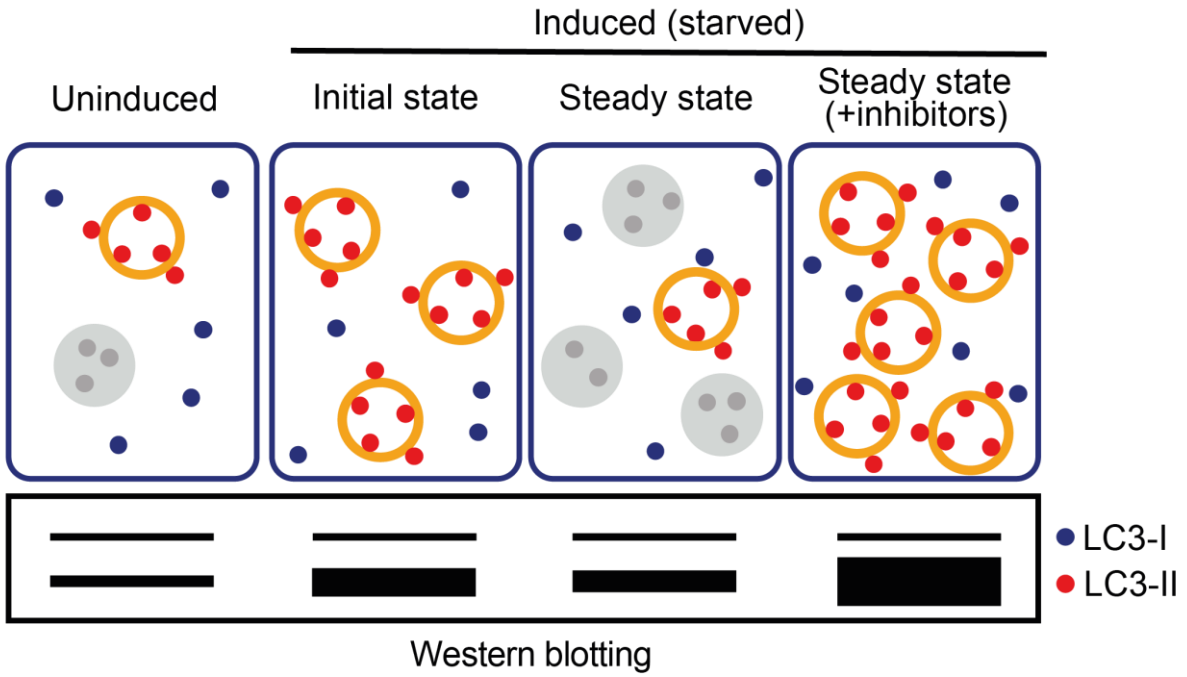

Figure 9 I Schematic overview of changes in LC3 levels upon autophagy modulation.
Autophagosome (orange) formation is induced upon starvation, resulting in an increase of LC3-II (red dots) levels. During steady state under starvation conditions, the number of autolysosomes (grey) exceeds the number of newly formed autophagosomes. Upon treatment with autophagy blockers such as Bafilomycin or Chloroquine, LC3-II escapes lysosomal clearance and accumulation occurs. Figure adapted from Ueno *et al.*[92].

However, results from LC3-II western blots or TR-FRETs are often misinterpreted as an accumulation of LC3-II can reflect autophagic upregulation as well as inhibition of autophagosome degradation. Autophagosome lysosome fusion blockers such as Bafilomycin or Chloroquine have been shown to induce an increase of LC3-II due to reduced clearance. In order to discriminate between autophagy induction and fusion blockers, p62, an additional marker for autophagic clearance can be introduced. p62 is a selective autophagy receptor, translocating ubiquitinated cargo to

autophagosomes and is itself subjected to autophagic degradation[90]. p62 levels are slightly increased upon autophagy induction followed by a decrease at later time points, whereas fusion blockers lead to a strong increase in p62 levels[90]. The combination of LC3-II levels and p62 levels gives a clearer picture about autophagic activity.

1.2.8 RFP-GFP-LC3 and RFP-LC3-GFP-LC3$^{\Delta G}$ probe for quantifying autophagic flux

Another approach to assess autophagic flux is to monitor the transition from autophagosomes into autolysosomes. For that purpose, fluorescent probes such as the mRFP-GFP-LC3 have been developed[93]. The probe is based on the sensitivity of GFP/EGFP in acidic environments when the signal is quenched at low pH. mRFP in turn is relatively stable even within the acidic lysosomal environment.When localized to the autophagosome, the mRFP-GFP-LC3 probe emits red as well as green light, which can be illustrated as yellow signals in merged images. Once the autophagosome fuses with the lysosome, the environment changes to low pH, resulting in quenched GFP signals. Consequently, the autolysosomes appear as a red signal. By determination of the ratio of GFP to mRFP signal, changes in autophagic flux can be monitored[93].

GFP-LC3-RFP-LC3$^{\Delta G}$, another advanced probe, has been developed to circumvent artefacts based on the fact that the RFP may be degraded in the lysosome. GFP-LC3-RFP-LC3$^{\Delta G}$ is a fusion protein consisting of GFP-LC3 and RFP-LC3, where the C-terminal glycine of the RFP-LC3 is deleted[94]. The fusion protein is translated as one molecule, and subsequently cleaved by Atg4 into the same numbers of GFP-LC3 and RFP-LC3$^{\Delta G}$. During autophagy, GFP-LC3 is PE conjugated and inserted into the autophagosomal membrane, whereas RFP- LC3$^{\Delta G}$ cannot be conjugated to PE, staying in the cytosol as an internal control. The autophagic activity can be quantified by the GFP/RFP ratio. For autophagy induction, a reduction of the GFP/RFP ratio is expected as the GFP-LC3 is degraded.

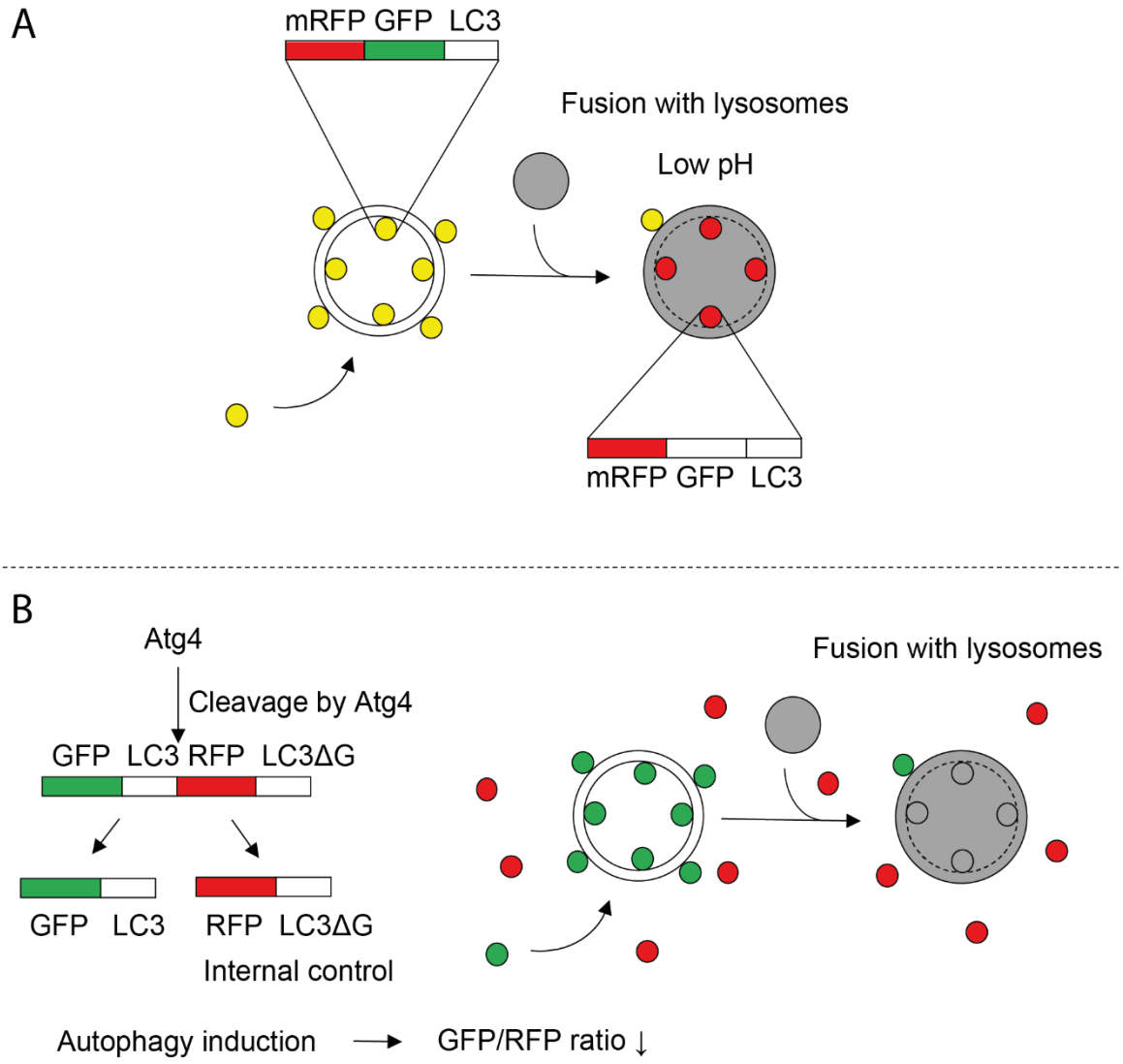

Figure 10 I Principle of the different red-green sensors for monitoring autophagic flux.
(**A**) The mRFP-GFP-LC3 probe, with quenched GFP fluorescence in the acidic environment of the autolysosome whereas the mRFP is stable at low pH. Autophagy induction increases the number of GFP and mRFP positive puncta (yellow). Upon autophagosome lysosome fusion, the puncta turn red as the GFP signal is quenched. (**B**) The GFP-LC3-RFP-LC3$^{\Delta G}$ probe that releases an internal control. Atg4 cleaves the probe into GFP-LC3 and RFP-LC3$^{\Delta G}$. Autophagic flux can be determined by calculating the ratio between GFP/RFP. Figure adapted from Yoshii *et al.*[89]

1.3 The role of Autophagy in neurodegenerative diseases

Due to the fact that autophagy plays a key role in maintaining cellular homeostasis, its dysfunction is contributing to the onset of neurodegenerative diseases such as Alzheimer's disease, Huntington's disease and Parkinson's disease[71,95]. Via autophagy, misfolded proteins, protein aggregates and damaged organelles such as mitochondria are degraded, and its constituents are recycled. Particularly for neurons in the brain, which do not divide and persist for the whole lifetime, autophagy plays an

important role. As autophagy is able to prevent the formation of protein aggregates, it contributes to the prevention of the onset of neurodegenerative diseases[95]. So far, many studies have demonstrated the neuroprotective effect of autophagy[29,95,71].

Since neurons have unusual large expanses of dendritic and axonal cytoplasm, prevention of the accumulation of dysfunctional organelles as well as cellular waste is complicated. Furthermore, neurons cannot undergo cell division as they are post-mitotic cells, which prevents “waste dilution” by apportionment to daughter cells as observed in mitotic cells[24,96], neurons are even more dependent on a functional and potent protein quality control system. Young neurons have been shown to be very efficient in clearing autophagic substrates, despite the long distance the autophagosomes needs to travel along the microtubules to meet lysosomes located mainly in the cell body. However, neurons are particularly vulnerable to impairments of the proteolytic clearance of cellular waste, as with dysfunctional autophagy, aggregation prone proteins accumulate and form protein aggregates. The cytotoxic effect of protein aggregates has been shown to lead to neurodegeneration as a result of deregulated cellular mechanisms such as transcription and impaired axonal transport[24].

Studies in Atg5 or Atg7 knockout mice revealed an increase of polyubiquitinated inclusion bodies accompanied by behavioral defects[97-98]. Furthermore, the depletion of FIP200 in mouse neurons showed a reduction of autophagosome formation resulting in cerebellar degeneration and progressive neuronal cell loss[99]. Silencing of the autophagy receptor p62 in mice results in an increased formation of neurofibrillary tangles and abnormal behavior in response to neurodegeneration[100]. These and many other studies indicate a crucial role of autophagy in maintaining homeostasis and prevention of neurodegeneration.

A common hallmark of neurodegenerative diseases is the accumulation of pathological abnormal proteins, developing neurofibrillary tangles of Tau proteins in AD, Lewy-bodies of α-synuclein in PD or huntingtin aggregates of polyglutamine-expanded huntingtin in HD. Such neurodegeneration related protein aggregates are mainly targeted by the autophagy pathway. As aging is a common risk for the development of neurodegenerative diseases and autophagic activity decreases with increasing age, it is thought that dysfunctional autophagy contributes to the pathogenesis of neurodegenerative diseases. Recent studies demonstrated that activation of autophagy increased clearance of aggregation prone proteins such as polyQ-

expanded huntingtin and Tau[101-102]. In contrast, pharmacological inhibition of autophagy by 3-MA or Bafilomycin lead to an increased HTT aggregate burden in mice as well as in cultured cells[103-104].

1.4 BRET assays for detection of Protein-Protein Interactions (PPI)

Bioluminescence resonance energy transfer (BRET) is a natural phenomenon occurring in various marine organisms such as *Renilla reniformis*, *Aequorea victoria* and *Oplophorus gracilirostris*, where energy is transferred from a luminescent donor to a fluorescent acceptor protein in a non-radiative manner[105]. One requirement for successful BRET is the close proximity of less than 10 nm between the donor and the acceptor protein. The strict dependence on molecular proximity between BRET donor and acceptor molecules makes it a suitable tool for analyzing protein-protein interactions (PPI) in living cells. Since its first use in 1999 by Xu et al. the BRET technique has been used for analysis of thousands of PPIs[106-107].

1.4.1 BRET principle

BRET, like Fluorescence resonance energy transfer (FRET) is a biophysical method based on the non-radiative diploe-dipole transfer of energy from a donor to an acceptor molecule which in turn emits light of a different wavelength[108]. Unlike FRET, BRET is based on the use of a luciferase protein as donor, and not dependent on an external light source for donor excitation[109]. A luciferase is a general term to describe an enzyme catalyzing light emitting reactions. Bioluminescence is referred to reactions catalyzed by luciferases to produce light by oxidation of a substrate molecule[109]. Usually, BRET assays are designed to use one of the well characterized luciferases such as Nano luciferase (NLuc)[110], Renilla luciferase (RLuc)[111] or Firefly luciferase (FLuc)[112].

For BRET experiments, the luciferase and the fluorophore molecules are fused to the proteins of interest in a manner similar to FRET experiments. It is important that the excitation spectrum of the acceptor protein overlaps with the emission spectrum of the donor luciferase. It has been shown that EGFP, and YFP-derived fluorescent proteins such as mCitrine work well as acceptors for BRET assays[113]. The presence of the bioluminogenic substrate induces the light emission of the luciferase in response to substrate oxidation (**Figure 11A**). The energy transfer that occurs in BRET is highly

dependent on the distance and orientation of the donor and acceptor molecules with the efficiency of the BRET decreasing with the sixth power of their distance[113]. Thus, BRET assays are a suitable tool to distinguish between a physical interaction and a protein co-localization in the absence of interaction.

A

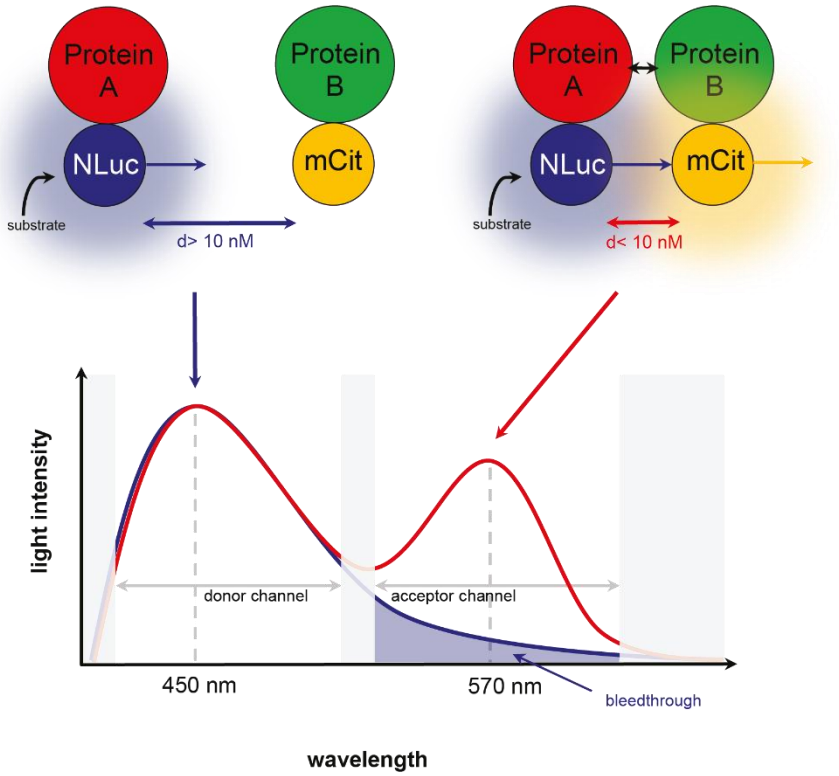

B

BRET ratio:

$$\frac{acc.channel}{don.channel} - corr.fact.$$

Bleedthrough correction factor:

$$\frac{acc.channel\ (don.only)}{don.channel\ (don.only)}$$

Figure 11 I Schematic overview of the BRET assay to study protein-protein-interactions. **(A)** Fusion proteins A and B with NLuc and mCitrine are co-expressed. Upon addition of the substrate Furimazine, luminescence signals are measured at 450 nm (NLuc light emission) and 570 nm (mCitrine light emission). Figure adapted from Sana *et al.*[114] **(B)** Calculation of the BRET ratio.

The quantification of BRET takes place by measuring the luminescence of the donor and the acceptor independently and the calculation of the BRET ratio by dividing the acceptor signal by the donor signal. The BRET ratio is corrected for donor bleed-through (overlap of the emission spectra of the donor with the emission spectra of the acceptor) by subtracting the BRET ratio of a donor only sample (**Figure 11B**). In case of an interaction, the acceptor protein emits light, which results in an increased BRET

ratio. In turn, if no interaction between the target proteins takes place, only the donor signal is detected, leading to a low BRET ratio.

1.4.2 Donor saturation assays for quantitative analysis of PPIs

Due to the fact that a high BRET ratio indicates an interaction of two proteins but does not give information about the specificity of the interaction, the BRET ratio itself cannot be used to get information about the affinity of two proteins to each other. In order to get information about the affinity of two proteins to each other and the specificity of the interaction, donor saturation assays can be conducted.

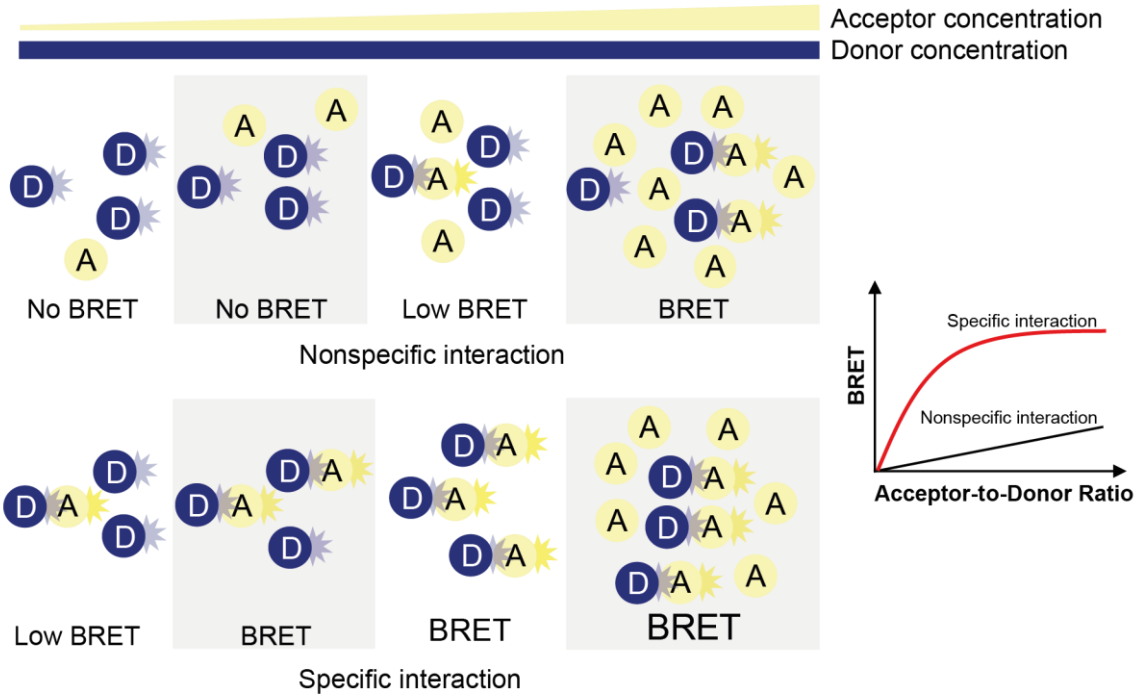

Figure 12 I Schematic overview of BRET donor saturation assays.
For donor saturation assays, constant amounts of donor tagged proteins are tested against an increasing amount of acceptor tagged proteins. A hyperbolic curve shape indicates a specific interaction whereas a non-specific interaction shows a linear relationship. Figure adapted from Wade et al.[116].

For the quantitative BRET saturation assay, a constant amount of donor fusion protein is co-expressed with increasing amounts of acceptor fusion protein (**Figure 12**). Hypothetically, a hyperbolic curve should be obtained for a specific interaction between the donor fusion protein and the acceptor fusion protein. Here, the BRET ratio increases with increasing quantity of acceptor fusion proteins until the donor fusion protein is saturated ($BRET_{max}$). In contrast, if the measured BRET signal is due to random collisions between the donor and acceptor in response to a high acceptor expression, a linear relationship is expected. $BRET_{50}$ values obtained from donor

saturation assays can be used as measure for the affinity of two proteins for each other[115].

1.5 Purpose of the presented work

Autophagy is a highly conserved catabolic mechanism, essential for maintaining cell homeostasis. Dysregulation of autophagy is related to many diseases, including cancer and neurodegenerative disorders. Accumulation of aggregation prone proteins such as α-synuclein in Parkinson's disease or Tau in Alzheimer's disease are indicative of an insufficient degradation of these proteins.

This project aims to enhance the turnover of aggregation prone proteins by interventions in the autophagy system to treat neurodegenerative diseases.

In order to induce the degradation of aggregation prone proteins via the autophagy pathway, the following specific aims were addressed:

1. Establishment and validation of BRET assays for the quantitative analysis of autophagy related protein-protein interactions
2. BRET based focussed screen of autophagy related protein-protein interactions for the identification of novel drug development targets
3. Modulation of autophagy related protein-protein interactions with the aim of autophagy induction
4. Development of a novel approach for targeted degradation of aggregation prone proteins

By investigating novel approaches for induction of autophagy as well as targeted degradation of aggregation prone proteins, this work aims for the identification of new treatment approaches to combat neurodegenerative diseases.

2 Material and Methods

2.1 Material

2.1.1 Lentiviral particles

Table 1 I Lentiviral particles for transduction of mammalian cells

Reagent	Vect. ID.	Supplier
pLV[Exp]-Puro-TRE3G-(HTT Ex1 46Qmix co-EGFP-FKBP mut)	VB201103-1074xzd	Vector Builder
pLV[Exp]-Puro-TRE3G-(HTT Ex1 19Qmix co-EGFP-FKBP mut)	VB201103-1073zjk	Vector Builder

2.1.2 Cell lines

The human embryonic kidney 293 (HEK293) cell line was obtained by CLS (Cat. No.: 300192) and HeLa cell line were obtained by ATCC (Cat. No.: CCL-2). iPSC derived neurons were obtained from Evotec stem cell division.

2.1.3 Chemicals and reagents

Table 2 I Reagents for cell culture and transfection

Reagent	Cat. no.	Supplier
MEM medium	51200-038	Gibco
DMEM medium, high glucose, HEPES	21063-029	Gibco
Fetal bovine serum (FBS)	10500-064	Gibco
Penicillin-Streptomycin (10,000 U/mL)	15140-122	Gibco
MEM NEAA	11140-050	Gibco
L-Glutamine	25030-024	Gibco
OPTIMEM	11058-021	Gibco
HBSS starvation buffer	14025-092	Gibco
TrypLE-express	12604-013	Gibco
TransIT-293	MIR2704	Mirus
Elution buffer	1014608	Qiagen

Table 3 I Reagents for iPSC culture and differentiation

Reagent	Cat. no.	Supplier
DMEM/F12 + Glutamax	10565-018	Gibco
MACS NeuroBrew 21 w/o vitamin A	130-097-263	Miltenyi Biotec
Y-27632-dihydrochlorid ROCKi	Y0503-1MG	Sigma
BDNF	B3795-5UG	Sigma
GDNF	130-129-542	Miltenyi Biotec
cAMP	D0627-250MG	Sigma
DAPT	D5942-25MG	Sigma
L-ascorbic acid	A4544-500G	Sigma

Table 4 I Reagents for plate coating

Reagent	Cat. no.	Supplier
Phosphate buffered saline (PBS)	14190-094	Gibco
Water for injection (WFI)	A12873-01	Gibco
Fibronectin from human plasma	F0895-5MG	Sigma

Table 5 I Reagents for gateway cloning

Reagent	Cat. no.	Supplier
10x TAE buffer	A1691	Applichem
Gateway LR Clonase II enzyme mix	11791-020	Invitrogen
Ampicillin Na-salt	K029.1	Roth
S.O.C. medium	15544034	Invitrogen
Qiagen Plasmid Plus Maxi Kit	12961	Qiagen

Table 6 I Reagents for BRET assay

Reagent	Cat. no.	Supplier
NanoGlo Furimazine	N113A	Promega
NanoGlo Endurazine	N257B	Promega
Phosphate buffered saline (PBS)	14190-094	Gibco

Table 7 I Reagents for BCA assay

Reagent	Cat. no	Supplier
Pierce BCA protein assay kit	23227	Thermo Scientific

Pre-diluted standard, Serum albumin	23208	Thermo Scientific

Table 8 I Reagents for immunocytochemistry

Reagent	Cat. no.	Supplier
Phosphate buffered saline (PBS)	14190-094	Gibco
Water for injection (WFI)	A12873-01	Gibco
Triton X-100	X100-100ML	Sigma
Bovine serum albumin (BSA)	A7979-50ML	Sigma
Para-formaldehyde 32% (PFA)	15714-S	EMS
Normal goat serum	005-000-121	Jackson IR
Hoechst 33342 solution 20 mM	62249	Thermo Scientific
Pre-diluted prot. assay standards	23208	Thermo Scientific

Table 9 I Reagents for SDS-PAGE and Western Blot

Reagent	Cat. no.	Supplier
Methanol	1.06009.2500	Merck
Bolt MES SDS running buffer (20x)	B0002	Novex
Pierce WB transfer buffer (10x)	35040	Thermo Scientific
Tris-Glycine SDS running buffer (10x)	LC2675	Novex
Tris-Glycine transfer buffer (25x)	LC3675	Novex
Tris-Glycine SDS sample buffer (2x)	LC2676	Novex
Bolt sample reducing agent (10x)	B0009	Novex
Phosphatase inhibitor	04 906 837 001	Roche
Protease inhibitor (with EDTA)	05 892 970 001	Roche
Magnesium chloride ($MgCl_2$)	63020-1L	Fluka
RIPA buffer	R0278-500ML	Sigma
Benzonase	70746-10KUN	Millipore
Pierce ECL western blotting substrate	32106	Thermo Scientific
Super Signal West Femto	34095	Thermo Scientific
Precision Plus Protein standard	161-0373	Bio Rad

Table 10 I Reagents for Protein Simple Jess Western analysis

Reagent	Cat. no.	Supplier
EZ Standard Pack 1	PS-ST01EZ	Bio-Techne

Antibody diluent 2	042-203	Bio-Techne
Streptavidine HRP	042-414	Bio-Techne
Luminol-S	043-311	Bio-Techne
Peroxide	043-379	Bio-Techne
Wash buffer	042-202	Bio-Techne
10x sample buffer	02-195	Bio-Techne

Table 11 I Reagents for Fractionation assay

Reagent	Cat. no.	Supplier
Tris-HCl	T2194-1L	Sigma
Sodium chloride ($NaCl_)$	S7653-1KG	Sigma
Water for injection (WFI)	A12873-01	Gibco
Triton X-100	X100-100ML	Sigma
Phosphatase inhibitor	04 906 837 001	Roche
Protease inhibitor (with EDTA)	05 892 970 001	Roche
Sodium-dodecyl-sulfate (SDS) solution	05030-500ML-F	Sigma
Phosphate buffered saline (PBS)	14190-094	Gibco

Table 12 I Reagents for TR-FRET assay

Reagent	Cat. no.	Supplier
TRIS-EDTA buffer solution	93302-100ML	Sigma
PicoGreen dsDNA reagent	P11495	Invitrogen
Triton X-100	X100-100ML	Sigma
Phosphatase inhibitor	04 906 837 001	Roche
Protease inhibitor (with EDTA)	05 892 970 001	Roche
Phosphate buffered saline (PBS)	14190-094	Gibco

Table 13 I Reagents for CTG assay

Reagent	Cat. no.	Supplier
CellTiter-Glo®	G756A	Promega

Table 14 I Reagents for Luminescence based co-precipitation assay

Reagent	Cat. no.	Supplier
NanoGlo Furimazine	N113A	Promega
Magnesium chloride ($MgCl_2$)	63020-1L	Fluca

PMSF	93482-50ML	Sigma
Dithiothreitol (DTT)	7016L	Cell Signaling
TBS 10x	1060.1	Roth
Tween20	P2287-100ML	Sigma
Blocker BSA in TBS-T 10%	37520	Thermo Scientific
Roti-Stock 10x TBS-T	1061.1	Roth
Benzonase	70746-10KUN	Millipore
HEPES	15630-049	Gibco
Water for Injection (WFI)	A12873-01	Gibco
Glycerol	G8773	Sigma
Sodium deoxycholate	D-6750	Sigma
Sodium Chloride (NaCl)	S7653	Sigma
EDTA	E9884	Sigma
Sodium fluoride (NaF)	S7920	Sigma
Sodium orthovanadate	S6508	Sigma
Tetra-sodium pyrophosphate	P8010	Sigma
Protease inhibitor (w/o EDTA)	04 693 159 001	Roche
NP-40	NP40-100ML	Sigma
Phosphate buffered saline (PBS)	14190-094	Gibco

Table 15 I Reagents for MSD assay

Reagent	Cat. no.	Supplier
Probumin® BSA	8.21006	Sigma
MSD read buffer GOLD	R92TG-1	MesoScale
Tween20	P2287-100ML	Sigma
Phosphate buffered saline (PBS)	14190-094	Gibco

Table 16 I Reagents for generation of stable cell lines

Reagent	Cat. no.	Supplier
Polybrene	PL0001	VectorBuilder
Puromycin, 10mg/mL	A11138-03	Gibco
Geneticin; G418	11811-064	Gibco
Hygromycin B	10687010	Invitrogen
DMSO	D8418-50ML	Sigma
FBS, Qualified; HI	10500-064	Gibco

2.1.4 Buffer solutions and media

TR-FRET lysis buffer	0.4% Triton X-100 1 tabl./10mL Protease inhibitor 1 tabl./10mL Phosphatase inhibitor in 1x PBS
RIPA lysis buffer	2 mM $MgCl_2$ 0.01% Benzonase 1 tabl./10mL Protease inhibitor 1 tabl./10mL Phosphatase inhibitor in RIPA buffer
CSK lysis buffer	25 mM Tris-HCL 150 mM NaCl 1% Triton X-100 1 tabl./10mL Protease inhibitor 1 tabl./10mL Phosphatase inhibitor in WFI
DMEM complete medium	10% FBS 1% penicillin/streptomycin in DMEM medium
MEM complete medium	10% FBS 1% penicillin/streptomycin 2 mM L-Glutamine 1x MEM-NEAA in MEM medium
iPSC differentiation medium	1x N2 supplement B 1x MACS NeuroBrew 21 w/o vitamin A 10 µM ROCKi 20 ng/mL BDNF 20 ng/mL GDNF

	200 µM cAMP 10 µM DAPT 200 µM L-ascorbic acid in DMEM/F12 + Glutamax
Lysis buffer for BRET in lysates	0.5M EDTA 4% Triton X-100 100% Glycerol 100mM PMSF 1 tabl./10mL Protease inhibitor 1 tabl./10mL Phosphatase inhibitor in PBS
HBSS starvation buffer	1% FBS in HBSS buffer
Lysis buffer for luminescence based co-precipitation assay	50 mM HEPES 150 mM NaCl 10% Glycerol 1% NP-40 0.5% Sodium deoxycholate 20 mM NaF 1.5 mM $MgCl_2$ 1 mM EDTA 1 mM DTT 1x Benzonase 1x Protease inhibitor 1 mM PMSF 1 mM sodium orthovanadate 2 mM tetra-sodium pyrophosphate in WFI
Washing buffer for luminescence based co-precipitation assay	1x TBS 0.1% Blocker BSA in TBS

	0.05% Tween 20 in WFI
MSD wash buffer	0.2% Tween20 1x PBS
MSD blocking buffer	0.5% Probumin® BSA in MSD wash buffer
Cell freezing medium	90% FBS 10% DMSO

2.1.5 Antibodies

Table 17 I Antibodies for Western Blot

Antigen	Clone	Host	Label	Cat. no.	Supplier
DDK (FLAG)	OTI4C5	mouse	none	TA50011-100	Origene
mouse IgG		goat	HRP	32230	ThermoFisher
rabbit IgG		goat	HRP	31402	ThermoFisher
mouse IgG		goat	680RD	926-68070	LI-COR
rabbit IgG		goat	800CW	926-32211	LI-COR
GAPDH	14C10	rabbit	none	2118S	CellSignaling
MAP1-LC3B		rabbit	none	ab51520	abcam
α-tubulin	B512	mouse	none	T5168	Merck
GFP		rabbit	none	ab290	abcam
HA-tag	C29F4	rabbit	none	2367	CellSignaling

Table 18 I Antibodies for immuno-cytochemistry

Antigen	Clone	Host	Label	Cat. no.	Supplier
HaloTag		rabbit	none	G9281	Promega
rabbit IgG		goat	AF647	A32733	ThermoFisher

Table 19 I Antibodies for JESS assay

Antigen	Clone	Host	Label	Cat. no.	Supplier
GFP		rabbit	none	ab290	abcam

GAPDH	14C10	rabbit	none	2118S	CellSignaling
Flotillin		rabbit	none	ab41927	abcam
rabbit IgG		goat	HRP	043-426	Bio-techne

Table 20 I Antibodies for TR-FRET assay

Antigen	Clone	Host	Label	Cat. no.	Supplier
LC3-II		rabbit	D2	L7543	Sigma
LC3-II		rabbit	Terbium	2324	CST
p62		rabbit	D2	P0067	Sigma
p62	2C11	mouse	Terbium	H00000878-M01	Abnova

Table 21 I Antibodies for Luminescence based co-precipitation assay

Antigen	Clone	Host	Label	Cat. no.	Supplier
GFP nanobody		cameloid	biotin	Gtb-250	Chromotek

Table 22 I Antibodies for MSD assay

Antigen	Clone	Host	Label	Cat. no.	Supplier
Human HTT N-term. (AA7-13)	MW1	mouse	Sulpho-tag	-	Evotec SE
HTT polyQ stretch	2B7	mouse		-	Evotec SE

2.1.6 Compounds

Table 23 I Compounds

Compound	Cat. no.	Supplier
Rapamycin	S1039	Selleckchem
Navitoclax	S1001	Selleckchem
Venetoclax	S8048	Selleckchem
Bafilomycin	B1793-10UG	Sigma
Chloroquine	PHR-12581	Sigma
FPZ	F4765-1G	Sigma
Torin1	S2827	Selleckchem
Torin2	S2817	Selleckchem
SW063058	-	Evotec SE
SW076956	-	Evotec SE

3MA	M9281-100MG	Sigma
ATACs	-	Evotec SE
neg. ATAC	-	Evotec SE

2.1.7 Consumables

Table 24 I Consumables

Consumable	Cat. no.	Supplier
384 well low volume plate, white	784080	Greiner
384 well low volume plate non-binding, black	784900	Greiner
384 well plate, transparent	781101	Greiner
96 well plate, µclear, white, advanced TC	655983	Greiner
96 well cell carrier ultra plate, black	6055302	Perkin Elmer
NeutrAvidin coated 384 well plate (white)	15512	Thermo scientific
Costar® 6-well clear TC-treated plate	3526	Corning
T25 cell culture flask	690 160	Greiner Bio-One
T175 cell culture flask	660 160	Greiner Bio-One
50 mL falcon tubes	227 261	Greiner Bio-One
2 mL Cryovials	122 263	Greiner Bio-One
Jess assay capillary cartridge	009-050	Bio-techne
Jess assay plate 12-230 kDa	043-165	Bio-techne

2.1.8 Software

Table 25 I Software

Software	Company
Graphpad Prism 9	GraphPad Software
ImageJ 1.49c	National Institutes of Health
Compass for SW 4.0.0	Bio-Techne
CytoScape 3.7.1	CytoScape
Discovery Studio Visualizer 19.1.0	Biovia
SnapGene 5.1.5	SnapGene
Spotfire Analyst 10.3.3	TIBCO
PyMOL 2.1	Schrödinger

Instant JChem 15.1.19	Chem Axon

2.2 Methods

2.2.1 Cell culture techniques

2.2.1.1 Maintenance culture of mammalian cells

All cell culture experiments were carried out by using immortalized, adherently growing cell lines. According to their specific properties, the cells were used for BRET assays, fractionation assays, TR-FRET assays, ICC assays as well as for sample collection for Western Blots.

The human embryonic kidney 293 (HEK293) cell line was routinely cultured in high glucose Dulbecco´s Modified Eagle´s Medium (DMEM) containing HEPES. HeLa cells (derived from Human cervical carcinoma cells) were cultured in Modified Eagle's Medium (MEM) containing 1x MEM Non-Essential Amino Acids Solution (NEAA). As standard, 10% heat inactivated Fetal Bovine Serum (FBS) and 1% Penicillin/Streptomycin were supplemented to each culture medium. Cells were incubated in T175 cell culture flasks at 37°C and 5% CO_2. Before reaching 90% confluence, cells were subcultured every 2-3 days. For this purpose, the culture medium was removed and TrypLE express was added for cell detachment from the cell culture flask. The cells were incubated for 3 minutes at 37°C with 5% CO_2, followed by the addition of standard culture medium which stopped the reaction. The cells were suspended in the culture medium. After counting the cells with a Countess cell counter, a certain volume containing the desired cell number was seeded into new flasks.

2.2.1.2 Maintenance of iPSC derived cortical neurons

Human cortical neurons were differentiated from human iPSC cells by the Evotec SE stem cell facility and transferred to the assay development team 7 days post differentiation. The iPSC derived neurons were routinely cultured in DMEM/F12 medium + Glutamax. As standard, N2 supplement-B, B21 (MACS NeuroBrew-21 w/o vitamin A), GDNF+BDNF, cAMP, AA and DAPT were supplemented to the medium.

2.2.1.3 Plate coating

In order to increase the cell adhesion to the cell culture plates, the plates were coated with a 0.001% solution of fibronectin. A 0.1% solution of fibronectin was diluted 1:100 in distilled water and added to the culture plate (40 µL for 96 well plates and 10 µL for 384 well plates). After an incubation of at least 4 h at 37°C with 5% CO_2, the plate was washed 1x with distilled water and 1x with PBS (100 µL for 96 well plates and 40 µL for 384 well plates). If not used immediately, the plates were stored at 4°C until further use.

2.2.1.4 Transient DNA transfection mediated by TransIT-293

The reverse transfection method was used for plasmids; therefore, the cells were seeded onto multi well plate after the addition of a transfection mix. At least 24 h prior to plating, HEK293 or HeLa cells were plated in a T175 flask so that the cells reached 70-80% confluency the following day. The transfection mix was prepared according to the manufacturer´s instructions using a ratio of 0.3 µL of TransIT-293 per 0.1 µg of plasmid DNA. The total amount of transfected DNA was dependent on the plate format (25 ng per 384 well, 100 ng or 200 ng per 96 well and 2000 ng per 6 well) and was kept constant by filling up with pcDNA3.1(+) empty vector. After addition of the transfection mix, HEK293 or HeLa cells were seeded onto the suitable culture plate for each experiment.

2.2.1.5 Compound treatment

In order to treat the cells with tool compounds as well as to test compounds, the compounds were diluted to a 10x concentration in culture medium. The 10x compound solutions were transferred to the cells to obtain a 1x final compound concentration. The final DMSO concentration was below 0.3% in all experiments, and solvent controls were always used to exclude solvent effects. The compounds treated cell cultures were incubated at 37°C with 5% CO_2 for the desired period.

2.2.1.6 Generation of cell lysates

For WB and Jess assays, HeLa cell lysates were generated by adding 300 µL or 30 µL of RIPA lysis buffer[117] to a 6 well or 96 well plate before freezing at -80°C. After thawing,

the lysates were placed on a plate shaker for 20 min at 4°C before being transferred to 1.5 mL Eppendorf tubes. The lysates were stored on ice until further processing.

2.2.1.7 Generation of stable pools using lentivirus transduction

In order to generate stable pools of HeLa cells, for each lentivirus and MOI (multiplicity of infection) one T25 flask plus one extra flask for cell number determination were prepared. One day before transduction, 1.5E^{06} cells were seeded in 6 mL into a T25 flask and incubated overnight at 37°C and 5% CO_2.

For lentivirus transduction, the cell number of the spare T25 flask was determined in order to calculate the volume of lentivirus to be added to the cells. Based on the cell number the volume of lentivirus was calculated as follows, where TU is the transfection unit:

$$vol.of\ lentivirus\ [\mu L] = \frac{desired\ MOI}{virus\ titer\ in \frac{TU}{\mu L}} \times vol.of\ medium\ in\ T25\ flask[mL] \times cell\ count\ of\ ctr.flask/mL$$

In order to enhance the efficiency of the lentiviral transduction, polybrene (5 µg/mL) was added to the cells before the calculated volume of the lentivirus was added. The cells were incubated for 24 h at 37°C with 5% CO_2, before the medium was changed for fresh medium. After a further 24 h of incubation, the construct specific selection markers were added to the culture medium at the following concentrations:

- Puromycin 0.4 µg/mL
- G418 100 µg/mL
- Hygromycin 200 µg/mL

The cells were incubated for a further 24 h before transferring 0.5E^{06} cells in 30 mL culture medium containing the selection antibiotics to a T175 flask. From this point on, the selection antibiotics will be supplemented to the culture medium as standard for culturing. The cells were incubated for 72 h before splitting into fresh culture flasks. Depending on the detection marker of the transduced proteins, the characterization of the cell lines took place by WB or ICC. For long term storage, the cells were frozen and stored in liquid nitrogen until further use. For that purpose, 4E^{06} cells were frozen in 1 mL of freezing medium (90% FBS; 10% DMSO).

2.2.2 Molecular biology techniques

2.2.2.1 Gateway cloning of fusion constructs

In order to clone the plasmids coding for the BRET fusion constructs, Gateway cloning was performed. The gateway cloning is based on the heterologous DNA sequences (flanked by modified att recombination sites) between vectors[118]. The plasmid cloning method was performed by using two recombination reactions - the BP and LR reactions. Here, entry and destination vectors from Evotec SE were used. The destination vectors, encoding N- and C-terminally tagged fusion proteins were generated based on pcDNA3.1 (+) backbone. Acceptor destination vectors pcDNA3.1(+)-V5-NLuc-2GS-GW, pcDNA3.1(+)-GW-2GS-NLuc-V5, pcDNA3.1(+)-FLAG-mCitrine-2GS-GW and pcDNA3.1(+)-GW-2GS-mCitrine-FLAG were amplified by internal cloning facility. Entry vectors obtained from BP reaction were ordered from GeneArt (Thermofisher). For the LR-reaction, 150ng of the destination vector was incubated for 1 h at 25°C with 50-150ng of the entry vector in Gateway LR Clonase enzyme mix containing Proteinase K solution 2 µg/µL. The LR reaction product was transformed into TOP10 *E.coli* by using the heat-shock procedure[119]. Competent TOP10 *E.coli* were exposed to a heat shock for a maximum of 1 min at 42°C, before adding the SOC medium for 1 h incubation at 37°C by shaking at 550 rpm on Eppendorf ThermoMixer. The transformation mix was plated on LB agar plates, containing 100 µg/mL Ampicillin, and incubated at 37°C overnight. A selection of colonies grown on the agar plates were transferred for further cultivation and proliferation (16 h at 37°C) to LB medium containing 100 µg/mL Ampicillin. The cloning product was purified by using the Maxi Prep kit from Qiagen, according to manufacturer's instruction. For quality control purposes, the maxi prep product was checked via control digest for the correct inserts and sent to LGC Genomics for sequencing.

2.2.3 Biochemical methods

2.2.3.1 BRET assay

In general, all BRET assays were performed in a 96 well format 48 h after DNA transfection, encoding the fusion proteins of interest according to the DNA transfection protocol described above (2.2.1.4). 48 h post DNA transfection 100 µL of the culture medium was removed and 10 µL of a Furimazine dilution (1:50 in PBS) was added to the remaining 100 µL resulting in a final substrate dilution of 1:500. After 5 min of incubation at 37°C with 5% CO_2, luminescence and fluorescence signals were measured using a PHERAstar (BMG Labtech) plate reader. Measurement took place at 37°C for living cells and at RT for lysates. The fluorescence emission at 530 nm was determined following excitation at 495 nm. Luminescence emission was measured at 450-80 nm (donor channel) and 570-100 nm (acceptor channel). A "total luminescence" reading was subsequently measured at a spectrum between 400 nm and 700 nm.

The BRET ratios were calculated for each condition by dividing the acceptor channel at 570-100 nm (LWL) by the donor channel at 450-80 nm (SWL). A correction for donor bleedthrough was performed by subtraction of a correction factor (cf) calculated from the transfection condition containing only the donor fusion protein.

$$BRET\ ratio = \frac{LWL}{SWL} - cf$$

$$cf = \emptyset \left(\frac{LWL_{NanoLuc}}{SWL_{NanoLuc}}\right)$$

For studies aiming for the modulation of interactions, the calculated BRET ratios were normalized to the respective untreated controls to give the nBRET in %.

$$nBRET\ ratio = \frac{BRET\ ratio\ sample}{BRET\ ratio\ untreated\ control}\ x\ 100$$

2.2.3.1.1 Donor saturation assay

In order to determine the binding affinity of two proteins to each other and the specificity of the interaction, donor saturation assays were performed. For that purpose, HEK or HeLa cells were transfected with a constant amount of NLuc fusion protein as BRET donor in presence or absence of increasing amounts of mCitrine fusion protein as BRET acceptor. As a standard, 0.5-1 ng plasmid DNA of donor fusion protein were co-transfected with 1-100 ng plasmid DNA of acceptor fusion protein in a 96 well format. In theory, for a specific interaction of protein A with protein B, a hyperbolic increase of the BRET ratio is expected. For a specific interaction, the increase in BRET signal reaches a plateau when all donor molecules are saturated with acceptors (BRETmax). In contrast, for a non-specific interaction, a linear increase with increasing acceptor concentrations of the BRET ratio is expected [116]. Due to the fact that the BRETmax is also defined by the spatial distance and the orientation between the reporter proteins to each other (NLuc and mCitrine), the BRETmax cannot be used as a quantitative measure for relative given binary interaction. Therefore, the $BRET_{50}$, which represents the acceptor/donor ratio (A/D) where 50% of the BRETmax is reached, is calculated. For compound treatment studies, an A/D ratio in the range of the $BRET_{50}$ was used.

2.2.3.1.2 Expression normalization

Due to the fact that the expressed ratio of donor and acceptor fusion constructs does not necessarily represent the transfected ration on a DNA level, an expression normalization based on fluorescence and luminescence levels of the tandem construct (mCitrine-NLuc) was performed. Based on the assumption that the ratio between Donor and Acceptor of the tandem construct is exactly 1:1, a correction factor was calculated by using following equation:

$$tanden\ corr.fact. = \frac{total\ luminescence\ signal}{fluorescence\ signal}$$

In order to determine the correct donor to acceptor (D/A) ratio for each sample, the following calculation was performed:

$$corr.D/A\ ratio = \frac{tand.corr.fact.* fluorescence\ signal}{total\ luminescence\ signal}$$

The corrected D/A ratios were used for the X-axis to plot the donor saturation curves.

2.2.3.1.3 Donor saturation assay using cell lysates

In order to determine the ability of small LIR peptides to bind to LC3, donor saturation assays were performed using HEK cell lysates. For that purpose, HEK293 cells were transiently transfected with NLuc-LC3B plasmids. After 48 h of expression, the cells were lysed in BRET lysis buffer for 30 min on ice. Cell debris was removed by 10 min centrifugation at 1000 rpm and at 4°C. For donor saturation assay, a constant amount of NLuc-LC3 containing cell lysate was added to a white low volume 384 well plate before increasing concentrations of acceptor (TMR) labelled LIR peptides were added. After 1 h incubation at room temperature on a plate shaker, fluorescence and luminescence signals were measured using a PHERAstar (BMG Labtech) plate reader. The fluorescence emission at 580 nm was determined following excitation at 540 nm. Luminescence emission was measured at 450-80 nm and 610-LP nm. BRET ratios were calculated as described in 2.2.3.1.

2.2.3.2 Competition assay using cell lysates

In order to confirm the binding of peptides to a target protein, competition assays were performed. For that purpose, HEK cell lysates were incubated for 1 h with labelled peptides (hot probe), before increasing concentrations of unlabeled peptides (cold probe) were added. After 1h of incubation the fluorescence and luminescence was measured and the BRET ratios were calculated as described in 2.2.3.1.3 and 2.2.3.1.

2.2.3.3 Kinetic studies

In order to perform kinetic studies, the cells were handled as described in 2.2.3.1 with the exception that Endurazine was used as substrate, which ensures a steady release of Furimazine. By using Endurazine experiments of several hours to days are possible[105]. The change of the substrate from Furimazine to Endurazine, requires a 1 h pre-incubation at 37°C with 5% CO_2 to ensure proper release of Furimazine. This is because the substrate Endurazine needs to be hydrolyzed by endogenous esterases. After 1 h of substrate incubation, the compounds were added and the plate was measured immediately on a Tecan SPARK plate reader at 37°C with 5% CO_2. As standard, an interval of 30 minutes was set for 48 h or 72 h. For preventing excessive

evaporation of the culture medium, kinetic BRET measurements took place by using a gas permeable transparent foil covering the plate. The data for each time point was analyzed as described in 2.2.3.1.

2.2.3.4 Immunocytochemistry (ICC)

For ICC, cells were fixed and stained for nuclei with 4% PFA and 250 nM Hoechst33342 in PBS for 15 min at room temperature, protected from light. After incubation, cells were washed 3x with PBS. For blocking unspecific binding of antibodies to proteins, a blocking solution with 10% normal goat serum, 1% BSA and 0.1% Triton X-100 in PBS was added for 1 h at room temperature (RT). After blocking, the cells were incubated with the primary antibody (AB) diluted in 5% normal goat serum, 1% BSA and 0.1% Triton X-100 in PBS for 1 h at room temperature. Before secondary antibody incubation (1 h at RT), the cells were washed 3x with PBS. After secondary antibody incubation the cells were washed again 3x with PBS. After washing, the culture plate was sealed with an adhesive aluminum foil and stored at 4°C until imaging at the OPERA Phoenix workstation. The images were acquired at 40x magnification using a water immersion objective with laser excitation. The following settings were used (**Table 26**):

Table 26 I Fluorescence imaging settings

Fluorescence channel	Excitation (nm)	Emission (nm)
Hoechst (nuclear stain)	405	456
EGFP	488	522
Alexa Fluor 647	640	706
Alexa Fluor 568	561	599

2.2.3.5 ICC image quantification

In order to quantify the images obtained by ICC, an automated script analysis was set up. The quantification was split into several consecutive steps, which processes the detection of the individual cell, the detection of HTT aggregates and the determination of the soluble HTT. In order to define the individual cells, the nuclei were detected by using the Hoechst channel signal. For that purpose, objects above a minimum brightness, size and shape were considered as nuclei. For the determination of the cytoplasm, the EGFP channel intensity was used to estimate the perinuclear region.

Based on the fact that the EGFP signal can potentially be influenced by compound activity, the cytoplasm detection was combined with a ring like region around the nucleus, which was used as a backup in case the EGFP signal was too weak for cytoplasm determination.

For the quantification of HTT aggregates, a threshold was applied and the detected regions were further filtered by attributes such as size, shape and signal to background ratio. Cells containing at least one HTT aggregate were considered as aggregate positive cells. In order to determine the intracellular soluble HTT amount, a texture analysis based on the perinuclear EGFP intensity was performed separately from the aggregate detection. Based on the quantitative data obtained from the imaging script, the following readouts were calculated:

Table 27 I ICC image quantification - QC-readouts

Readout	Description
Cell count (more accurately nuclei count)	sum of all nuclei per field and then per well

Table 28 I ICC image quantification - HTT assay readouts

Readout	Description
rationumber EGFP pos	ratio of all EGFP positive cells to all detected cells (per well)
number_EGFP_pos	sum of all EGFP positive cells per well
Agg_number_total	sum of all HTT-aggregates in the whole well
Agg_number_per_EGFPpos_cells	sum of all HTT-aggregates divided by the sum of all EGFP positive cells

Table 29 I ICC image quantification - Soluble HTT readouts

Readout	Description
EGFP_Intensity_vs_MedianBG_Whole Cell	Mean value per well of EGFP intensity in the whole cell divided by median EGFP intensity in the (local) background
EGFP_MedianIntensity_vs_MedianBG _WholeCell	Median value per well of EGFP Intensity in the whole cell divided by median EGFP intensity in the (local) background

2.2.3.6 BCA assay for determination of protein concentration of cell lysates

The protein concentration of cell lysates was determined against a standard curve of known concentrations of bovine serum albumin (BSA). 5 µL of standard or lysate were added in quadruplicates to a clear 384 well plate. 45 µL of BCA working reagent (1:1 mixture of reagent A and reagent B, according to manufacturer's instructions) were added to the samples. The microplate was sealed and incubated for 30 min at 37°C before measuring the absorbance at 562 nm wavelength using a PHERAstar (BMG Labtech) plate reader.

2.2.3.7 SDS-PAGE and Western Blot (WB)

For analysis of protein levels, HEK and HeLa cell lysates were prepared for protein separation on polyacrylamide gels by adding SDS sample buffer and sample reducing agent. The samples were heated to 95°C for 5 minutes (75°C for 10 minutes for LC3 WB) and loaded onto a 6-12% Bis-Tris gel (16% Tris-Glycine gel for LC3 WB) along with a molecular weight marker for reference. Gels were run at 140 V for 60 min (120 min at 100 V and 4°C for LC3 WB) in running buffer. The progress of the gel electrophoresis was monitored by observation of the tracking dye bromophenol blue which was included in the sample buffer. By using the Western Blotting (WB) technique, proteins separated by gel electrophoresis are transferred to a 0.45 µm PVDF membrane (0.2 µm for LC3 WB) for 1 h at 20 V (15 V for LC3 WB).

The proteins were transferred by wet transfer procedure. Therefore, for every gel to be blotted, two stacks of filter paper and a sponge pad were soaked in transfer buffer. A PVDF membrane was cut to gel size and activated by short incubation in methanol.

The SDS gel was transferred onto one of the filter sponge stacks placed on a wet transfer cassette. The PVDF membrane and the second filter sponge stack were piled on top and potential air bubbles removed by gently applying pressure onto the stack from the middle towards the edges. The transfer cassette was closed, placed inside the transfer tank and filled with transfer buffer. Electroblotting was performed by administering 20 V for 60 min (15 V for LC3 WB).

In order to prevent unspecific binding of the antibodies during incubation steps, membranes were firstly blocked in blocking buffer (5% BSA in TBS-T). The incubation was carried out under gentle agitation for 60 min at RT. For specific labelling of a given protein, the respective antibody was diluted in 5% BSA in TBS-T and applied to the

blocked membrane. The membranes were then incubated for 1 h at RT or overnight at 4°C on a plate shaker. Next, the membrane was washed 3x for 5 min in TBS-T to eliminate unbound antibodies and was incubated with the respective species-specific secondary antibody diluted in 5% BSA in TBS-T. After incubation of 1 h at RT or overnight at 4°C, the membrane was washed again 3x for 5 min in TBST for residual antibody removal. All utilized antibodies were conjugated to the reporter enzyme horseradish peroxidase (HRP). Under cleavage of a chemiluminescent agent, the HRP produces a luminescence signal, which was detected by a Licor C-digit device. Hence, the washed membranes were air dried and covered with ECL or WestFemto solution and incubated for 30 sec at RT before placed into the dark chamber for image acquisition. The signals were quantified by using ImageJ software.

2.2.3.8 Protein Simple Jess Western analysis

In order to determine protein levels, Jess western blots were also performed. The Jess assay is a fully automated capillary-based immunoassay. For that purpose, protein concentration of HEK293 and HeLa cell lysates were determined as described in 2.2.3.6. Samples were diluted using 0.1x sample buffer and 5x fluorescent master mix to achieve a final concentration of 1x master mix according to the manufacturer's instructions. The prepared samples were denatured for 5 min at 95°C and stored on ice until further use. Primary antibodies were diluted to the final concentration in antibody diluent. 5 µL of sample, 10 µL of antibody diluent, 10 µL of primary antibody, 10 µL of HRP conjugated secondary antibody, 15 µL of Luminol peroxide and 500 µL of wash buffer were dispensed to the assay plate according to the plate layout. The assay plate is centrifuged for 5 min at 1000xg before loading into the instrument. The proteins were separated and detected in the individual capillaries. The digital images were collected and analyzed by Compass software. The protein levels were reported as area under the peak representing the intensity of the signal. For EGFP, GAPDH and Flotillin, antibody dilutions of 1:100, 1:250 and 1:25, respectively, were used. For the secondary antibody, anti-rabbit HRP secondary antibody was used.

2.2.3.9 Fractionation assay

For fractionation assays, HeLa cell lysates were generated by adding 300 µL of CSK lysis buffer[117] to a 6 well plate before freezing at -80°C. After thawing, the lysates were

placed on a plate shaker for 20 min at 4°C before transferring the lysates to 0.5 mL protein LoBind tubes. The protein concentration was determined by preforming a BCA assay as described in 2.2.3.6. In order to separate the soluble and insoluble (aggregated) proteins of the total cell lysates, the samples were fractionated by using ultra centrifugation. All samples were adjusted to the same protein concentration, with 400 µL of the homogenate transferred into an ultracentrifugation tube. The samples were centrifuged for 30 min at 106,000xg and 4°C (TLA_100.3 (6tubes)). After centrifugation the supernatant was transferred into a fresh tube and stored on ice. The pellet was washed with 400 µL of fresh CSK lysis buffer and centrifuged again for 30 min at 106,000xg. This time the supernatant was discarded and the pellet was re-suspended in 200 µL of CSK lysis buffer containing 0.5% SDS. In order to dissolve the pellet completely, the samples were sonicated for 30 sec. (70%, 0.9 cycle) by using an ultrasonic processor (UP50H; Hielscher). The final samples were stored at -80°C until further use.

2.2.3.10 TR-FRET assay

For LC3-II and p62 level determination in cell lysates, cells were lysed in 16 µL/well (384 well) of ice cold TR-FRET lysis buffer for 30 min on a plate shaker at 500 rpm and at room temperature. The plate was centrifuged for 1 min at 200xg and stored at -80°C. For the TR-FRET assay, the plate was defrosted for 1 h at RT and centrifuged for 1 min at 200xg. 1 µL/well of the antibody mix (donor: Terbium; acceptor: D2 conjugated to LC3 and p62 antibodies) was combined with 5 µL of cell lysate on a separate 384 well assay plate. Following centrifugation at 200xg for 1 min, the plate was incubated for 24 h at RT on a plate shaker at 500 rpm and for 24 h at 4°C in the fridge.
For the LC3-II or p62 readout, the assay plate was stored at RT for 5 min After centrifugation at 200xg for 1 min, the TR-FRET measurement was performed using a PHERAstar (BMG Labtech) plate reader. For each well, the donor was excited at a wavelength of 337 nm, with the emission of the donor and acceptor being measured at wavelengths of 615 nm and 665 nm. From the measured fluorescence values, the TR-FRET ratio was calculated in order to minimize medium interferences:

$$TR-FRET\ ratio\ (665\ nm/615\ nm) = \frac{emission\ at\ 665\ nm}{emission\ at\ 615\ nm} \times 10.000$$

The specific TR-FRET signal is expressed as a percentage of Delta F (DF%), and calculated as follows:

$$DF\% = \frac{(665\,nm/615\,nm)sample - (665\,nm/615\,nm)blank}{(665\,nm/615\,nm)blank} \times 100$$

As a readout for toxicity, a PicoGreen assay was performed on the same assay plate. PicoGreen is a dsDNA specific reagent that exhibits a >1000x fold enhancement of fluorescence upon DNA binding. For that purpose, 2 µL of a PicoGreen solution diluted 1:25 in TRIS-EDTA buffer was added to the assay plate and incubated for 30 min at RT. A fluorescence measurement (Ex 485 nm, Em 535 nm) took place subsequently at the PHERAstar (BMG Labtech) plate reader. The PicoGreen signal is expressed as a percentage of Delta F (DF%) and calculated as follows:

$$DF\% = \frac{(535\,nm)sample - (535\,nm)blank}{(535\,nm)blank} \times 100$$

2.2.3.11 CTG assay

In order to determine cell toxicity, CellTiter-Glo® (CTG) assays were performed. The CTG assay is based on the quantification of adenosine triphosphate (ATP) which represents the presence of metabolically active cells. For that purpose, 14 µL of cell lysates in TR-FRET lysis buffer were combined with 10 µL of CTG reagent on a white low volume 384 well plate. After 30 min incubation at RT on a plate shaker with 500 rpm, the luminescence signal was determined using a PHERAstar (BMG Labtech) plate reader. The “total luminescence” was measured at a wavelength between 400-700 nm at room temperature.

2.2.3.12 Luminescence based co-precipitation assay

LuTHy assay is a double readout consisting of a BRET assay followed by a luminescence-based precipitation assay (LuC) for the quantitative analysis of binary PPIs[115]. The BRET assay was performed as described in 2.2.3.1 before the cells were lysed in Luminescence based co-precipitation lysis buffer (96 well; 40 µL) for 30 min on ice. The lysates were stored on ice until precipitation assay. A NeutrAvidin coated 384 well plate was washed 3x with 50 µL of washing buffer before coating with 20 µL of biotinylated GFP nanobodies (diluted in washing buffer (1500 ng/mL). The plate was sealed and incubated for 2 h at RT. After plate coating, the plate was washed 3x with

50 µL of washing buffer. For later LuC calculations, the input measurement of crude cell lysates is required. Therefore, 5 µL of the cell lysate was added to a white small volume 384 well plate. After addition of 5 µL of Furimazine solution, (diluted 1:100 in PBS) the luminescence and fluorescence was measured using a PHERAstar (BMG Labtech) microplate reader. For the co-precipitation assay 20 µL of fresh lysates were added to the nanobody coated NeutrAvidin plate. The plate was sealed and incubated for 1 h at room temperature. After incubation, the plate was washed 3x with 50 µL of lysis buffer. Immediately after adding 25 µL of Furimazine solution (1:100 diluted in PBS) to the lysates, the Luminescence and fluorescence measurement took place.
For the LuC data analysis, the LuC ratios from the co-precipitation assay are calculated according to Trepte *et al,* 2018[115]. Therefore, the luminescence-precipitation ratio (PIR) of the Tandem (NLuc-mCitrine) control was calculated as follows:

$$PIR_{(Tan)} = \frac{NLuc_{(prec)}}{4xNLuc_{(input)}}$$

With $NLuc_{(prec)}$ being the total luminescence measured after the co-precipitation and $NLuc_{(input)}$ being the total luminescence measured in cell extracts directly after lysis.
Subsequently, the LuC ratios of all interactions of interest are calculated and corrected for the PIR_{Tan} ratio as follows:

$$LuC\ ratio = \frac{NLuc_{(prec)}\ /\ 4x\ NLuc_{(input)}}{PIR_{(Tan)}}$$

2.2.3.13 MSD assay

For the MSD assay detecting soluble levels of HTT proteins, the MULTI-ARRAY® 384-well plate was coated with the capture antibody (2B7 binding to the N-terminus of HTT). For that purpose, 10 µL of the diluted antibody, diluted in carbonate-bicarbonate buffer to 5 µg/mL, was added to the MSD assay plate. The plate is sealed and centrifuged at 1000xg for 10 sec in order to ensure that the antibody dilution covers the bottom of each well. For incubation, the plate was shaken on a plate shaker at 350 rpm for 5 min before being stored at 4°C for further overnight incubation. To prepare for the blocking step, the coating antibody solution was removed by spilling off the plate. The plate was washed 2x with 35 µL of MSD washing buffer before 35 µL of MSD blocking solution was added. The blocking buffer was incubated for 60 min at 350 rpm at room

temperature. After incubation, the plate was washed 2x with 35 µL of MSD washing buffer. Samples were pre-diluted 1:10 in lysis buffer and 10 µL of this mix was added to the assay plate. The plate was incubated for 60 min at 350 rpm at room temperature before 2x washing with 35 µL of MSD washing buffer. For detection of the immobilized HTT proteins, 10 µL of the detection AB (MW1 conjugated with SULPHO-TAG), diluted in carbonate-bicarbonate buffer to a concentration of 1 mg/mL, was added to the MSD assay plate. After 60 min of incubation on a plate shaker at 350 rpm and RT, the plate was washed 2x with 35 µL of MSD washing buffer. 35 µL/well of MSD read buffer GOLD was added to the plate and the electrochemiluminescence was measured by the MESO SECTOR S600 plate reader.

2.2.3.14 Statistical analysis

For testing the normality of the distribution of the data, an ordinary one-way analysis of variance (ANOVA)-test was performed. The analysis of statistical significance was determined by using Bonferoni post hoc analysis. The defined levels of significance are:
not significant (ns) ≥0.05,
significant (*) 0.01-0.05
very significant (**) 0.001-0.01
highly significant (***) <0.001
All statistical analysis has been done by using GraphPad Prism 9 software.

3 Results

3.1 Screening for and modulation of autophagy related PPIs

There are many recent publications reporting autophagy related PPIs[120], which are summarized and accessible in different PPI databases[121]. Such databases like Biological General Repository for Interaction Datasets (BioGRID), Molecular INTeraction database (MINT), Database of Interacting Proteins (DIP), Human Protein Reference Database (HPRD) and IntAct molecular interaction database (IntAct) list thousands of different PPIs from various organisms whereas the majority of interactions account for proteins from *Saccharomyces cerevisiae* and *Homo sapiens*[121]. In order to provide an overview of all listed PPIs, the Human Integrated Protein-Protein Interaction Reference (HIPPIE) database integrates the *Homo sapiens* interactions listed in 10 source databases[122]. Another feature of the HIPPIE database is that the interactions are scored by the number of publications the interaction has been described in, as well as the experimental system the interaction was determined by. However, no quantitative information about the affinity of the interacting proteins is given. So far, different experimental techniques for the identification of PPIs have been developed. Besides the well applied yeast two-hybrid system (Y2H), co-IP based, fluorescence resonance energy transfer (FRET) based and proximity ligation assays (PLA) contributed to qualitative detection of PPIs[123]. In order to describe PPIs in a quantitative manner, BRET assays have been proven to be a suitable tool[124]. Based on a similar assay principle like FRET assays, BRET assays utilize a Nano luciferase (NLuc) as donor. NLuc relies on the substrate (Coelenterazine or Furimazine) to emit high intensity luminescence. This property enables the NLuc-fused proteins to be expressed at endogenous-like levels[125]. By using BRET assays it is possible to determine the strength of interactions in living cells by calculation of $BRET_{50}$ values from donor saturation experiments[126-127].

As this project aims for the modulation of autophagic pathways by stimulation or inhibition of PPIs, BRET assays are an eligible tool. In order to validate the BRET assay, the well described interaction between the Bcl-2-Antagonist of Cell Death (BAD) and Bcl-2-like protein 1 (BCL-2L1) was tested. BAD is a BH3 domain containing protein involved in the control of the cell cycle and the regulation of metabolism. BCL-2 family proteins are pro survival regulators and are able to bind to the BH3 domain of various proteins. A fixed amount of Nano-Luciferase (NLuc)-tagged BAD as BRET donor was

co-transfected with increasing amounts of mCitrine-tagged BCL-2L1 as BRET acceptor. Co-transfection with mCitrine only served as a negative control.

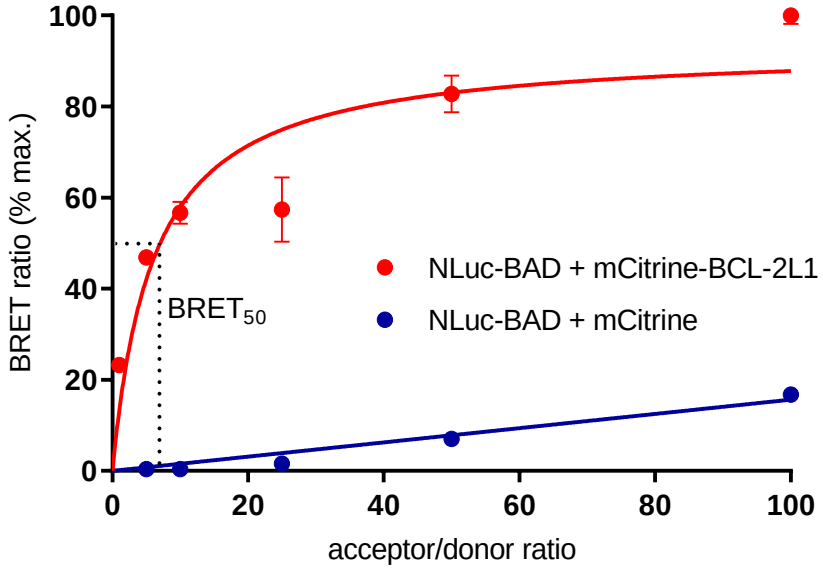

Figure 13 I BAD and BCL-2L1 show specific interaction in BRET donor saturation assay.
Specific interaction between BAD and BCL-2L1 with a $BRET_{50}$ of 6.1. Constant amounts of NLuc-BAD and increasing amounts of mCitrine-BCL-2L1 were transiently expressed in HEK293 cells. Data are presented in percentage of the maximum BRET ratio obtained for the BAD-BCL-2L1 interaction. mCitrine alone is expected not to interact with BAD and was included as negative control. Data are means ± SD of quadruplicate samples.

NLuc-BAD and mCitrine-BCL-2L1 showed an increase of the BRET ratio upon increase of the acceptor/donor (A/D) ratio (**Figure 13**). The hyperbolic curve indicates that the interaction is specific. The calculated $BRET_{50}$ value of 6.1 implies that on a DNA level an excess of six times of the acceptor is needed to saturate 50% of the donor. The negative control condition NLuc-BAD and mCitrine showed just a slight increase in BRET signal with a linear relationship between BRET ratio and A/D ratio, indicating an unspecific signal. Thus, the results confirm that the BRET assay is a valid tool for studying PPIs in living cells.

Since this work aims for the modulation of autophagy related PPIs, we analyzed whether the BRET assay could capture these typed of modulations positively or negatively affecting the interaction between proteins. Therefore, we assessed the interaction between the proteins Beclin1 (BECN1) and B-cell lymphoma 2 (BCL-2), as there are two well characterized mutations which have been reported to prevent the direct interaction between BECN1 and BCL-2[128].

BECN1 is an essential initiator of autophagy as well as a key determining factor as to whether cells undergo autophagy or apoptosis. BECN1 interacts with BCL-2 family members via its BH3 domain, leading to the inhibition of apoptosis and autophagy[129]. Recently, the point mutation F123A within the BH3 domain as well as deletion of the BH3 domain (d112-123), have been shown to disrupt the interaction with BCL-2[128].

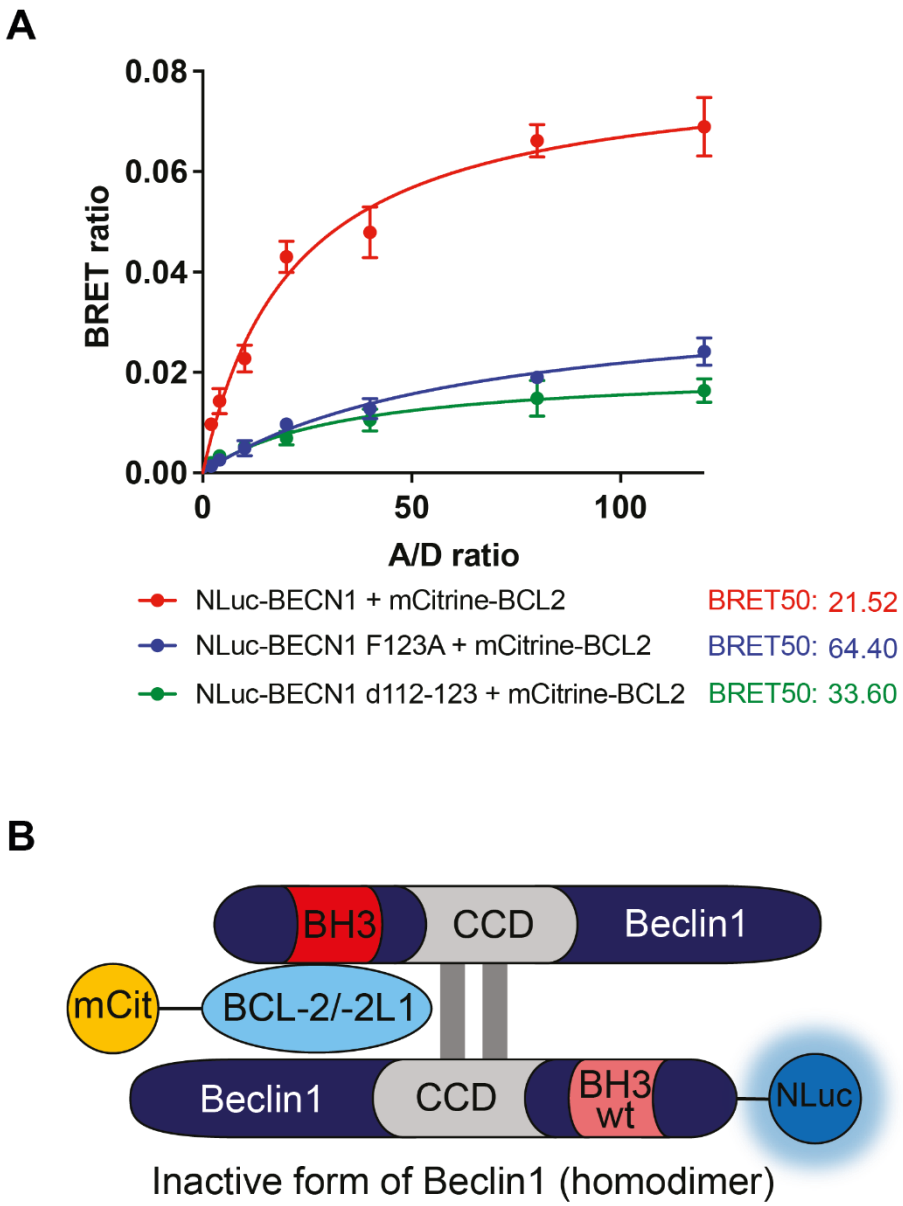

Figure 14 I BECN1 mutations show a reduced BRET ratio for interaction with BCL-2.
(A) Specific interaction of BECN1-BCL-2 PPI was confirmed by BRET assay with a $BRET_{50}$ of 31.1. BECN1 mutations (previously reported to disrupt interaction with BCL-2) modulate binding between BECN1 and BCL-2 leading to higher $BRET_{50}$ values around 85. Fixed amounts of NLuc-BECN1wt/mt and increasing amounts of mCitrine-BCL-2L1 were transiently expressed in HEK293 cells. Data are presented in percentage of the maximum BRET ratio obtained for the BECN1-BCL-2 interaction. Data are means ± SD of triplicate samples. **(B)** In its inactive state, Becn1 forms homodimers via its CCD domain explaining the remaining interaction of mutant BECN1 and BCL2.

In order to test the specificity of the BRET assay to detect the influence of mutations, we performed donor saturation assays between wildtype, mutant BECN1 and BCL-2. The interaction between NLuc-BECN1 as donor and mCitrine-BCL-2L1 as acceptor showed a concentration dependent increase of the BRET (**Figure 14A**). The hyperbolic curve indicates that the interaction is specific. The point mutation F123A as well as the deletion mutation of amino acids 112-123 of the Beclin1 BH3 domain showed a strong decrease of the maximum BRET signal reached. Also, the $BRET_{50}$ value dropped from 31.5 to 64.4, indicating a reduced ability of mutated BECN1 (mt-BECN1) to interact with BCL-2. The hyperbolic relationship for the mutations indicates that there is some remaining interaction between the BECN1 and BCL-2 proteins. Due to the fact, that BECN1 forms homodimers with its CCD domain, it is possible that heterotrimers between endogenous BECN1 bound to BCL-2 and the mt-BECN1 form. The wt-BECN1 of these heterotrimers can still interact with mCitrine-BCL-2 proteins which results in the remaining BRET signal (**Figure 14B**).

Another PPI to demonstrate the sensitivity of BRET assay to detect a full inhibition of a PPI mediated by point mutations is the interaction between STX1A and STXBP. Both interactions are described to be involved in exocytosis as well as membrane fusion[130].

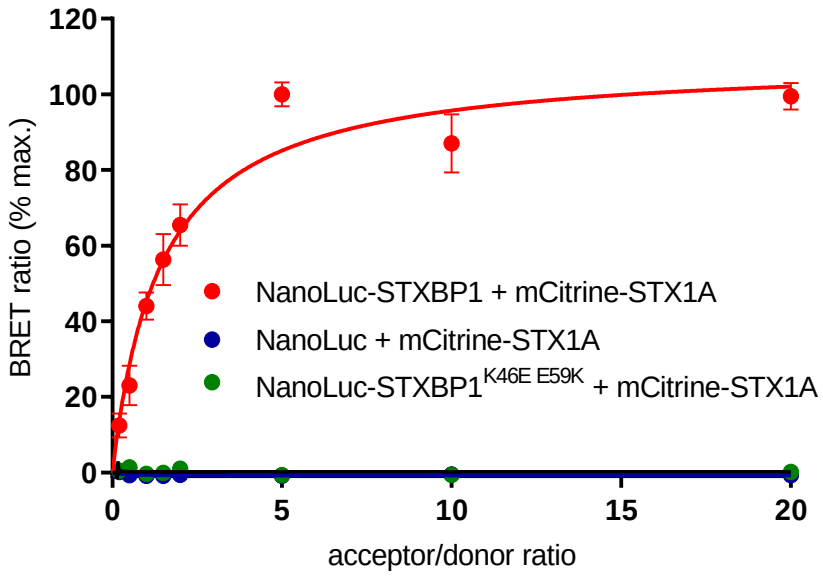

Figure 15 I STXBP mutation completely inhibit binding to STX1A.
Specific interaction of STX1A-STXBP was confirmed by BRET assay with a BRET50 of 1.4. STXBP mutation (previously reported to disrupt interaction with STX1A) completely prevent STXBP from binding to STX1A. Fixed amounts of NLuc-STXPBwt/mt and increasing amounts of mCitrine-STX1A were transiently expressed in HEK293 cells. Data are presented in percentage of the maximum BRET ratio obtained for the STX1A-STXBP1 interaction. Data are means ± SD of triplicate samples.

Using ICC and Yeast two-hybrid (Y2H) assays, Han *et al.* showed that a double point mutation of STXBP loses its ability to bind to STX1A[130]. In order to validate the BRET assay for detection of point mutation mediated prevention of a PPI, we have performed donor saturation assays between wildtype and mutant STXBP with STX1A. The hyperbolic curve for STXBP and STX1A indicates a specific interaction. The low $BRET_{50}$ value of 1.4 indicates a high affinity of the interaction partners to each other. The point mutation of STXBP leads to a complete loss of interaction with STX1A. This data confirms the findings of Trepte *et al.* who demonstrated the impact of point mutations on detected PPI via BRET assays[115]. Taken together, this data demonstrates the sensitivity of the BRET assay to detect changes within the interaction between two proteins caused by point or deletion mutations (**Figure 15**).

Another aim of this project is the modulation of autophagic pathways by small molecule compounds. Therefore, the BRET assay was further validated to show feasibility to detect pharmacological modulation of PPIs. As case study, the induction of the interaction between FKBP and FRB and the dissociation of the BAD-BCL-2L1 interaction have been chosen. The 12-kDA FK506 binding protein (FKBP) and FKBP-rapamycin binding domain (FRB), the 100-amino acid domain of the mammalian target of Rapamycin (mTOR), do not interact under physiological conditions. However, it has been shown that the mTOR inhibitor Rapamycin can facilitate the interaction between FKBP and FRB[131] (**Figure 16A**), making this interaction a good tool for testing compound mediated induction of PPIs. In contrast, the BH3 mimetic compounds Navitoclax is an anti-cancer drug binding to hydrophobic grooves of BCL-2 family members, preventing the binding of BH3 domain containing interaction partners in a competitive manner[129] (**Figure 16B**). The interaction between BAD and BCL-2L1 can be disrupted by BH3 mimetics. Chiang *et al.* have shown in an AlphaLISA assay that treatment of the BECN1-BCL-2 interaction with Navitoclax inhibits the interaction in a concentration dependent manner[132]. As multiple proteins bind with its BH3 domain to BCL-2L1 and BCL-2, the BH3 mimetic Navitoclax is expected to block the interaction between the BH3 only protein BAD and BCL-2L1. For examining the induction together with the inhibition of PPIs, interactions between NLuc-FKBP and mCitrine-FRB along with NLuc-BAD and mCitrine-BCL-2L1 were challenged using Rapamycin or Navitoclax, respectively.

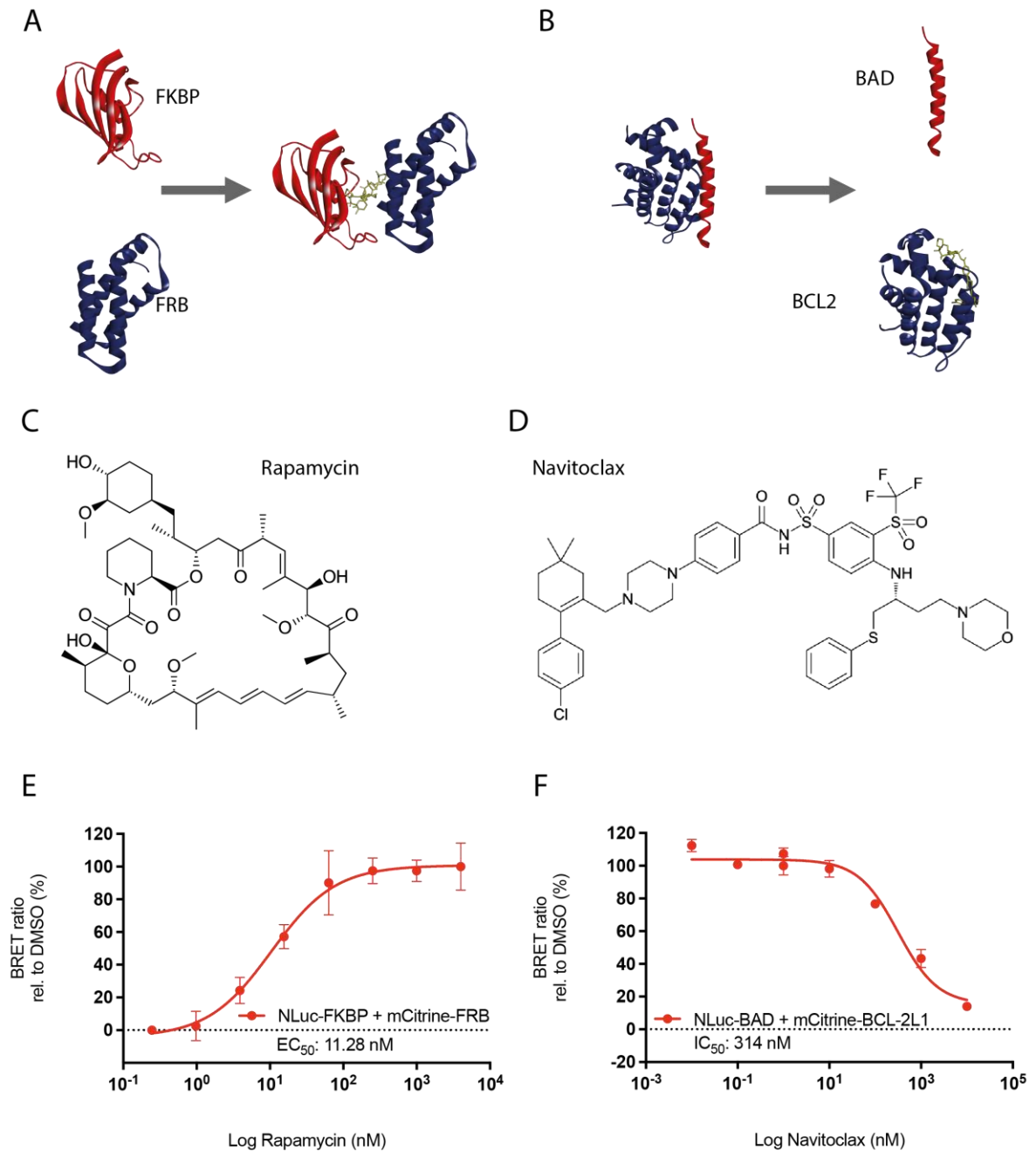

Figure 16 I Pharmacological modulation of reference PPIs.
(A) Rapamycin inducing FKBP and FRB interaction (PDB 1NSG[133]). **(B)** BAD-BCL-2 interaction dissociated by competitive binding of Navitoclax to BCL-2 (PDB 2BZW, 4LVT[133]). **(C)** Structure of Rapamycin and **(D)** Navitoclax. **(E)** 2 h Rapamycin treatment induces the PPI between NLuc-FKBP and mCitrine-FRB in a concentration dependent manner with an EC_{50} of 11.28 nM. **(F)** 16 h Navitoclax treatment induces a dissociation of NLuc-BAD and mCitrine-BCL-2L1 in a concentration dependent manner with an IC_{50} of 314 nM. Data are presented in percentage of the BRET ratio recorded for the DMSO control. Data are means ± SD of quadruplicate samples.

The BRET assay showed that a 2 h treatment with Rapamycin induces the interaction between FKBP and FRB in a concentration-dependent manner (**Figure 16E**), as indicated by an increase in BRET signal. Upon 16 h of Navitoclax treatment, the BAD-

BCL-2L1 interaction shows a clear decrease in BRET indicating the dissociation of BAD and BCL-2L1 (**Figure 16F**).

In summary, the data indicates that BRET assays are a suitable tool for the detection of small molecule induced modulation of PPIs. In order to verify the FKBP-FRB interaction in an orthogonal assay, a luminescence-based precipitation assay (LuTHy) was performed. The LuTHy assay is a combination of the classical BRET assay in living cells and a luminescence based co-precipitation assay (LuC) of cell lysates obtained from the BRET assay cells[115]. For that purpose, the mCitrine construct is immobilized by using NeutrAvidin coated plates and biotinylated nanobodies against the mCitrine tag. In case of an interaction of the target proteins, the NLuc tagged protein is co-precipitated and can be detected by the luminescence signal.

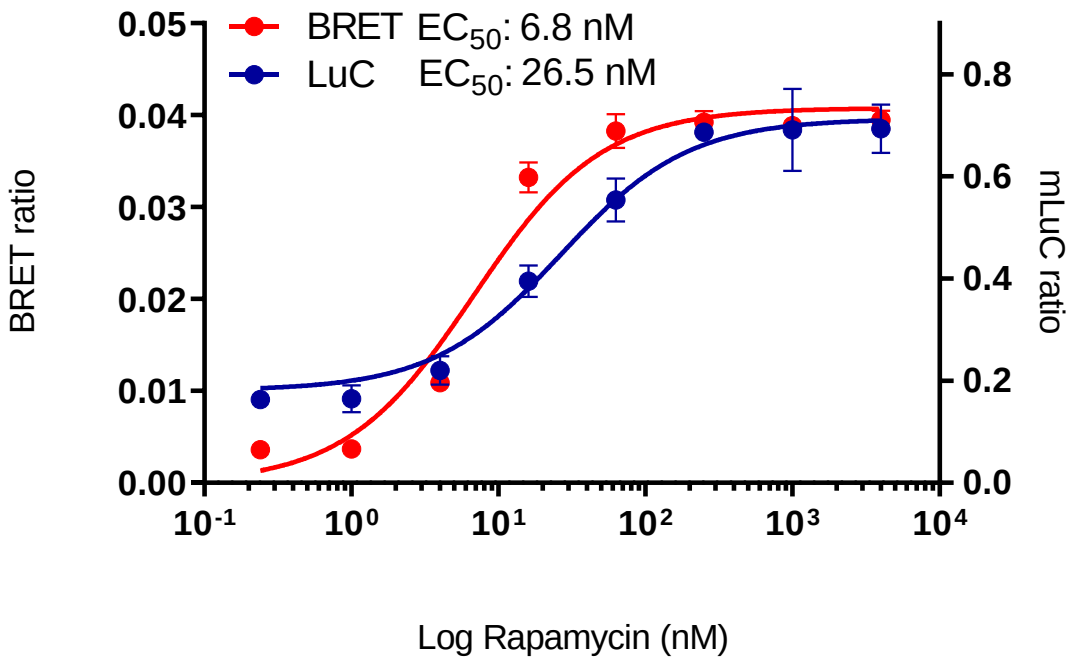

Figure 17 I BRET assay data correlates with data obtained by LuC assay.
2 h Rapamycin treatment induces the PPI between FKBP and FRP in BRET as well as Co-IP assay in a concentration dependent manner with EC_{50} values of 7 and 27 respectively. 0.5 ng of NLuc-FKBP and 5 ng of mCitrine-FRB were transiently co-expressed in HEK293 cells for 46 h before 2 h compound treatment. After BRET assay, the cells were lysed and tested in co-IP assay. Data are presented in BRET ratio as well as LuC ratio. Data are means ± SD of quadruplicate samples.

The LuC assay confirmed the Rapamycin induced interaction between FKBP and FRB measured previously using a single BRET assay (**Figure 17**). For both techniques, a concentration-dependent increase in PPI was observed upon Rapamycin treatment. The calculated EC_{50} values are in the same low nanomolar range as observed in the

previous assay (**Figure 16E**). In comparison to the EC_{50} obtained from BRET assay, The EC50 observed from LuC assay is slightly higher. This might be due to the fact that some of the interactions are lost during the lysis process. Taken together, the BRET assay was validated as a suitable and sensitive tool for the quantitative analysis to detect the effect of point mutations as well as pharmacological intervention.

Protein-Protein interactions are involved in a wide range of biological processes, such as signal transduction, metabolism and the cell cycle[134]. Analyzing PPI networks may help to identify new drug targets and can give insights into the mode of action of compounds. In recent years many PPIs have been described by different experimental methods such as yeast two-hybrid (Y2H), mass spectrometry and Luminescence based assays[123]. However, many methods suffer from limitations, as they do not provide quantitative information about the affinity of two proteins to each other. By using the BRET assay, we aim to analyze autophagy related PPIs in a quantitative manner in order to get new insights into the dynamic processes of autophagy.

For the quantitative analysis of autophagy-related PPIs, a number of relevant PPIs within the autophagy pathway was selected. The chosen PPIs are involved in the different stages of autophagy such as initiation, cargo sequestration or the autophagosome lysosome fusion event. The majority of analyzed PPIs originate from a collection of interactions around BECN1 and STX17 which are involved in autophagy induction[129] and autophagosome lysosome fusion event respectively[135]. Due to the fact that autophagy induction is studied as a potential therapy in neurodegenerative diseases[29], PPIs around the autophagy initiator BECN1 have been selected. BECN1 was described as a key player in autophagy induction[129] and analysis of BECN1 related PPIs may reveal new drug targets. In the past, the initiation of autophagy attracted most attention in research, the later stages of autophagy were much less studied[136]. To get more insights into the autophagosome lysosome fusion and interactions of the Q_a-SNARE protein STX17 (which is described to be directly involved in the autophagosome lysosome fusion event[135]), PPI analysis occurred. The majority (around 80%) of analyzed PPIs were listed in the HIPPIE database. Apart from these PPIs, further interactions were chosen, based on recent publications.

In order to analyze which of the selected key interactions of the autophagic pathway can be confirmed in living cells, donor saturation assays were performed. Table 30 summarizes all tested PPIs and lists as measure of confidence, the HIPPIE score, as well as number of publications the PPIs were described in (**Table 30**).

Table 30 I Protein-protein interactions analyzed in BRET assay

PPI	HIPPIE score	# of publications	$BRET_{50}$	Interaction detected	Process involved
BAD-BCL-2L1	0.99	30	4.9	yes	
BECN1-VSP34	0.97	30	-	no	
IGBP1-PPP2CA	0.97	16	1.5	yes	
BECN1-BCL-2	0.90	34	61.4	yes	
BECN1-BCL-2L1	0.90	31	17.9	yes	
BECN1-ATG14	0.90	19	16.7	yes	initiation
BECN1-Ambra1	0.90	9	221.8	yes	
DYNLL1-Ambra1	0.86	2	133.4	yes	
Ambra1-BCL-2	0.79	1	-	no	
ULK1-Ambra1	0.75	2	103.3	yes	
BECN1-DACT1	0.63	1	32.7	yes	
ULK1-IRGM	0.63	1	541.2	yes	
BECN1-IRGM	0.63	1	401.1	yes	
ULK1-ATG14	-	-	-	no	
FKBP1A-FRB	-	-	11.7	yes	
ATG12-TRIM50	-	-	5.5	yes	
ATG16L1-ATG5	0.96	11	5.9	yes	
ATG16L1-ATG16L1	0.71	4	19.7	yes	nucleation
ATG16-IRGM	0.63	1	-	no	
SQSTM1-SQSTM1	0.97	21	207.7	yes	cargo
MAP1LC3B-SQSTM1	0.90	15	85.0	yes	recruitment
SNAP29-STX7	0.89	5	34.3	yes	
SNAP29-STX17	0.88	2	81.8	yes	
STX17-VPS16	0.73	1	142.1	yes	
STX17-VPS33A	0.73	1	-	no	
STX17-VPS39	0.72	1	-	no	
STX17-VAMP8	0.63	1	60.9	yes	fusion
SNAP29-VAMP8	0.63	1	47.6	yes	
MAP1LC3A-IRGM	-	-	-	no	
MAP1LC3A-STX17	-	-	84.8	yes	
MAP1LC3B-STX17	-	-	272.8	yes	
STX17-IRGM	-	-	-	no	

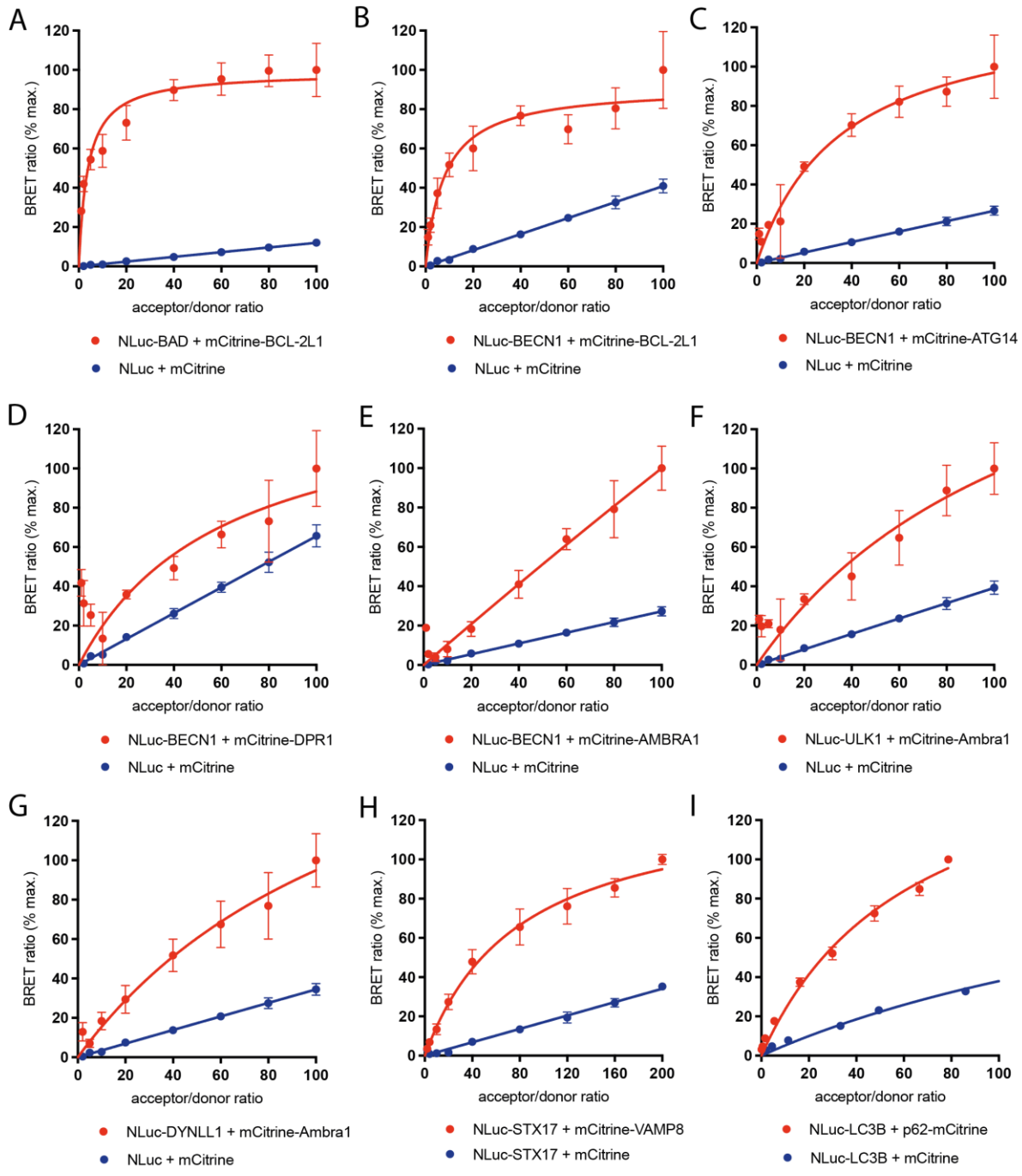

Figure 18 I Selected donor saturation assays of confirmed autophagy related PPIs.
HEK293 cells were transiently transfected for 48 h with BRET constructs for **(A)** NLuc-BAD and mCitrine-BCL-2L1 and donor tagged proteins against mCitrine conditions were included as positive and negative controls. The shown interactions only represent a selection of confirmed interactions and does not depict all analyzed interactions. Data are presented in percentage of the maximum BRET ratio for the respective interaction. Data are means ± SD of triplicate samples.

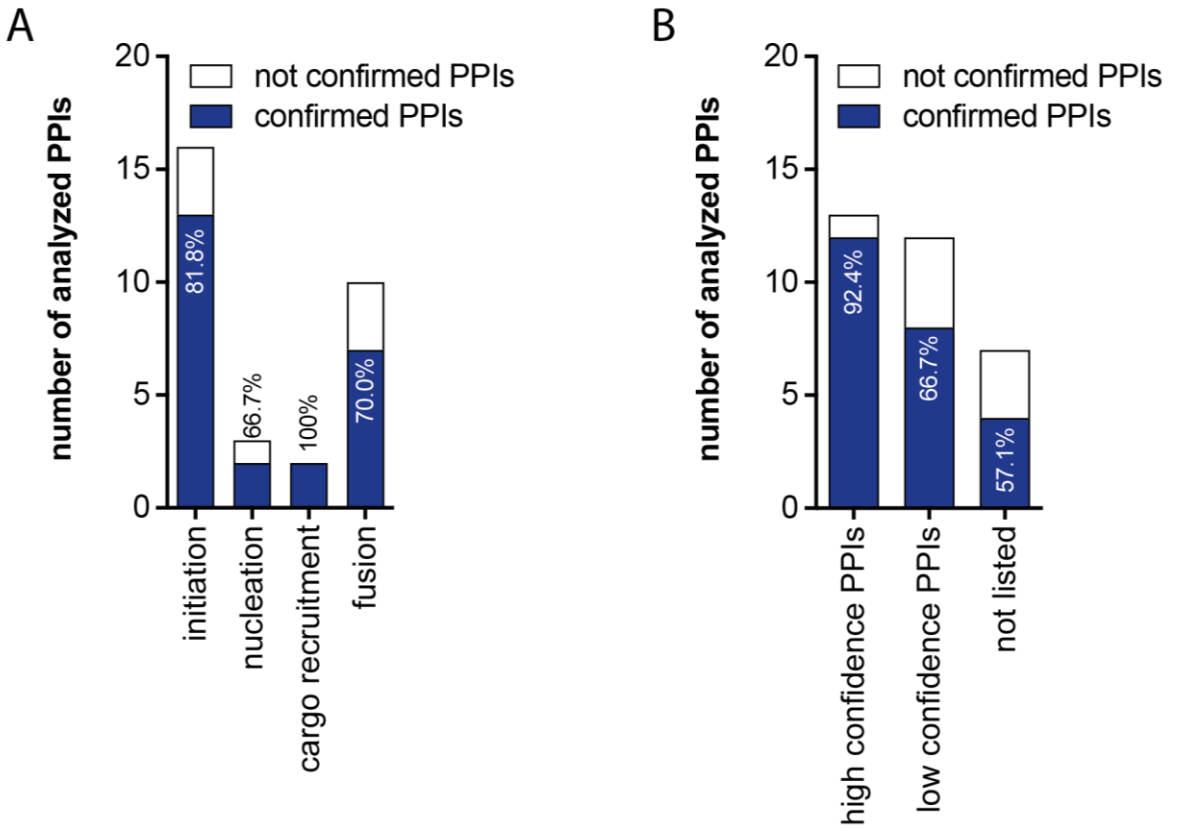

Figure 19 I Binning of protein-protein interactions.
Number of analyzed protein-protein interactions annotated according to their function in the autophagic pathway (**A**) and according to their HIPPIE score (**B**). High confidence PPIs (HIPPI score >0.80); low confidence PPIs (HIPPIE score <0.80). The indicated numbers represent the proportion of confirmed PPIs within each group.

Specific interaction was found for the majority (24 out of 32) of the analyzed PPIs at different stages of the autophagy pathway, summarized in Table 30. The BRET donor saturation assay confirmed many published PPIs, whilst some interactions listed in the HIPPIE database could not (**Figure 18**). The confirmation rate among the PPIs of the different stages of the autophagy pathway is more than 60% relatively stable (**Figure 19A**). It becomes apparent that the PPIs with high HIPPI score (>0.80) are more likely (92.4%) (12 out of 13) to be found in BRET assay, whereas interactions with low HIPPIE score (<0.80) and not listed PPIs show only 66.7% (8 out of 12) and 57.1% (4 out of 7) confirmation rate (**Figure 19B**). In some cases, new PPIs were detected which were so far not listed in the HIPPIE database. This might be due to the fact that the HIPPIE database is incomplete and was not updated since February 2019. From these two interactions, the LC3A and LC3B interaction with STX17 has already been shown by Kumar *et al.* in 2018 using co-IP assay[135]. In contrast, the interaction between TRIM50 and ATG12 has to date not been reported at all.

The results of this focused PPI screen have been graphically summarized in a network. The network shows two main clusters representing the interactions of the initiation step as well as of the autophagosome lysosome fusion event. The interaction of the nucleation as well as cargo recruitment are due to the low number of analyzed interactions represented as single interactions (**Figure 20**).

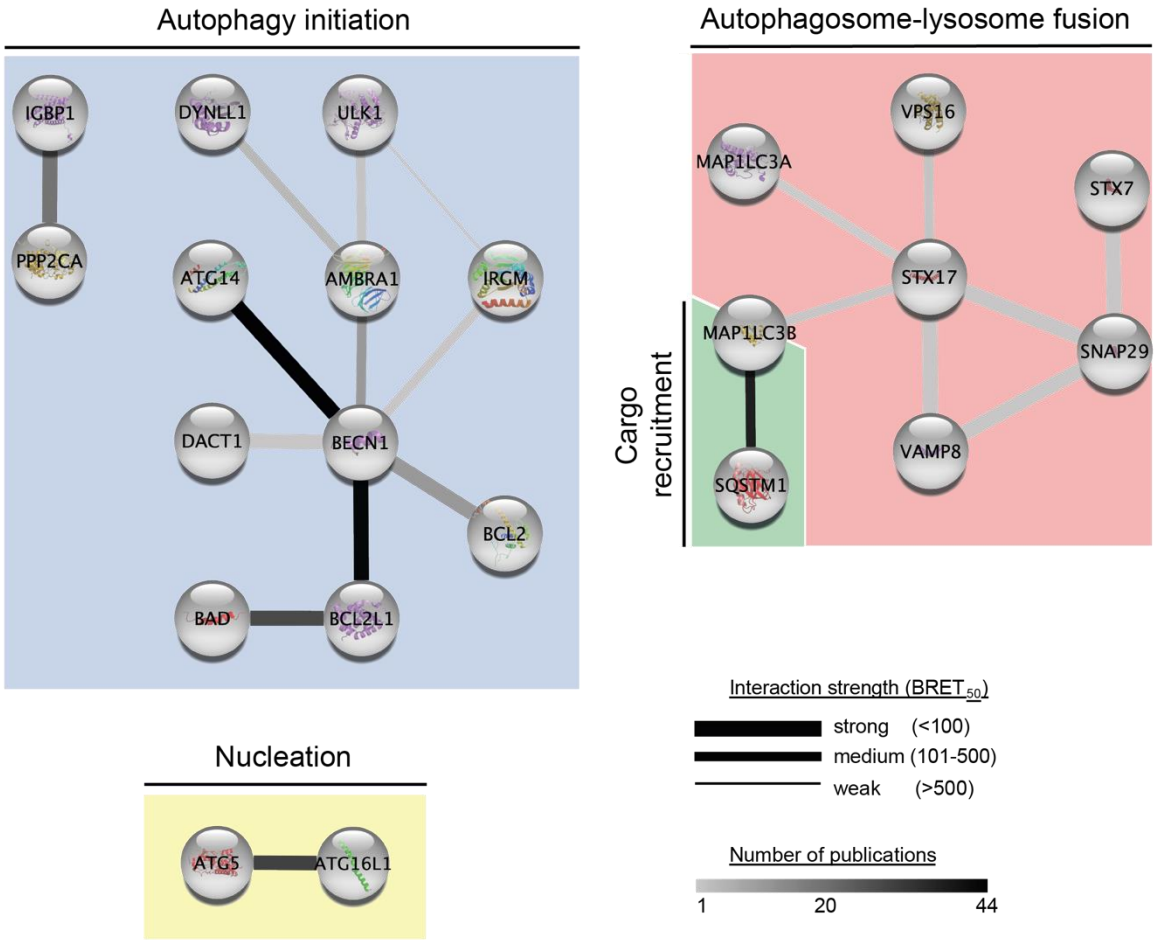

Figure 20 I Interactome network of PPIs detected by BRET assay.
Summary of all detected PPIs with BRET assay. Edge width represents the affinity of the tested interaction partners based on the acquired $BRET_{50}$ value (thin = weak to bolt = strong interaction). The color gradient of the edges indicates the classification of the interaction based on the number of publications the interaction is found in (light = 1 to dark = 44).

Taken together, the quantitative data of the focused screen reveals that high confidence PPIs are more likely to be found in BRET assays compared to low confidence interactions. The generated network may act as starting point for further investigation and modulation of certain PPIs.

Based on the focused PPI screen, the STX17-VAMP8 PPI attracted our interest, as this interaction could potentially be used as a new readout for measuring autophagic flux. STX17 is a Q_a-SNARE protein located in the autophagosomal membrane and is

directly involved in the autophagosome lysosome fusion event by interacting with the R-SNARE protein VAMP8[135]. For the autophagosome-lysosome fusion event, the interaction between STX17 and VAMP8 is crucial (**Figure 21A**). Thus, we hypothesized that quantifying this interaction would allow discrimination between autophagy stimulation and inhibition, as the fusion event between the autophagosome and lysosome is measured. Once autophagy is induced, an increase of the STX17-VAMP8 interaction is expected, whereas a reduced BRET signal is anticipated when autophagy is inhibited.

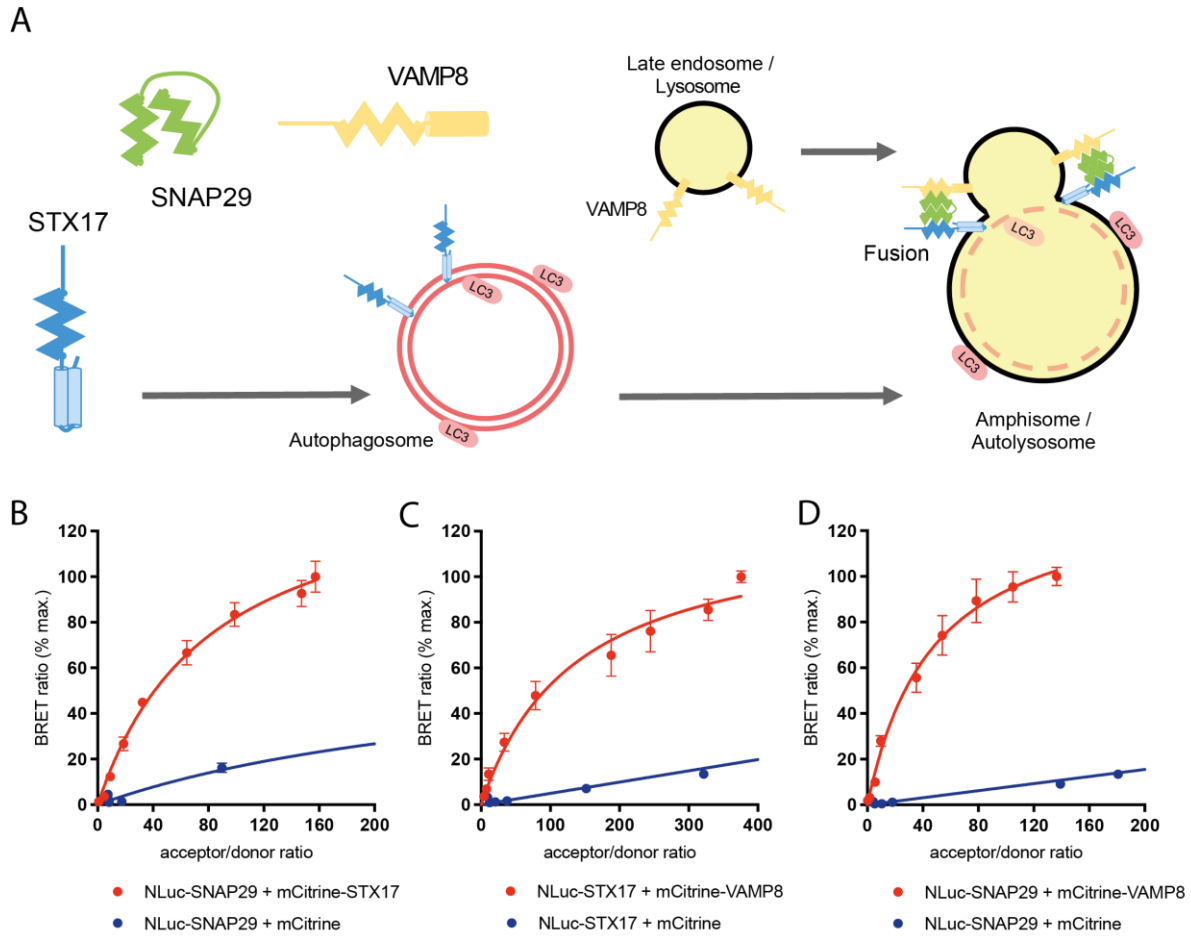

Figure 21 I The process of autophagosome-lysosome fusion.
(A) The outer autophagosomal membrane fuses with the late endosomal/lysosomal membrane. This process is mediated by the autophagic SNARE complex comprising STX17, SNAP29, and VAMP8 (figure modified from Itakra *et al.*, 2012, Cell)[138]. **(B-D)** Specific interaction of SNAP29-STX17, STX17-VAMP8 and SNAP29-VAMP8 interactions confirmed by BRET assay. Constant amounts of NLuc-tagged and increasing amounts of mCitrine-tagged proteins were transiently expressed in HEK293 cells for 48 h. The D/A ratio was normalized to the D/A ratio of mCitrine-NLuc construct. Data are presented in percentage of the maximum BRET ratio obtained for the respective interaction. Data are means ± SD of quadruplicate samples.

In order to confirm the fusion event related PPIs detected in the focused PPI screen, donor saturation assays for the interaction of STX17, VAMP8 and SNAP29 were performed. SNAP29 has been shown to facilitate the interaction between STX17 and VAMP8 by binding to both interaction partners[137]. A specific interaction between all three protein pairs could be shown (**Figure 21B-D**) as described by Dodson *et al.*[139]. For monitoring the fusion event between autophagosome and lysosome, the interaction between the autophagosomal STX17 and the lysosomal VAMP8 was selected. It is important that for the validation of the STX17-VAMP8 PPI as a marker for autophagic flux, its modulation can be detected. Using immuno-cytochemistry, Fu *et al.* have shown that the overexpression of BNIP3 interferes with the autophagosome lysosome fusion event. They demonstrated that the disruption of the STX17-VAMP8 PPI takes place by inhibition of the interaction between SNAP29 and VAMP8[137]. BNIP3 is a mitophagy receptor which shows expression and autophagy induction upon hypoxia[140]. In turn, Fu *et al.* also demonstrated that the overexpression of SNAP29 induces the interaction between STX17 and VAMP8[137]. Thus, we hypothesized that overexpression of BNIP3 inhibits and SNAP29 induces the interaction between STX17 and VAMP8. SNAP29 and BNIP3 overexpression have been performed in order to investigate the genetic modulation of the STX17-VAMP8 PPI. For this purpose, increasing amounts of HA-tagged SNAP29 or BNIP3 were co-expressed with NLuc-STX17 and mCitrine-VAMP8.

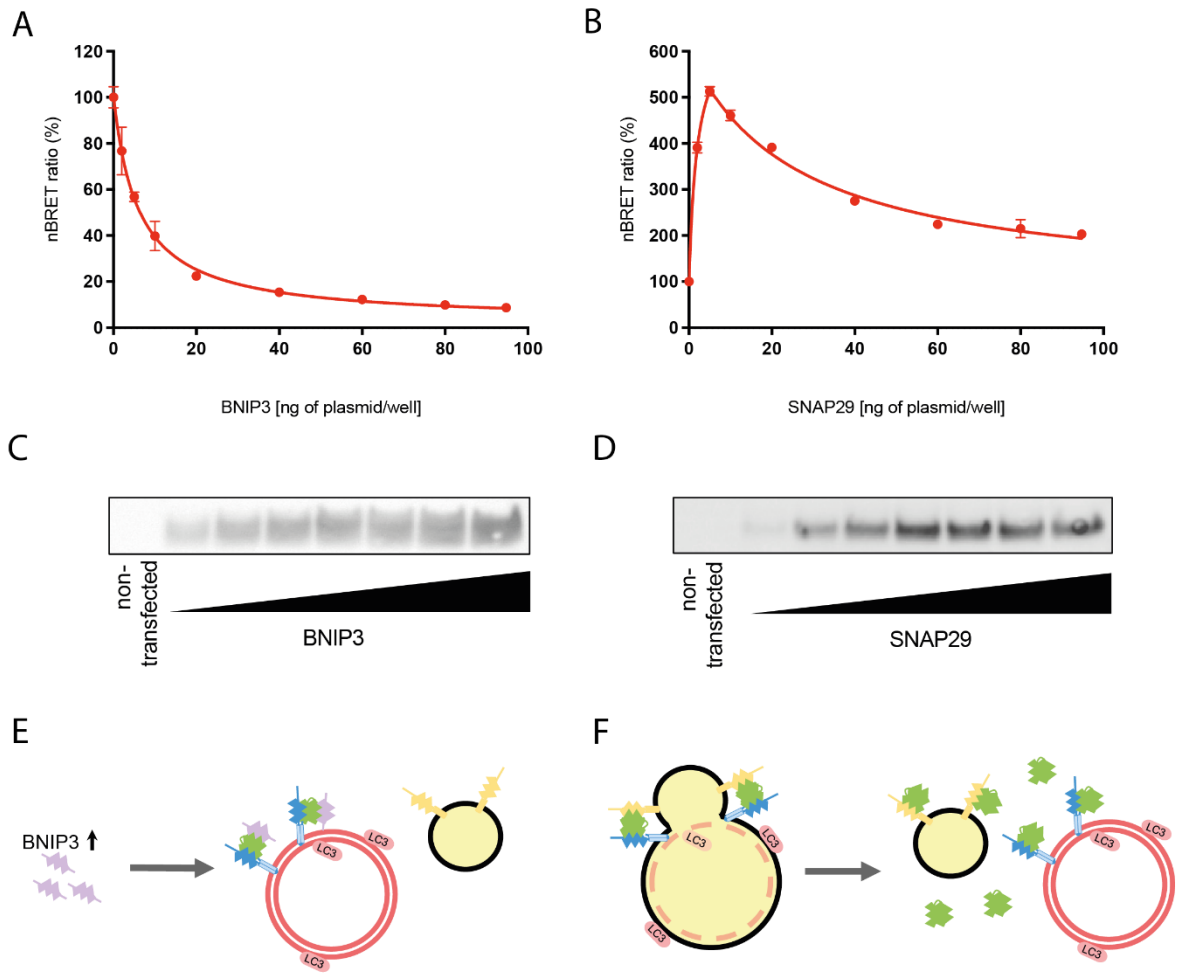

Figure 22 I Genetic modulation of STX17-VAMP8 interaction.
(A) Overexpression of BNIP3 leads to a reduction of the interaction between both interaction partners by preventing the interaction of SNAP29 with VAMP8. **(B)** Overexpression of SNAP29 leads to an increase of the interaction with hook effect at 5 ng of co-transfected SNAP29. **(C-D)** The overexpression of BNIP3 and SNAP29 is shown by Western Blot **(E)** BNIP3 plays an important role in autophagosome-lysosome fusion[137]. BNIP3 overexpression leads to a competitive inhibition of the SNAP29-VAMP8 PPI. **(F)** The autophagosome lysosome fusion is mediated by the interaction of SNAP29 with STX17 and VAMP8. Too strong overexpression of SNAP29 leads to a hook effect caused by the saturation of both interaction partners**.** Data are presented in percentage of the BRET ratio for the STX17-VAMP8 PPI without co-transfection of SNAP29 and BNIP3 proteins. Data are means ± SD of triplicate samples.

Our data reveals that an overexpression of SNAP29 or BNIP3 leads to a modulation of the interaction between STX17 and VAMP8. Binding of BNIP3 to SNAP29 leads to a decreased BRET signal, indicating a reduced interaction between STX17 and VAMP8 **(Figure 22B**). In turn, the overexpression of SNAP29 initially increases the interaction between STX17 and VAMP8. A hook effect is observed at 5 ng of DNA/well. Further increased overexpression of SNAP29 attenuates the interaction between STX17 and VAMP8 **(Figure 22A**). The hook effect is a common feature of three component systems[141], further confirming the ternary complex formation between

STX17, SNAP29 and VAMP8. The hook effect describes an auto-inhibition of ternary complex formation due to saturation of the interaction partners. Hook effects can be observed in treatments with bi-functional compounds as PROTACs[141] as well as in immuno-assays such as ELISA. Next to SNAP29, no further SNAP proteins have been described in the literature for their ability to induce PPI between STX17 and VAMP8 during the autophagosome lysosome fusion event. In order to determine the specificity of SNAP29 in inducing STX17-VAMP8 PPI, further SNAP proteins were analyzed in the BRET assay. The family of t-SNARES comprises next to SNAP29 three further members such as SNAP23, SNAP25 and SNAP47. Thus, we tested SNAP23 and SNAP25, two t-SNARE family proteins involved in the fusion of vesicles with the plasma membrane facilitating neurotransmitter release as well as vesicle transport and fusion142. Additionally, SNAP47, a protein also involved in autophagosome lysosome fusion143 was analyzed. SNAP47 has not been reported to interact with STX17 or VAMP8 but structurally exhibits the closest homology to SNAP29144.

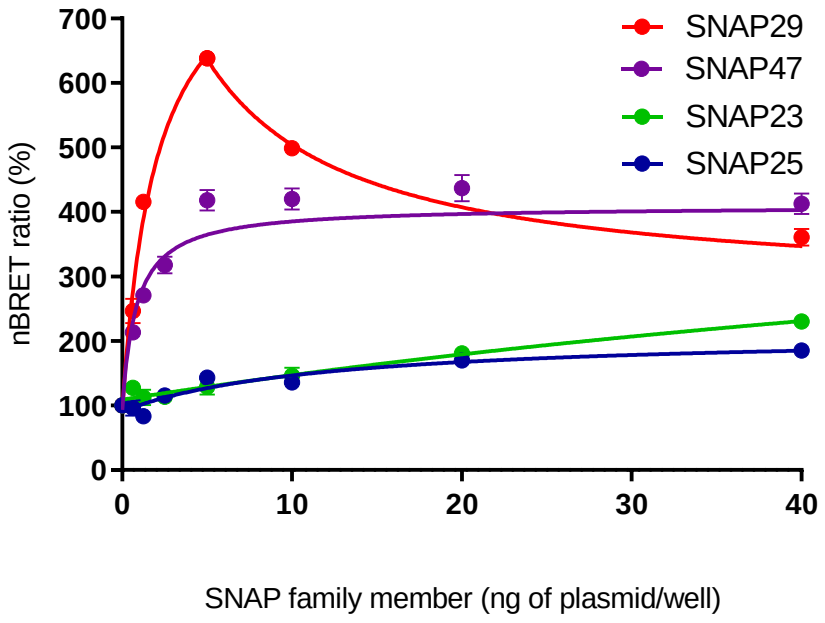

Figure 23 I SNAP29 and SNAP47 positively affect the interaction between STX17 and VAMP8. Other SNARE proteins such as SNAP23 and SNAP25 do not induce the interaction between STX17 and VAMP8 whereas SNAP29 leads to a strong increase of BRET signal with a hook effect at 5 ng of co-transfected SNAP29. SNAP47 also increases BRET signal. HEK293 cells were co-transfected with NLuc-STX17, mCitrine-VAMP8 and each of the indicated SNAP proteins for 48 h. Data are presented in percentage of the BRET ratio for the STX17-VAMP8 PPI without co transfection of SNAP proteins. Data are means ± SD of triplicate samples.

This data confirms the results from the previous study (**Figure 22**), where the overexpression of SNAP29 leads to an increased BRET signal. Co-expression of the

unrelated synaptosome proteins SNAP23 and SNAP25, showed a slight increase in BRET ratio, indicating that the modulation of the STX17-VAMP8 interaction is specifically mediated by SNAP29 (**Figure 23**). Interestingly, the overexpression of SNAP47 also induced the interaction between STX17 and VAMP8. As SNAP47 shows partial homology to SNAP29 and was reported to be involved in autophagic flux[143], it could indirectly induce the PPI between STX17 and VAMP8 by induction of other fusion related PPIs. Such PPIs could be between members of the HOPS complex and lysosomal membrane proteins such as STX7. This might also explain why a hook effect was not observed for SNAP47 overexpression.

Using the BRET assays, we have demonstrated that the interaction between two fusion related proteins can be modulated on a genetical basis. However, in order to validate this interaction as a potential sensor for autophagic flux, further research is needed.

Within our focused screen for autophagy related PPIs, we have confirmed the interaction between BECN1 and BCL-2 as well as BCL-2L1 with BRET50 values of 61.4 and 17.9, respectively. Liu *et al.* claim that the interaction between BECN1 and BCL-2 plays a crucial role in regulating autophagy and apoptosis[145]. Pattingre *et al.* reported that in its inactive state, BECN1 forms homodimers bridged by BCL-2/-XL and cannot promote autophagy[146]. According to Malik *et al.*, disruption of the BECN1-BCL-2 PPI by BH3 mimetic compounds has an autophagy inducing effect[147]. In order to investigate the pharmacological modulation of the interactions between BECN1 and BCL-2 as well as BCL-2L1, BRET assays were performed.

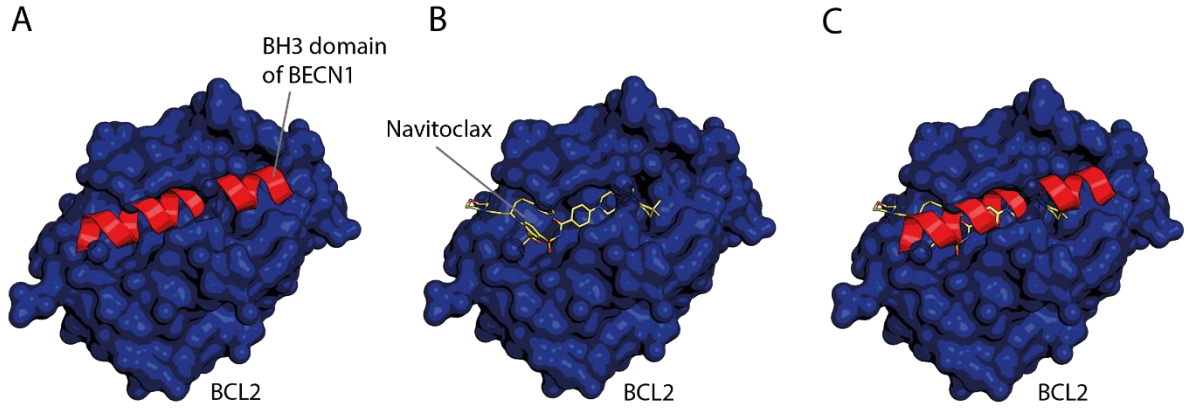

Figure 24 I Binding of the BH3 domain of BECN1 and Navitoclax to BCL2
(A) Binding of the BH3 domain of BECN1(red) to BCL2 (blue) (PDB 5VAY[133]). **(B)** Navitoclax (yellow) occupying the same binding site of BCL2 (PDB 4LVT[133]). **(C)** Superimposed structures of Navitoclax and the BH3 domain of BECN1 within the binding pocket of BCL2 (PDB 5VAY[133], PDB 4LVT[133]).

For that purpose, the effect of BH3 mimetic compounds Navitoclax (**Figure 24**) and Venetoclax were analyzed in both interactions. Navitoclax and Venetoclax are anti-cancer drugs binding to hydrophobic grooves of BCL-2 family members, preventing the binding of BH3 domain containing interaction partners in a competitive manner[129].

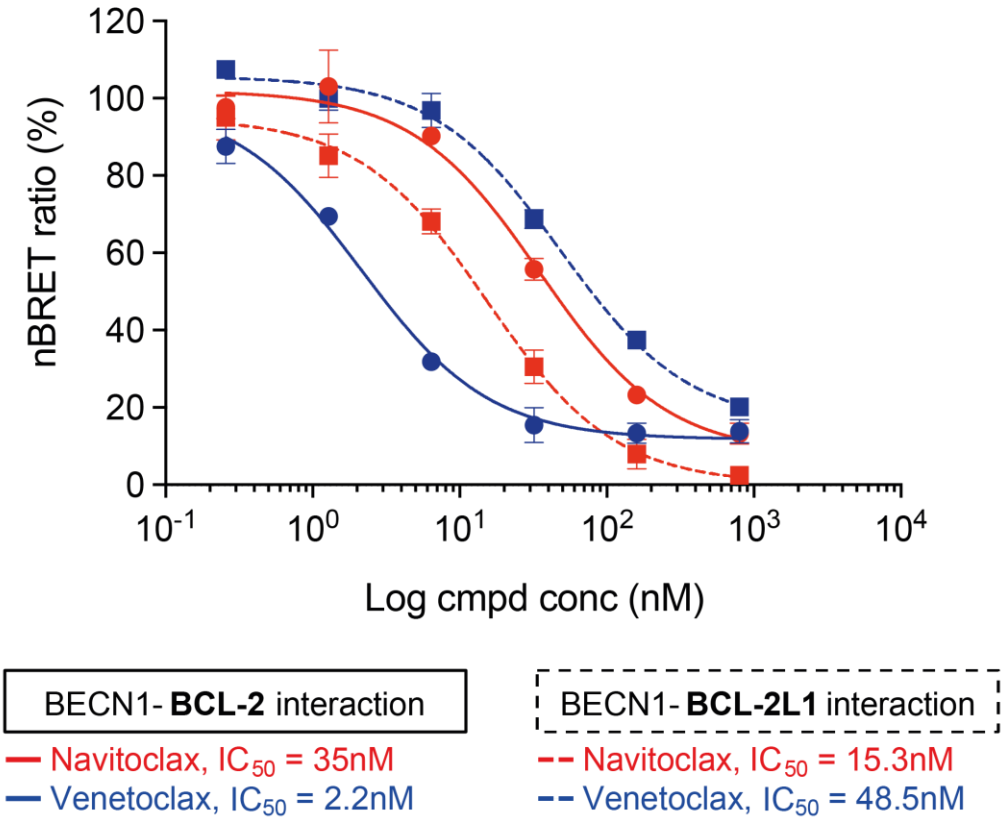

Figure 25 I BH3 mimetics inhibit BECN1-BCL-2/BCL-2L1 interactions.
HEK293 transiently co-expressing either NLuc-BECN1 and mCitrine-BCL-2 or NLuc-BECN1 and mCitrine-BCL-2L1 for 42 h before treatment with the indicated BH3 mimetics for 6 h. Navitoclax and Venetoclax treatment inhibited the BECN1-BCL-2 (solid line) as well as the BECN1-BCL-2L1 (dashed line) interactions in a concentration-dependent manner. Data are presented as percentage of the DMSO control. Data are means ± SD of triplicate samples.

The BRET data revealed that both BH3 mimetic compounds inhibit the interaction between BECN1 and BCL-2 as well as BCL-2L1 in a concentration dependent manner. The calculated IC_{50} values imply a selectivity of Venetoclax for the BECN1-BCL-2 interaction whereas Navitoclax shows no clear preference for either of the tested interactions. The non-selectivity of Navitoclax is in line with Samra *et al.* who described Navitoclax as BCL-2 and BCL-XL dual inhibitor[148]. This data reveals that BRET assays are not only detecting the modulation of protein-protein interactions, but also is a sensitive tool for detection of compound preferences for certain protein-protein interactions.

As confirmed in the previous experiment that treatment with BH3 mimetic compounds can disrupt the interaction between BECN1 and BCL-2/-XL, referring to Pattingre *et al.*[146], we hypothesized that treatment with BH3 mimetic compounds can induce autophagy.

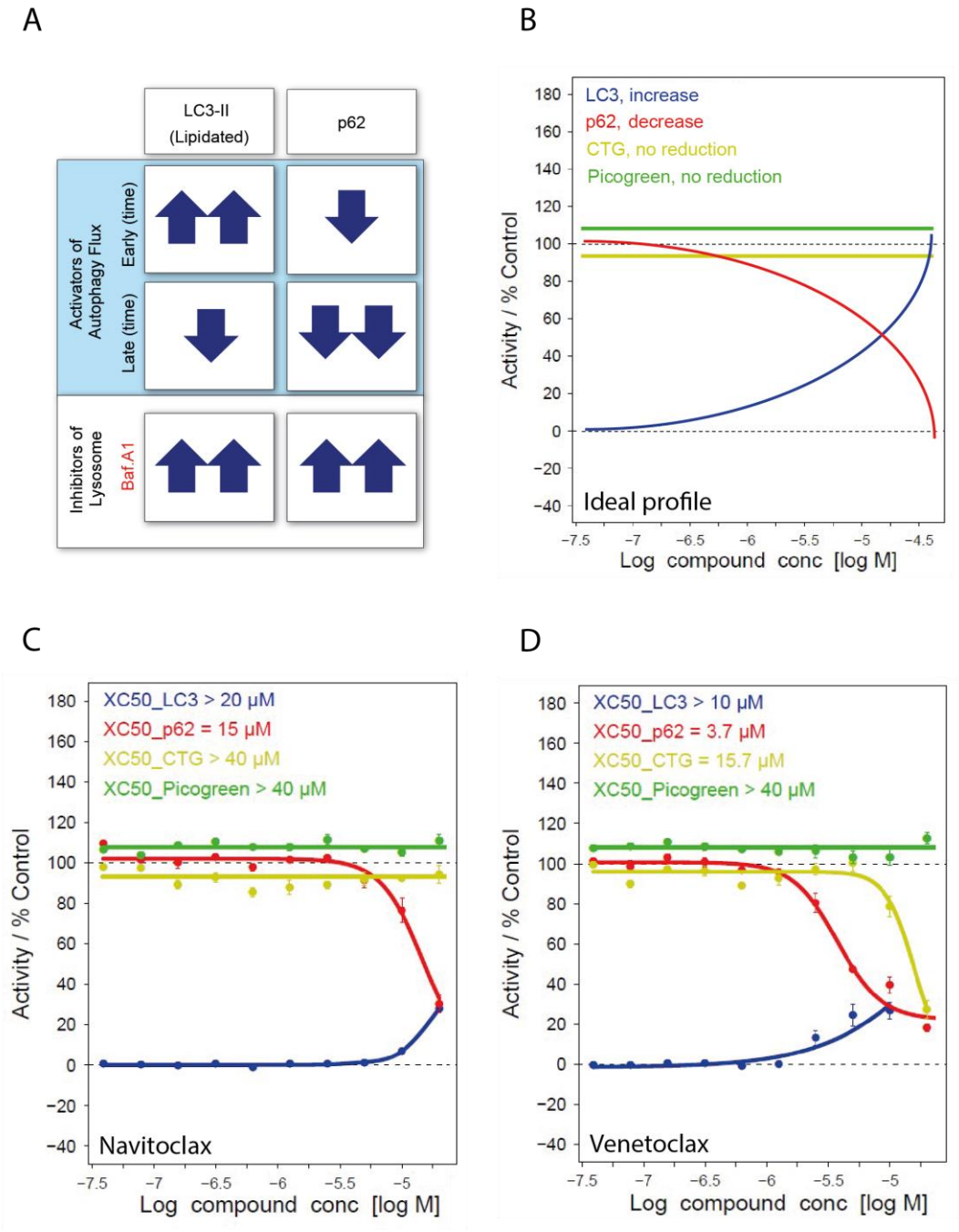

Figure 26 I Navitoclax and Venetoclax induce autophagy in HEK293 cells.
(A) Schematic overview of expected changes in LC3-II and p62 levels upon autophagy induction as well as lysosome inhibition. Schema adapted from Andreas Weiss (internal communication) **(B)** Ideal profile for LC3-II and p62 levels representing autophagy induction. **(C-D)** TR-FRET assays monitoring levels of the lipidated form of LC3 (LC3-II) and the autophagy receptor p62, reveal autophagy induction by Navitoclax and Venetoclax in HEK293 cells after 6 h treatment. The toxicity readout CTG shows no toxicity for Navitoclax **(C)**, whereas Venetoclax showed to be toxic at high concentrations **(D)**. The less sensitive toxicity readout PicoGreen was unobtrusive for both compounds **(C-D)**.

In order to test this, Navitoclax and Venetoclax were analyzed for their ability to induce autophagy. Therefore, TR-FRET assays for monitoring the levels of the lipidated form of LC3 (LC3-II) and p62 were performed. The combination of an increase of LC3-II and a decrease of p62 levels would indicate an autophagy-inducing effect (**Figure 26A-B**). As LC3-II formation is upregulated upon autophagy stimulation, a strong increase of LC3-II level is expected in the early phase of autophagy activation. Since LC3-II itself is subjected to autophagic degradation during the autophagic process, the expected increase in LC3-II in later stages of autophagy is expected to be less pronounced (**Figure 26A**). Due to the fact that accumulation of LC3-II may reflect either upregulation or inhibition of autophagosome degradation, monitoring LC3-II in isolation complicates its interpretation[90]. For discriminating autophagy inducers from blockers, p62 levels have been introduced as an additional marker for autophagic activity. p62 is an autophagy receptor which is subject for autophagosomal degradation and is expected to be decreased during autophagy (**Figure 26A**)[90]. Indeed, we find an autophagy-stimulating effect for both compounds (**Figure 26C-D**) confirming the observations of Reljic *et al.*[149]. The TR-FRET assay shows that Venetoclax is more potent in inducing autophagy, as Navitoclax only shows an effect at concentrations above 10 µM. The CellTiter-Glo® (CTG) readout, which is an indicator of toxicity, revealed that the positive autophagy-inducing effect of Venetoclax is accompanied with some toxicity at concentrations above 10 µM. The Navitoclax treatment showed no toxic side effects at the tested concentration range (**Figure 26B-C**). In the literature it has been described that BH3 mimetics produce not only an autophagy inducing effect, but also an apoptosis inducing effect, explaining the toxicity of BH3 mimetics[150]. Apoptosis induction takes place by the disruption of the interaction between the apoptosis regulator BCL-2 associated X Protein (BAX) and BCL-2 homologous antagonist/killer (BAK) with BCL-2 and BCL-2L1[151]. In order to identify compounds dissociating BECN1 from BCL2 without inducing toxicity by not affecting the interaction between BCL-2 and BAX as well as BAK, Chiang *et al.* performed Split-Luciferase and AlphaLISA screens[132]. To validate the general ability of BH3 mimetics to induce autophagy, two hit compounds from Chiang *et al.* were analyzed for their ability to disrupt the binding of BECN1 to BCL2. Both compounds, SW063058 and SW076956, have been previously reported to potently target this interaction[132].

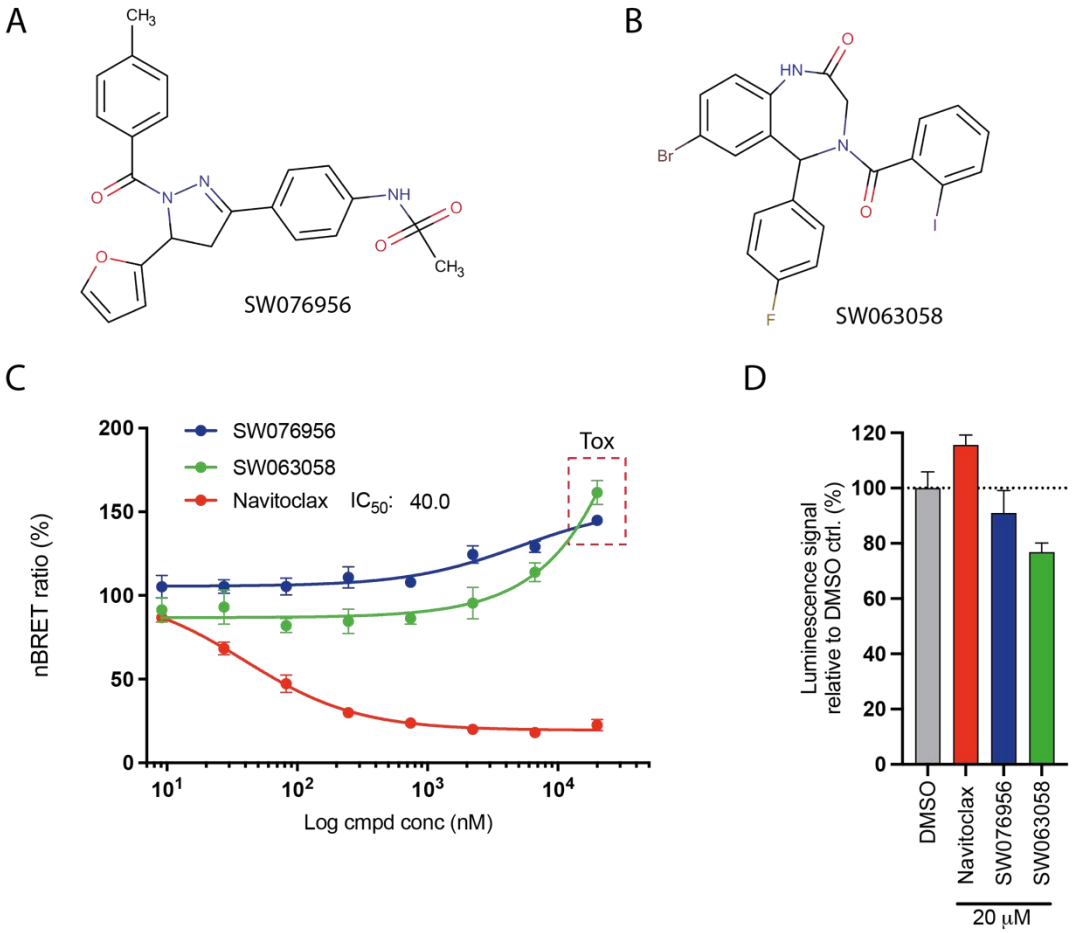

Figure 27 I The BH3 mimetics SW063058 and SW076956 do not displace BECN1 from BCL-2. HEK293 cells transiently co-expressing NLuc-BECN1 and mCitrine-BCL-2 for 42 h before treatment with the indicated BH3 mimetics for 6 h. Structure of **(A)** SW076956 and **(B)** SW063058. **(C)** SW076956 and SW063058 showed no effect after 6 h treatment. Positive control Navitoclax showed the expected profile. **(D)** Total luminescence signals suggest toxicity of SW063058 and SW076956. Data are presented as percentage of the DMSO control. Data are means ± SD of triplicate samples.

Based on the BRET data, no change in BECN1-BCL-2 interaction was found for both BH3 mimetic compounds from the Chiang paper (**Figure 27A-B**). The positive control Navitoclax showed the expected concentration-dependent decrease of the interaction between BECN1 and BCL-2. Since a reduction in total luminescence was seen at the highest compound concentration of 20 µM, toxicity of both compounds is assumed at this concentration (**Figure 27E**). In addition to its BECN1-BCL-2 disrupting activity, Chiang *et al.* also claimed an autophagy inducing effect of SW063058 and SW076956 in LC3-II Western Blot as well as immuno-cytochemistry studies[132]. Despite the fact that the BRET assay showed no BECN1-BCL-2 disrupting effect of SW063058 and SW076956, TR-FRET assays to confirm the autophagy inducing effect of SW063058 in HEK293 and human iPSC derived neurons has been performed.

additional LC3/p62 TR-FRET assays for SW063058 were performed in HEK293 cells as well as human iPSC derived neurons.

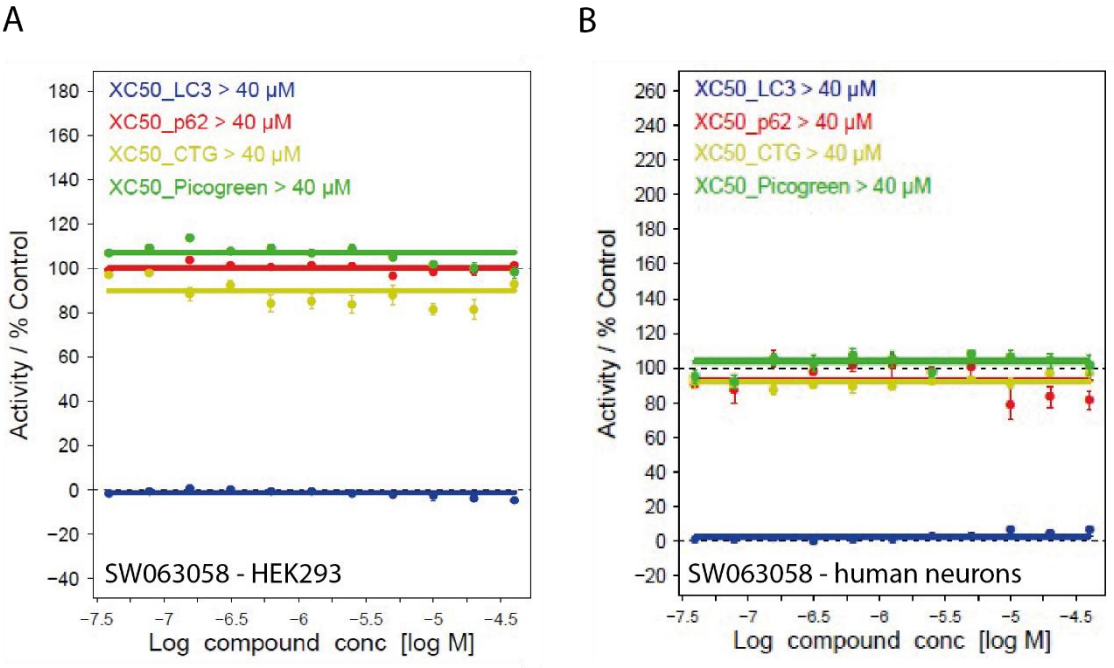

Figure 28 I SW063058 shows no autophagy inducing effect in HEK293 cells and human neurons. SW063058 does not show any autophagy modulating effect in p62 and LC3-II TR-FRET assay in lysates of HEK293 and human iPSC-derived neurons. HEK293 **(A)** and human iPSC-derived neurons **(B)** were treated for 6 h with SW063058 before lysis. Data were generated by Anja von Nordheim Hansen and are presented as % of DMSO control. Data are means ± SD.

The TR-FRET assay showed that the BH3 mimetic SW063058 has no autophagy-modulating effect, which is in line with the BRET data, which showed no BECN1-BCL-2 disrupting effect. Thus, only Navitoclax and Venetoclax (but not SW063058 or SW07695) potently reduced the interaction between BECN1 and BCL-2 whilst also inducing the autophagic cascade. For future perspective, there is more research necessary, which investigates the interplay between BECN1-BCL-2 disruption and BCL-2 dissociation from BAK and BAX and its influence on autophagy as well as apoptosis induction.

3.2 Development of autophagy targeting chimera for targeted degradation of protein aggregates

Within our focused screen, the well described key interaction between the autophagic receptor p62 and the autophagosomal membrane protein LC3B was confirmed. We hypothesized that this interaction can be utilized for targeted degradation of larger structures such as protein aggregates or organelles by bi-functional molecules

mimicking the activity of p62. Despite the fact that there is a controversial debate about the neurotoxic disease pathogenesis driving species, the majority of the early research has focused on aggregation inhibition and the induction of the proteolysis mechanisms[4]. With this part of the work, we aim to develop a new approach for selective degradation of protein oligomers and aggregates via the autophagy pathway. For this purpose, the target of interest needs to be connected to phagophores for its subsequent degradation.

As LC3 is a central protein in the autophagy pathway located in the membranes of phagophores and autophagosomes, it is an ideal effector for the connection of target structures to phagophores. Another key player in the selective autophagy pathway are autophagy receptors such as p62, NBR1 and optineurin[152]. These receptors are among other domains composed of an ubiquitin associated domain (UBA) for target binding and a LC3 interaction region (LIR). Such autophagy receptors are inborn bi-functional molecules, connecting target proteins with LC3-II of the autophagosomal membrane for its subsequent degradation. The approach of connecting target proteins with phagophores via Autophagy Targeting Chimera (ATAC) compounds mimics the natural function of endogenous autophagy receptors. In order to connect target proteins to LC3, we first analyzed the binding ability of different LIRs to LC3B proteins. LIRs are small peptides of around 12 amino acids[153] originating from various human proteins including autophagy receptors such as p62, NBR1 or Optineurin. However, LIR domains can also be found in proteins of other species such as parasites. Such Proteins, hijacking human autophagy, are the M2[154] of the influenza virus or the RavZ of *Legionella pneumophilia*[155]. These proteins can bind to LC3 by interaction of its LIR domain with the LIR docking site of LC3 which consists of two hydrophobic binding pockets[156]. In humans, seven ATG8 genes (LC3A, LC3B, LC3B2, LC3C, GABARAP, GABARAPL1 and GABARAPL2) are expressed with LC3B being best characterized in the literature and molecular structures are available[157-159]. Therefore, in a first experiment, it was investigated which LIR shows the best binding pattern to LC3B proteins. For this purpose, a donor saturation assay in HEK293 cell lysates has been performed. Here, cell lysates of donor tagged LC3B (NLuc-LC3B) were incubated with increasing concentrations of acceptor labelled (TAMRA (TMR)) LIR peptides (**Figure 29A**). For determination of non-specific binding of TMR to LC3B or NLuc, free TMR was included as negative control.

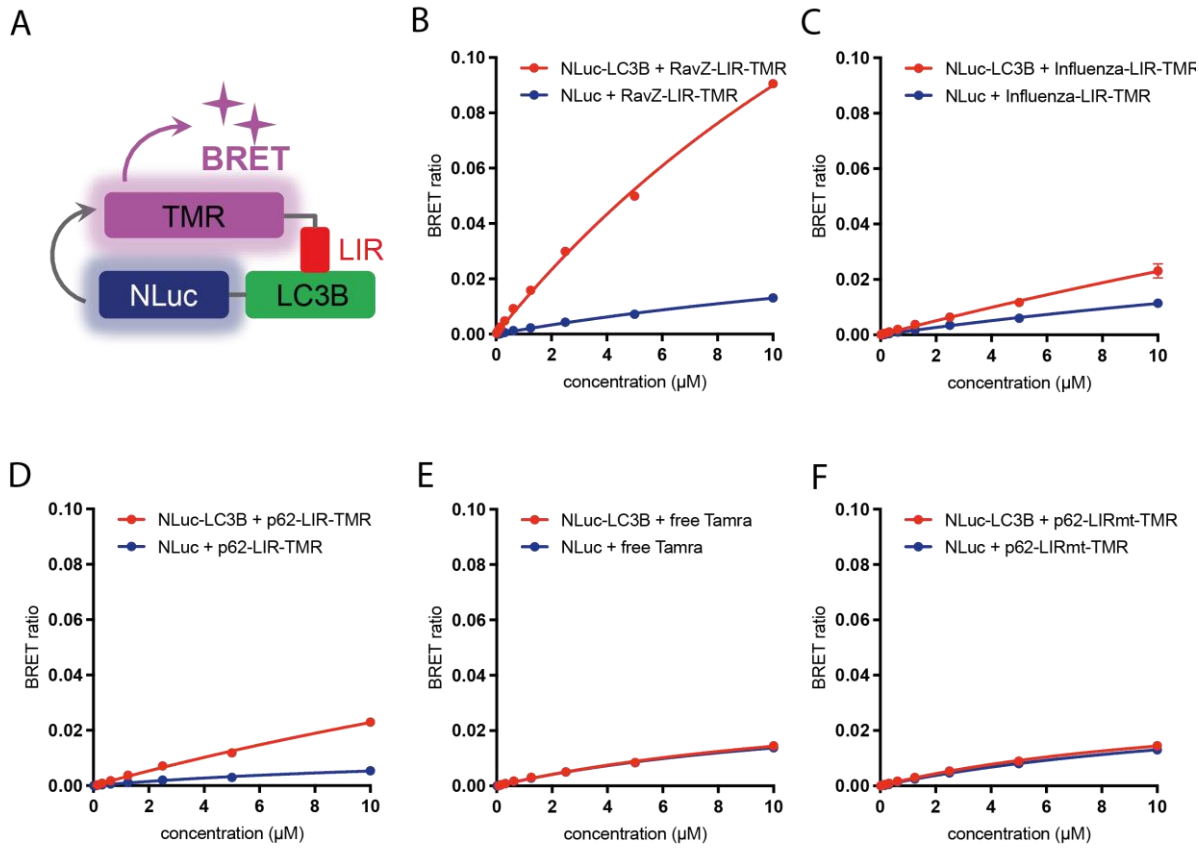

Figure 29 I BRET assay for LIR binding to LC3B in HEK293 cell lysates.
(A) Assay principle for BRET in cell lysates. **(B-F)** Results of the BRET assay for LIR binding to LC3B. Data are presented as BRET ratio for the indicated PPIs. Data are means ±SD of triplicate samples.

The results of donor saturation in HEK293 cell lysates shows a most robust binding of the RavZ-LIR to LC3B. Also, the Influenza and p62 LIRs show some affinity for LC3B, but not as high as the RavZ-LIR which originates from *Plasmodium falciparum* (**Figure 29B-D**). The canonical p62-LIR showed less affinity compared to RavZ-LIR. This is in line with the findings of Kwon *et al.* who described the N-terminal LIR of RavZ as more affine to LC3 then canonical LIRs[155]. The free TMR reveals that there is no interaction between TMR and NLuc (**Figure 29E**). Also, the negative control p62-LIRmt, where the conserved hydrophobic amino acids are switched to Serine, and the binding of the LIR to the hydrophobic binding pocket of LC3 is prevented, shows no binding to LC3B (**Figure 29F**). In order to confirm the binding of the RavZ LIR to LC3B, we have performed a competition assay, where TMR-labelled LIRs (hot probe) compete with unlabeled LIRs (cold probe) for the binding site of LC3B (**Figure 30A**). The competition assay shows that the unlabelled RavZ LIR competes with the TMR-labelled LIR for the LC3B binding site resulting in a concentration dependent decrease of the BRET signal (**Figure 30B**).

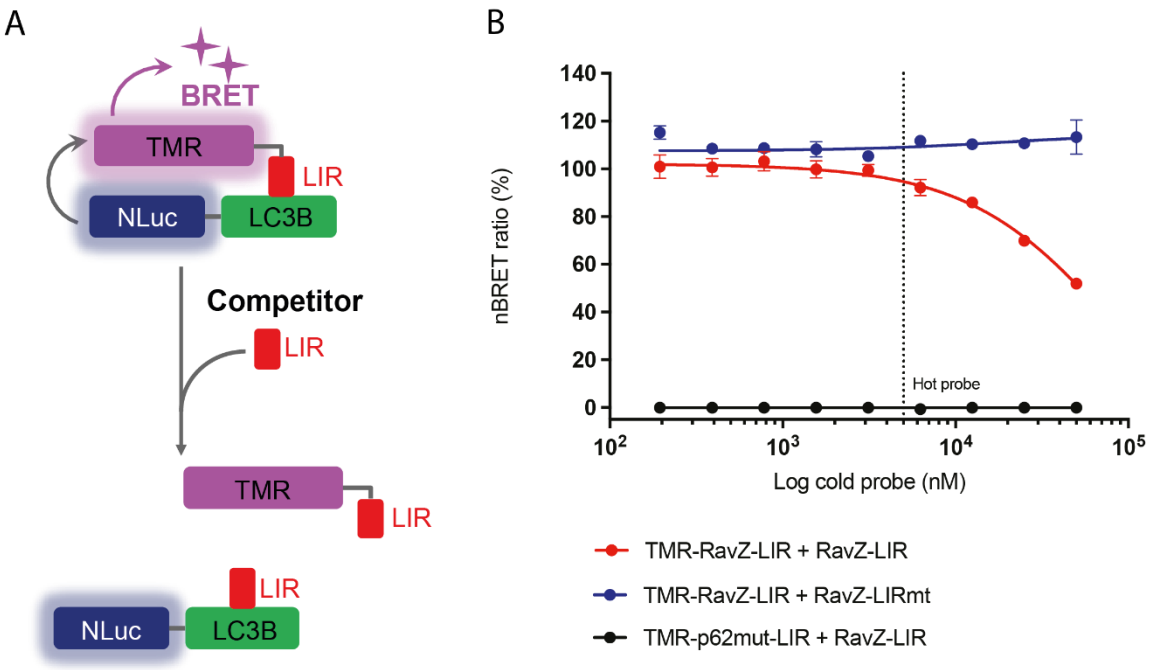

Figure 30 I Competition assay to confirm LIR binding to LC3B.
(A) Assay principle for competition assay in HEK293 cell lysates. **(B)** The concentration dependent decrease of BRET signal indicates the competition of unlabeled and labelled RavZ LIR for the binding site of LC3B. Stable amount of HEK293 cell lysates expressing NLuc-LC3B were incubated with increasing amounts of the cold probe (unlabelled LIR). RavZ-LIRmt condition serves as negative control. TMR-p62mt-LIR + RavZ-LIR combination has been added for background reduction. Data are presented in percentage of the BRET ratio for the 0 nM cold probe condition. The dashed line indicates the concentration of the hot probe. Data are means ±SD of quadruplicate samples.

The RavZ-LIRmt control, where the conserved hydrophobic amino acids were switched to Serine to prevent binding to the hydrophobic pocket of LC3, showed no effect indicating its inability to bind to LC3B. The TMR-p62-LIRmt which has been demonstrated to be unable to bind to LC3 has been used as negative control. As expected, no BRET signal was observed for TMR-p62-LIRmt. In order to validate the results in living cells, HEK293 cells were co-transfected with NLuc-LC3B and mCitrine-LIR encoding plasmids and the interaction between LIR and LC3B was assessed via BRET assay (**Figure 31A**). The BRET assay in living cells confirmed the robust binding of the RavZ-LIR to LC3B. As seen in the lysates, the Influenza-LIR showed very weak binding for LC3B. In contrast, the p62-LIR showed a very high binding to LC3B comparable to RavZ-LIR. The negative control p62-LIRmt showed as expected no binding to LC3B (**Figure 31E**). With the BRET assay in living HEK293 cells the results from the BRET in lysates were confirmed. Based on its robust binding to LC3B, the RavZ-LIR was found as the most suitable LIR for experiments aiming to connect protein aggregates to LC3B. Consequently, RavZ-LIR was chosen for proof-of-concept experiments.

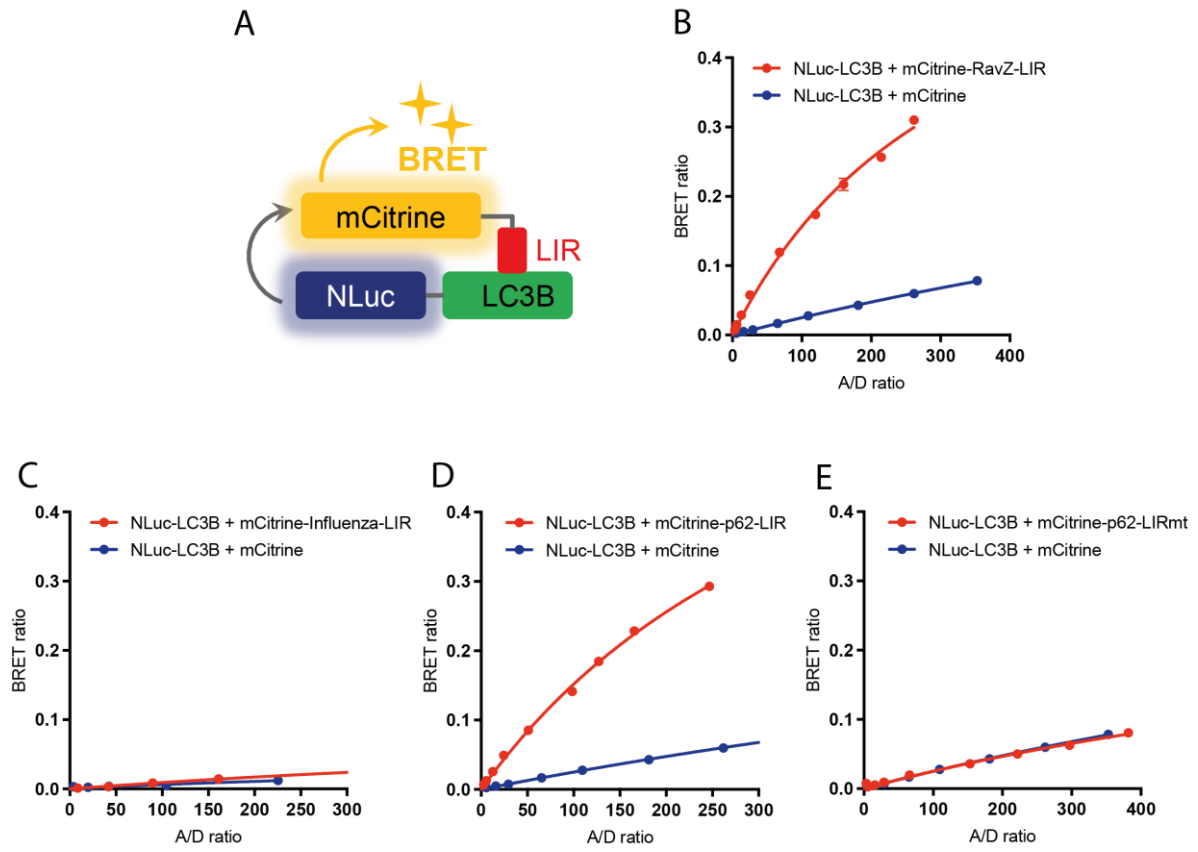

Figure 31 I BRET assay for LIR binding to LC3B in live HEK293 cells.
(A) Assay principle for BRET in live HEK293 cells. HEK293 cells were co-transfected with NLuc-LC3B and mCitrine-tagged LIRs for 48 h before BRET analysis. **(B-E)** Results of the BRET assay for LIR binding to LC3B. Data are presented as BRET ratio for the indicated PPIs. Data are means ±SD of triplicate samples.

For demonstrating the feasibility of the idea of connecting bulky cargo to phagophores for degradation, we aimed to analyze whether tagging a target with a LC3 interaction region (LIR) can mediate the degradation of the target. Therefore, Hela cells expressing Tau40$^{P301S/S320F}$ proteins were used, as this double mutation of Tau has been shown to readily aggregate upon overexpression in cells[117]. The Tau40$^{P301S/S320F}$ was tagged with EGFP and either a RavZ-LIR or RavZ-LIRmt (**Figure 32A**). These constructs were transiently expressed in HeLa cells for 48h and insoluble Tau40 aggregates as well as soluble Tau40 proteins were separated via biochemical fractionation. The fractionation assay reveals that tagging mutant Tau40 with a LIR leads to a slight reduction of proteins detected in the insoluble fraction (**Figure 32D+F+G**). If non-tagged or tagged with a non-functional LIR, the protein levels showed not to be affected.

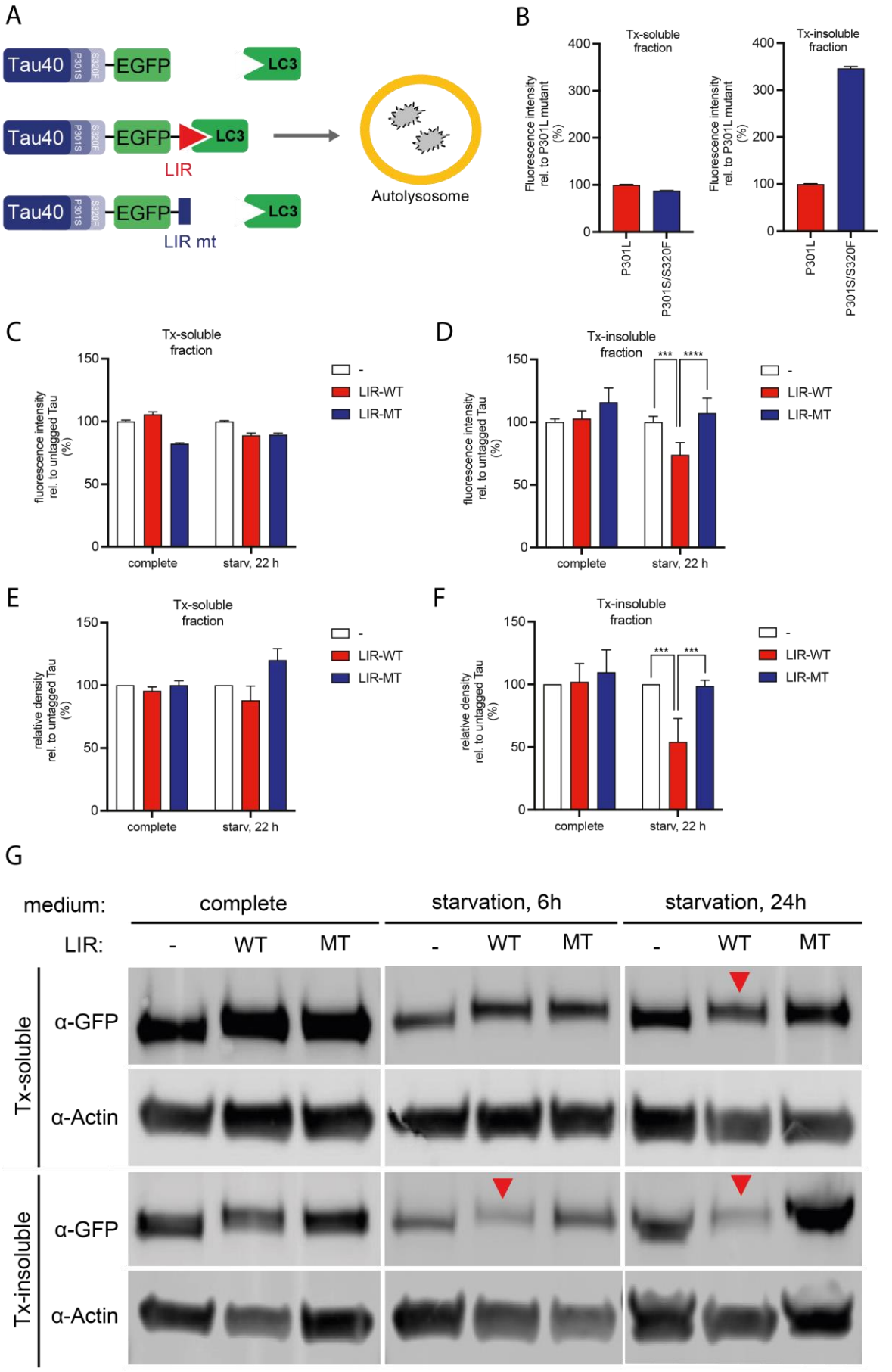
A
Tau40
P301S
S320F
EGFP
LC3
LIR
LIR mt
Autolysosome
B
Tx-soluble fraction
Tx-insoluble fraction
Fluorescence intensity rel. to P301L mutant (%)
P301L
P301S/S320F
C
Tx-soluble fraction
fluorescence intensity rel. to untagged Tau (%)
-
LIR-WT
LIR-MT
complete
starv, 22 h
D
Tx-insoluble fraction
***
****
E
Tx-soluble fraction
relative density rel. to untagged Tau (%)
F
Tx-insoluble fraction
G
medium:
complete
starvation, 6h
starvation, 24h
LIR:
WT
MT
Tx-soluble
Tx-insoluble
α-GFP
α-Actin

Figure 32 I LIR mediated degradation of Tau40 aggregates.
(A) Schematic overview of the LIR mediated degradation of double-mutant Tau aggregates in HeLa cells. **(B)** Fractionation assay showing the assay window between aggregation prone (P301S/S320F) Tau and non-aggregating Tau. **(C-D)** EGFP intensity of the Triton-X soluble and insoluble fraction. **(E-F)** Quantification of the WB for the Triton-X soluble and insoluble fraction **(G)** WB results of the fractionation assay. Cell lysates of HeLa cells transiently expressing the different Tau40 constructs for 48 h. Starvation took place by exchange of the complete medium for HBSS for 6 h or 24 h. Triton-X (1%) soluble and insoluble fractions were separated via biochemical fractionation. Proteins were determined via EGFP tag in WB and florescence plate reader. **(C-F)** Data are mean +SD obtained from 3 individual experiments. WB has been performed by Kristin Flechtner.

The fractionation assay reveals that tagging mutant Tau40 with a LIR leads to a slight reduction of proteins detected in the insoluble fraction (
Figure 32D+F+G). If non-tagged or tagged with a non-functional LIR, the protein levels showed not to be affected. In terms of soluble mutant Tau40 levels, no difference is observed (
Figure 32C+E+G). This data suggests that tagging Tau40 with a functional LIR leads to targeted degradation of insoluble Tau aggregates. If the cells were starved for 6 h or 24 h using HBSS buffer, an amplified degradation can be observed. For the 24 h starvation condition there is even a slight reduction in the soluble fraction detectable, suggesting that soluble proteins can also be targeted. The fact that the effect of the LIR tag is further induced by induction of autophagy suggests its autophagy dependent mode of action.

Having confirmed the targeted degradation of protein aggregates by connecting cargo to the phagophore, we want to test whether this connection can be mediated by bi-functional molecules. Due to there being no ligand available for LC3, a protein tagging system was developed. In order to make the LC3B and target proteins amendable for binding to an ATAC molecule, we fused the LC3B to a HaloTag and the target proteins such as Tau40 and HTT to a mutant FKBP1A. For both tags, the $FKBP1A^{F36V}$ and the HaloTag, well established binders are available. In 2018 Nabet *et al.* used a FKBP1A binder which shows preference for the F36V mutation[160]. This synthetic ligand of FKBP12 (SLF) has been successfully used before as a warhead to mediate the degradation of $FKBP1A^{F36V}$-tagged target proteins[52,160] in PROTAC experiments. In 2015, England *et al.* published the HaloTag as a tool for biochemical applications[161] and Buckley *et al.*[162] demonstrated that using the Halo-tag system for recruitment of proteins works for PROTAC development[162]. HaloTag describes a two-component system consisting of a 36 kDa protein and a chloroalkane ligand. The HaloTag can be genetically linked to other proteins, and the chloroalkane ligand can be connected to

fluorophores and other molecules of interest[110]. The chloroalkane binds covalently to the HaloTag making it a good tool moiety for bi-functional compound design. For the ATAC compounds, the SLF and the chloroalkane were connected via a polyethylene glycol (PEG) linker of different lengths (2x to 12x PEG linker) (**Figure 33A**). So far, the most common motif in PROTAC degrader structures is the PEG of varying length, making about 55% of published linkers[163]. The synthetic accessibility, flexibility and the ability to easily change the length of PEG linkers makes PEG advantageous over other linker moieties such as Alkyne, Triazoles and Piperazines[163]. Also in AUTAC design, PEG linkers have been applied[52].

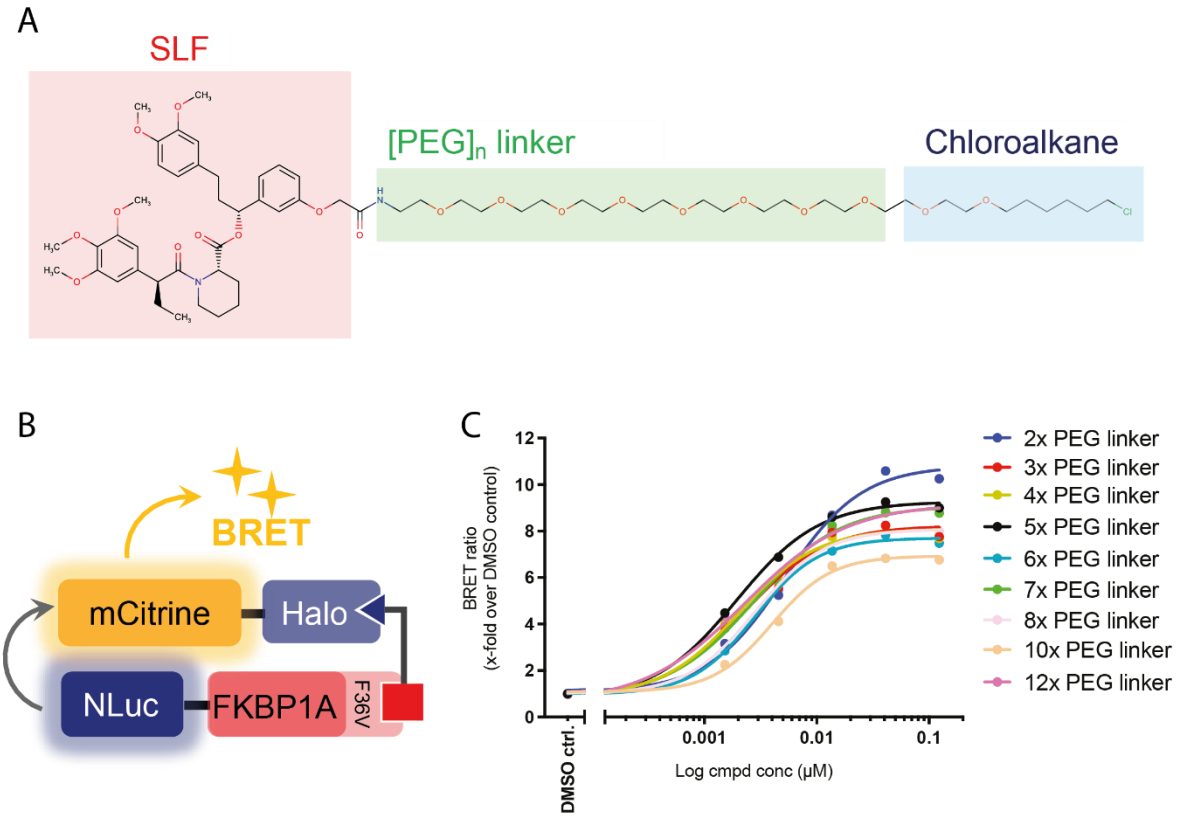

Figure 33 I ATAC compounds induce the interaction between FKBP1A^{F36V} and HaloTag.
(A) Structure of ATAC compounds consisting of a SLF moiety binding to FKBP1A^{F36V} and Chloroalkane binding to HaloTag connected via a PEG linker of various length. **(B)** Schematic overview of the BRET assay to assess the ATAC induced interaction between FKBP1A^{F36V} and HaloTag. **(C)** ATAC compounds induce the interaction between NLuc-FKBP1A^{F36V} and HaloTag in a concentration dependent manner. HEK293 cells transiently co-expressing NLuc-FKBP1A^{F36V} and mCitrine-HaloTag for 48 h were treated with compounds for 4 h. Data were generated by Stephanie Wieneke and are presented in x-fold over DMSO control for the indicated compounds. Data are means of duplicate samples.

As the bi-functional ATAC molecules are expected to induce the PPI of FKBP1A^{F36V} and HaloTag, a BRET assay to confirm functionality and cell permeability was

performed. Therefore, HEK293 cells transiently expressing NLuc-FKBP1A^{F36V} as BRET donor and HaloTag-mCitrine as BRET acceptor were treated with dilution series of ATACs for 4 h. The BRET assay showed that all compounds with varying linker-lengths induce the PPI between NLuc-FKPB1A^{F36V} and mCitrine-Halo in a concentration dependent manner (**Figure 33C**). Furthermore, the data indicates that the compounds are cell permeable. Due to the fact that all tested ATAC compounds show a similar pattern, the ATAC compound with a 10x PEG linker was chosen for further investigation.

In order to analyze the capability of ATAC compounds to induce the degradation of protein aggregates, an ICC based aggregation assay has been developed. As we found that HTT aggregates are easier to quantify in imaging assays than Tau40$^{P301S/S320F}$, we decided to switch from Tau to HTT aggregates. For that purpose, HeLa cells were transiently transfected with fusion constructs encoding the pathogenic huntingtin exon 1 containing a 46Q repeat expansion fused to EGFP and FKBP1A^{F36V} (HTT Ex1 Q46-EGFP-FKBP1A^{F36V}) and HaloTag-LC3 for 24 h before treatment with ATAC (10x PEG linker) for 24 h with 6 h starvation in HBSS supplemented with 1% FBS (**Figure 34A**). The compound effect on HTT aggregates was determined by assessing the number of aggregates per EGFP positive cell. The image-based aggregation assay shows a clear aggregation of the 46Q constructs, whereas the 19Q construct does not show any aggregation as expected (**Figure 34B**). Furthermore, a 24 h ATAC treatment decreases the number of HTT aggregates in a concentration dependent manner. A hook effect can be observed at 125 nM which indicates the point where both interacting partners are saturated with the compound. The hook effect is a common feature of bi-functional molecules such as PROTACs[141] and describes an auto-inhibition of ternary complex formation due to saturation of the interaction partners. The maximum effect at 125 nM represents ~65% of reduction of HTT aggregates (**Figure 34C**).

In order to confirm the findings of ATAC mediated HTT degradation using independent methods, BRET (**Figure 35A**) and fractionation assays were performed. Additionally, to further validate the effect of the ATAC compound, a negative control compound was tested. This compound is unable to bind to the HaloTag due to the absence of a Chlorine atom at the alkane moiety of the molecule (**Figure 35C**).

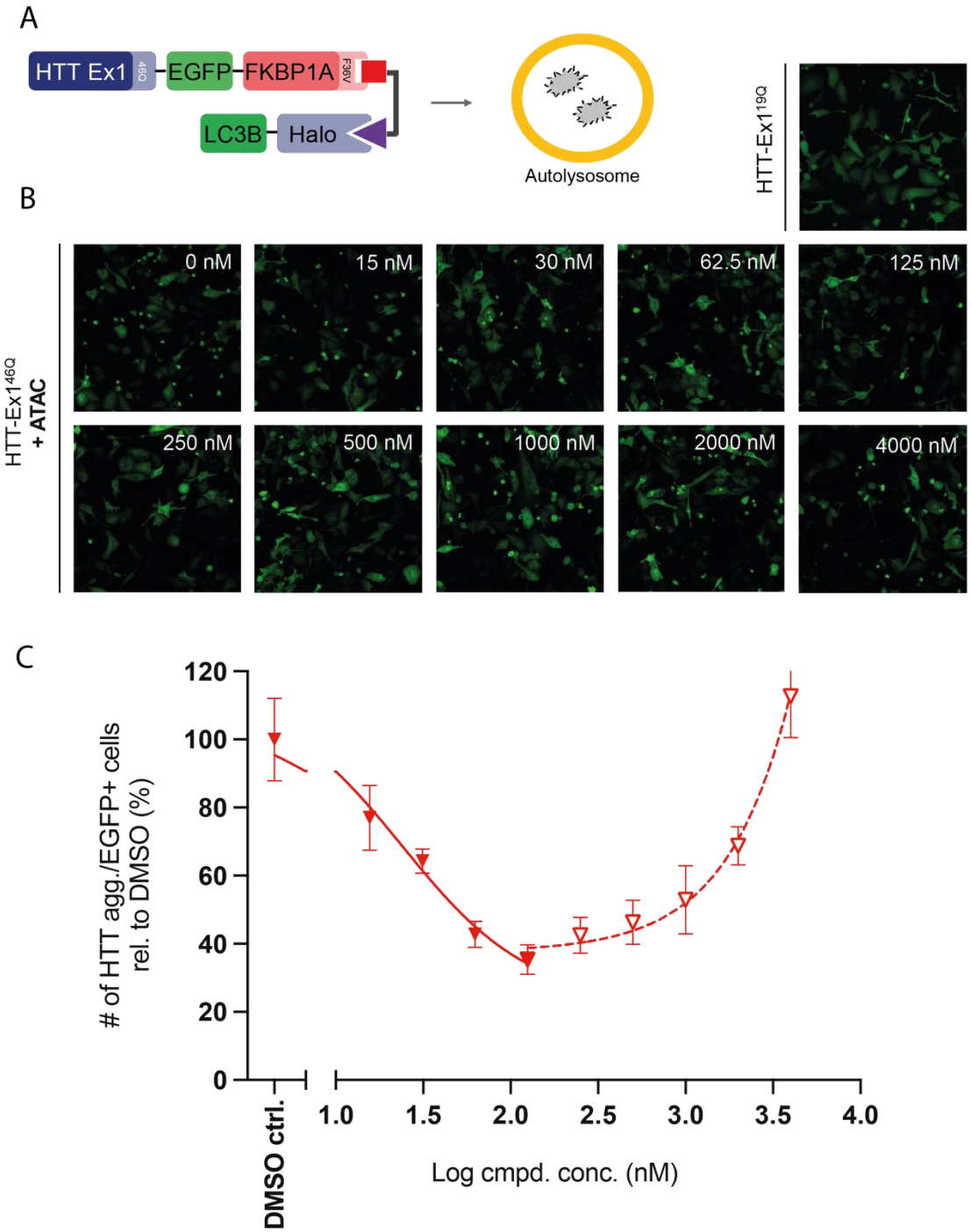

Figure 34 I ATAC mediates the degradation of HTT aggregates.
(A) Schematic overview of the ATAC mediated degradation of HTT aggregates. **(B)** Raw images of 19Q and 46Q HTT constructs with and without ATAC compound. HeLa cells co-expressing HTT Ex1 46Q-EGFP-FKBP1A^{F36V} and HaloTag-LC3B for 48 h were compound treated for 24 h including 6 h starvation with HBSS+1%FBS. **(C)** Concentration dependent degradation of HTT aggregates mediated by ATAC compound. Hook effect at 125nM of compound concentration with a max. effect of ~65%. Data are presented as number of aggregates per EGFP positive cell relative to the DMSO control condition. Data are means ± SD of six replicate samples.

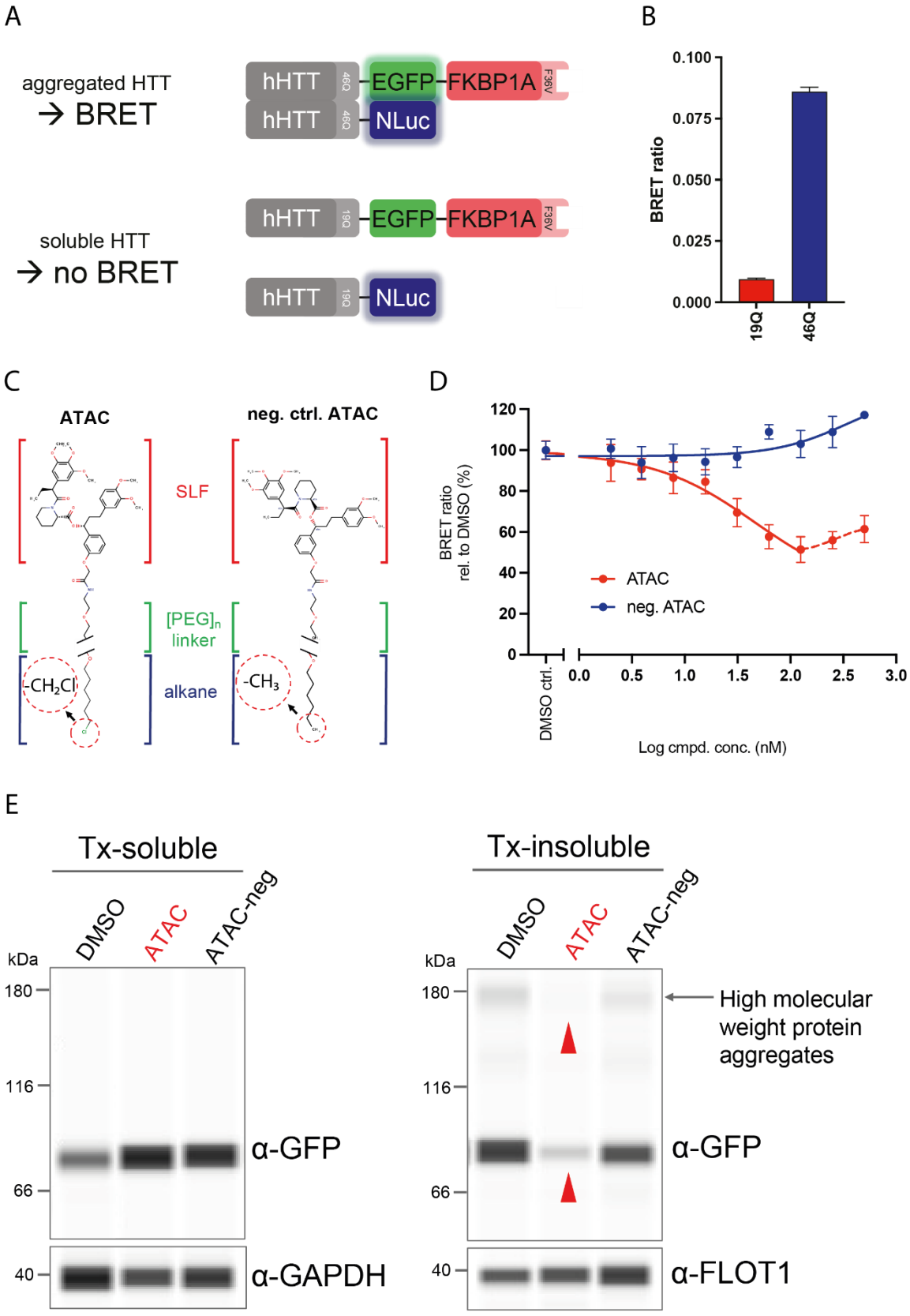

Figure 35 I ATAC mediated HTT degradation confirmed in orthogonal assays.
(A) Schematic overview of the BRET aggregation assay. **(B)** BRET aggregation assay showing the assay window between 19Q and 46Q HTT constructs. **(C)** Difference in structure of ATAC and neg. ctrl. ATAC compounds. **(D)** ATAC compound mediated degradation of HTT in a concentration dependent

manner. Hook effect at 125 nM of compound concentration with max. effect of ~50%. Data are presented in percentage of the BRET relative to the DMSO control condition. Data are means ± SD of six replicate samples. **(E)** Simple Western results for the protein levels of soluble and insoluble fractions. HeLa cells co-expressing HTT Ex1 46Q-EGFP-FKBP1A^{F36V} and Halo-LC3B for 48 h were treated for 24h with 125 nM of ATAC and negative control ATAC.

The BRET aggregation assay showed that the results previously obtained from the ICC assay can be reproduced using independent methods. Upon ATAC treatment, the BRET signal is decreased in a concentration dependent manner with a hook effect at 125 nM (**Figure 35D**). The treatment with the negative control ATAC (unable to bind to HaloTag due to substitution of the Chlorine atom by a Hydrogen atom) did not lead to a reduction in BRET signal. By using the fractionation assay with subsequent Simple Western blotting, the degradation of protein aggregates can be confirmed using independent methods (**Figure 35E**). The Triton-X soluble fraction representing soluble HTT proteins, does not show any degradation upon ATAC treatment. However, the Triton-X insoluble fraction representing aggregated HTT, does show a clear reduction in EGFP positive aggregates upon ATAC treatment. The high molecular weight bands of the insoluble fraction showed the same pattern of ATAC mediated degradation. The DMSO and negative control ATAC show no reduction in HTT protein levels, indicating, that the observed effect is mediated by the connection to phagophores.

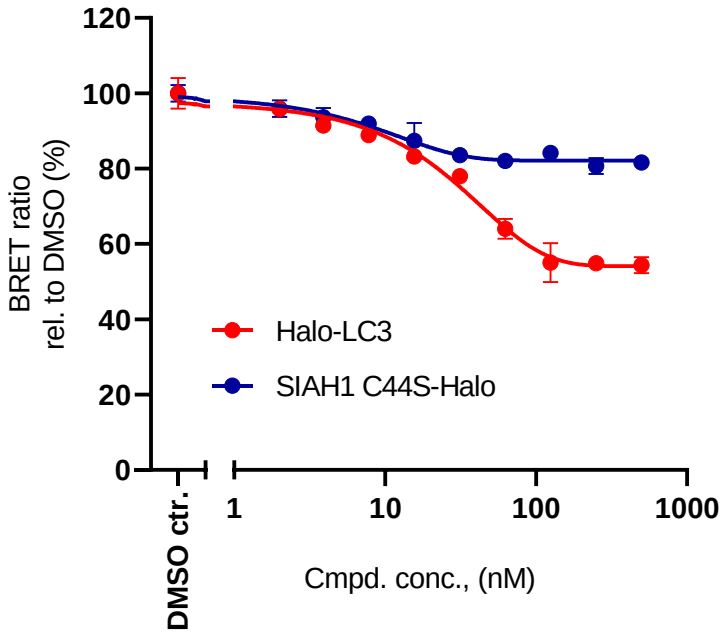

Figure 36 I BRET assay of SIAH1^{C44S} as negative control.
BRET assay shows no effect for the SIAH1^{C44S} negative control. HeLa cells were co transfected with HTT Ex1 46Q-EGFP-FKBP1A^{F36V}, HTT Ex1 46Q-NLuc and Halo-LC3B or Halo-SIAH1^{C44S} for 24 h before 24 h compound treatment. Data are presented in percentage relative to the DMSO control condition. Data are means ± SD of six replicate samples.

To investigate whether the observed effect is coming from LC3B mediated degradation, but not an artefact of ternary complex formation with HaloTag fusion, further negative controls were tested in BRET aggregation assay. For that purpose, HeLa cells were co-transfected with HTT Ex1 46Q-NLuc, HTT Ex1 46Q-EGFP-FKBP1A^{F36V} and Halo-LC3B or Halo-SIAH1^{C44S}. SIAH1 is an E3-ligase and is not involved in the autophagosomal pathway. Its point mutation C44S from SIAH1 has been shown to be catalytically inactive[164], indicating that a proteasomal degradation of the target can be excluded. The results showed that SIAH1^{C44S} recruitment does not induce degradation of HTT aggregates upon compound treatment. These results further confirm the autophagy driven MoA of ATAC compounds, as connecting the target to an autophagy unrelated protein does not show any effect. In order to confirm that the observed ATAC effect is due to the active degradation of protein aggregates and not a result of increased solubilization of the HTT proteins, a meso scale discovery (MSD) assay to monitor the level of soluble HTT was performed. The MSD assay is a sandwich immunoassay where HTT proteins are immobilized by capture antibodies. A sulpho-tag conjugated detection antibody binding to the immobilized HTT monitors protein levels via an electrochemiluminescence signal (**Figure 37A**).

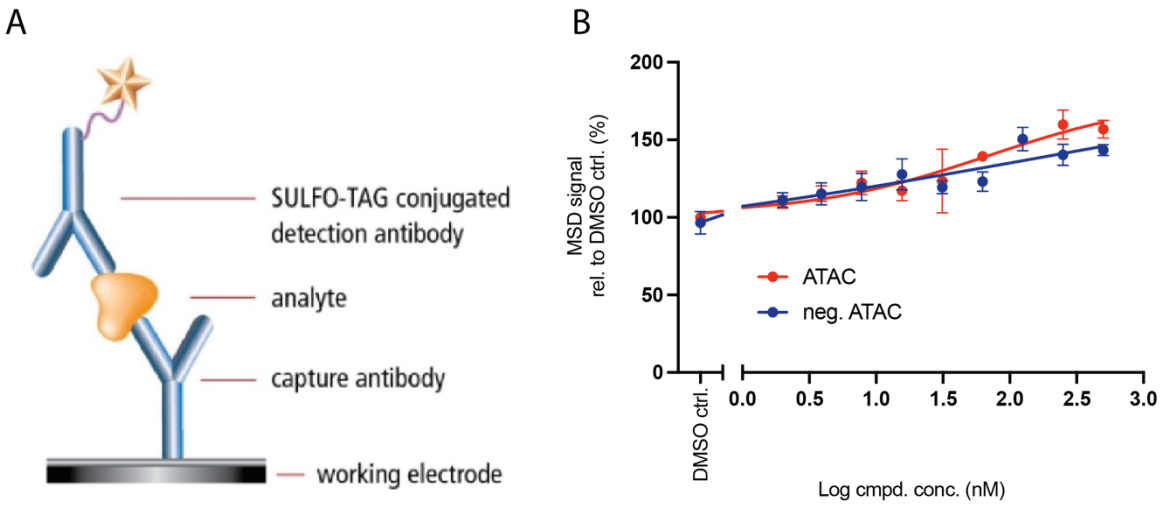

Figure 37 I Meso scale assay for determination of soluble HTT levels.
(A) Schematic overview of the MSD assay. **(B)** MSD assay shows a slight increase of soluble HTT levels upon compound treatment. HeLa cells were co transfected with HTT Ex1 46Q-EGFP-FKBP1A^{F36V} and Halo-LC3B for 24 h before 24 h compound treatment. Data were generated by Philipp Dante Zinn and are presented in percentage relative to the DMSO control condition. Data are means ± SD of quadruplicate samples.

The MSD assay showed a slight increase in soluble HTT levels upon compound treatment. Due to the fact, that there is no difference between the ATAC and negative control ATAC it can be assumed that the observed compound effect is not due to a solubilization of protein aggregates, but indeed an ATAC induced degradation of aggregates.

As we hypothesize that connecting cargo to the autophagosome will lead to its degradation via the autophagy pathway, next, we addressed its autophagy dependent mode of action (MoA). The most simple way of inducing autophagy is by exposing the cells to a starvation condition where the lack of amino acids, serum and carbohydrates triggers the cells into a state of nutritional stress[165]. In order to compensate for the lack of nutrients, the cellular recycling systems like autophagy or the UPS will be triggered to ensure sufficient amino acid supply. In order to induce autophagy in the HTT aggregation assays, HeLa cells were exposed to a nutrients starvation of 6 h at the end of the compound treatment period. Starvation is defined by the change of the culture medium for HBSS buffer supplemented with 1% FBS.

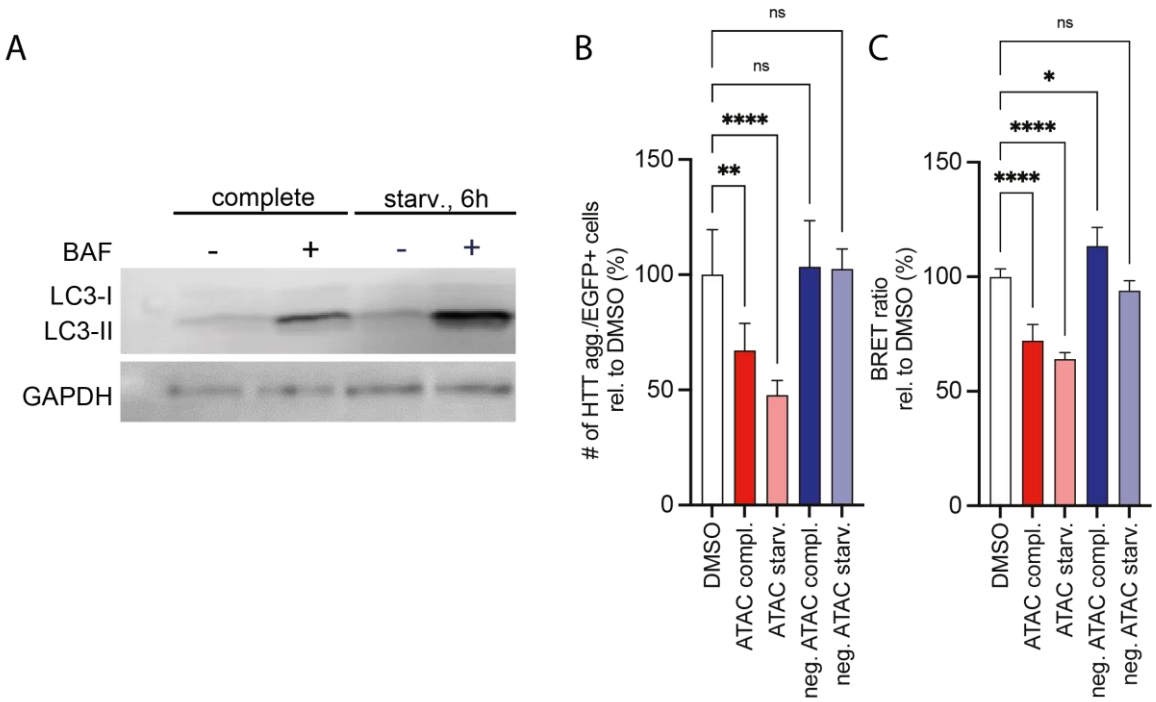

Figure 38 I ATAC mediated degradation is increased by starvation.
(A) LC3 WB for comparison of complete medium condition with 6 h partial starvation condition. HeLa cells were cultured for 24 h or 18 h in complete medium followed by 6 h partial starvation in HBSS with 1% FBS before lysis. **(B)** ICC assay to test the impact of starvation on ATAC mediated HTT degradation. **(C)** BRET assay for assessing starvation effect on HTT degradation mediated by ATAC compound. **(B-C)** HeLa cells were co transfected with HTT Ex1 46Q-EGFP-FKBP1A^{F36V}, HTT Ex1 46Q-NLuc and Halo-LC3B for 24 h before 24 h compound treatment with and without 6 h partial starvation with HBSS+1%FBS. Data are presented in percentage relative to the DMSO control condition. Data are means ± SD of six replicate samples. Statistical analysis was performed by one-way ANOVA with Dunnett *post hoc* test.

By using LC3 WB it was shown that the 6 h partial starvation leads to an increase of the LC3-II levels indicating a starvation induced autophagy stimulation (**Figure 38A**). The effect of starvation on the ATAC mediated HTT degradation was tested in an ICC as well as BRET assay. The results showed that in both assays the compound effect of the ATAC could be increased by starvation (**Figure 38B-C**). The fact that the starvation positively affects the ATAC effect, indicates that the ATAC MoA is autophagy driven. In order to confirm and validate the autophagy dependent MoA of the ATAC compound, autophagy inhibition was analyzed by small molecules as well as on a genetic level by protein overexpression. For that purpose, well known autophagy modulating compounds like Bafilomycin and 3MA were tested. Bafilomycin is described to inhibit the fusion of autophagosomes and lysosomes by suppressing the acidification of the lysosome[166]. 3MA is a PI3K inhibitor which has been shown to modulate autophagy upstream of autophagosome formation[167]. PI3K plays a key role in mTOR activation and hence is an important regulator of autophagy[168].

For testing autophagy inhibition on a genetic level, overexpression of ATG4B was tested. ATG4B plays a dual role in the LC3 conjugation system[81]. For LC3 to be inserted into the autophagosomal membrane, the conjugation of LC3 with phosphatidylethanolamine (PE) is essential. For that purpose, LC3 needs to be cleaved at its C-terminal end to expose a glycine where the PE conjugation can take place. ATG4B is the protease facilitating the cleavage of the C-terminal end of LC3. Despite its role in cleaving LC3, ATG4B plays a dual role in LC3 conjugation system as it has been shown that once overexpressed, it can delipidate LC3 by cleaving PE from LC3 and hence blocks autophagy[169]. In order to test the influence of autophagy blockage on ATAC mediated HTT degradation, ATG4B overexpression as well as Bafilomycin or 3MA treatment was tested in ICC and BRET aggregation assays. With a LC3B WB we demonstrated that the overexpression of the HA-ATG4B construct leads to a decreased LC3-II formation indicating an inhibition of autophagic activity (**Figure 39A**). ATG4B overexpression mediated autophagy inhibition showed a partial reduction of the ATAC mediated degradation of HTT (**Figure 39B**) which suggests that the ATAC MoA is autophagy dependent. This autophagy driven MoA can be further confirmed by chemical autophagy modulation attempts in ICC and BRET assay. Both assays show that blocking autophagy via Bafilomycin results in a decreased degradation of HTT aggregates (**Figure 39C-D**).

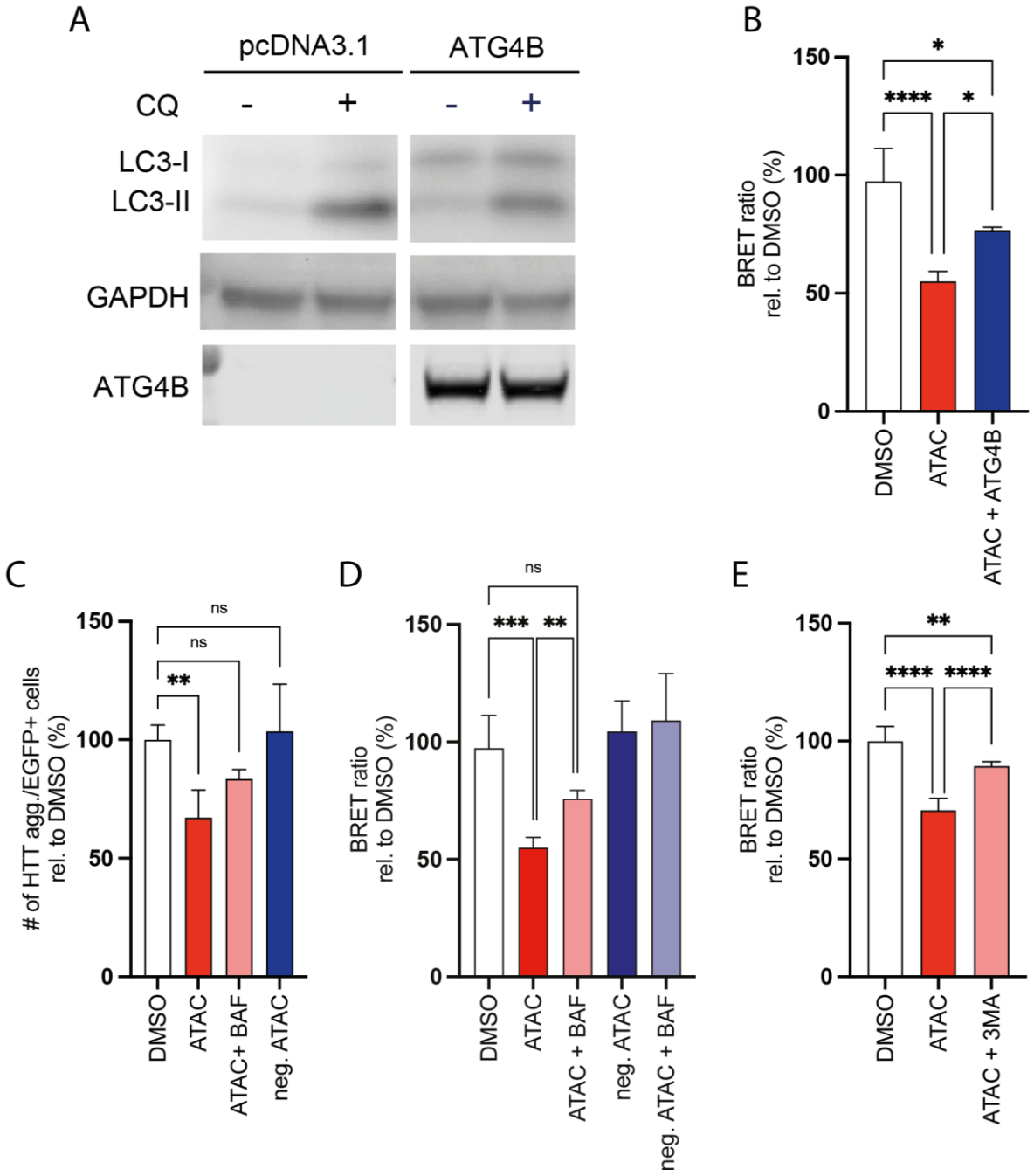

Figure 39 I Chemical and genetic autophagy modulation indicate autophagy driven MoA.
(A) LC3 WB for testing the autophagy inducing effect of ATG4B overexpression. HeLa cells were transiently transfected with empty vector or ATG4B for before lysis. **(B)** BRET assay shows a partial reduction of ATAC mediated HTT degradation upon overexpression with ATG4B. HeLa cells were co transfected with HTT Ex1 46Q-EGFP-FKBP1A^{F36V} and Halo-LC3B with and without co-transfection of HA-ATG4B for 24 h before 24 h compound treatment. Data are presented in percentage relative to the DMSO control condition. Data are mean ± SD. **(C-D)** ICC and BRET assay for assessing the effect of Bafilomycin co-treatment on HTT degradation mediated by ATAC compound. **(D-E)** BRET assay showing the partial reduction of ATAC compound effect on HTT degradation. HeLa cells were co transfected with HTT Ex1 46Q-EGFP-FKBP1A^{F36V} and Halo-LC3B for 24 h before 24 h compound treatment with and without 24 h co-treatment with the mentioned compounds (BAF 15 nM, 3MA 5 mM). Data are presented in percentage relative to the DMSO control condition. Data are means ± SD of six replicate samples. Statistical analysis was performed by one-way ANOVA with Dunnett *post hoc* test.

Also, the co-treatment with the autophagy modulator 3MA results in a decreased ATAC activity (**Figure 39E**) further suggesting an autophagy dependent MoA. Taken together, the autophagy modulation attempts of starvation, ATG4B overexpression and pharmacological inhibitors, the results indicate the autophagy dependent MoA of ATAC mediated HTT degradation. The design of bifunctional compounds like PROTACs are very complicated because the Target protein needs to be in the right orientation to the ubiquitinating E2- and E3-ligases. This makes it very labor intensive finding the right linker and linker-length. As for the ATAC approach, a simple connection between LC3 and the target structure is needed, and we hypothesize that the linker-length does not influence the compound efficacy substantially. In order to test the effect of linker-length on ATAC mediated HTT degradation, a BRET assay with ATACs of different linker-lengths (2x-12x PEG linker) (**Figure 40A**) was performed and compared to the compound which was used in previous experiments with 10xPEG linker.

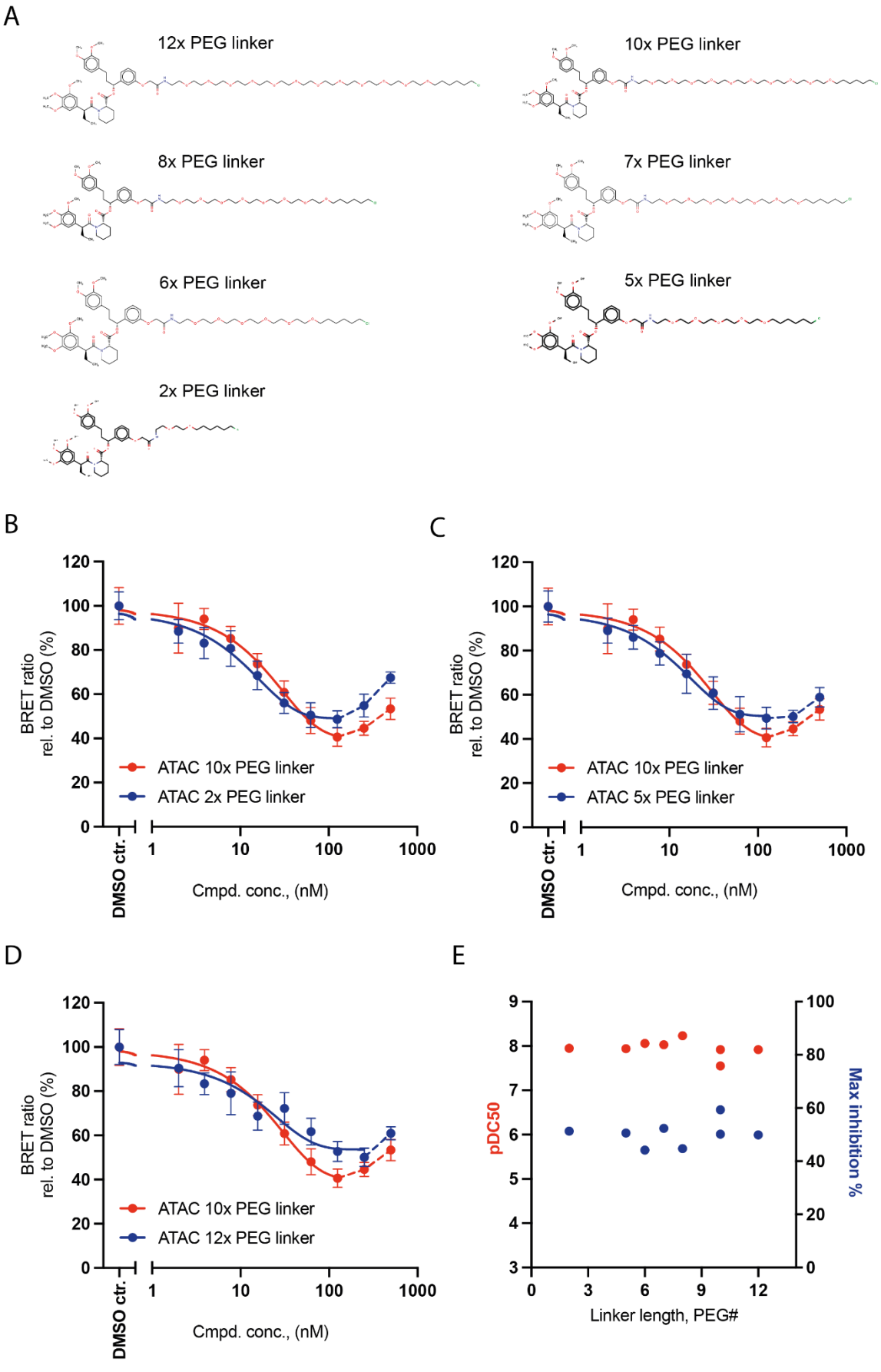
A
12x PEG linker
10x PEG linker
8x PEG linker
7x PEG linker
6x PEG linker
5x PEG linker
2x PEG linker
B
BRET ratio rel. to DMSO (%)
ATAC 10x PEG linker
ATAC 2x PEG linker
DMSO ctr.
Cmpd. conc., (nM)
C
BRET ratio rel. to DMSO (%)
ATAC 10x PEG linker
ATAC 5x PEG linker
DMSO ctr.
Cmpd. conc., (nM)
D
BRET ratio rel. to DMSO (%)
ATAC 10x PEG linker
ATAC 12x PEG linker
DMSO ctr.
Cmpd. conc., (nM)
E
pDC50
Max inhibition %
Linker length, PEG#

Figure 40 I Analyzing the influence of the linker-length on HTT degradation.

(A) Chemical structures of ATAC compounds with different linker-lengths tested in BRET assay. (**B-D)** BRET assay shows no difference between the HTT degradation mediated by compounds with different linker-lengths. HeLa cells were co transfected with HTT Ex1 46Q-EGFP-FKBP1A^{F36V}, HTT Ex1 46Q-NLuc and Halo-LC3B for 24 h before 24 h compound treatment. Data are presented in percentage relative to the DMSO control condition. Data are means ± SD of six replicate samples. **(E)** Summary of all tested compounds in terms of DC_{50} in pDC_{50} as well as the maximum inhibition in %.

The BRET assay showed that there is no difference between the effects of the ATAC compounds with different linker-length. Comparing the pDC50 and maximum inhibition of all tested compounds reveals that the linker-length does have a significant effect on ATAC activity (**Figure 40E**). This property of ATAC simplifies the compound design of ATACs profoundly. As a next step, we want to investigate the kinetics of ATAC mediated HTT degradation. For that purpose, a stable pool of HTT Ex146Q-EGFP-FKBP1A^{F36V} expressing HeLa cells has been generated by lentiviral transduction. In contrast to the transient expression system, the stable pool has an inducible promoter system (Tet on) with which the expression of the HTT construct can be selectively switched on and off in a Doxycycline dependent manner.

Before testing the stable HTT cells, their capability to serve as an aggregation model needs to be confirmed. In order to do so, the stable cells were assessed for their ability to express the HTT constructs and to form HTT aggregates upon Doxycycline treatment as well as the ATAC compound effect needs to be reproduced.

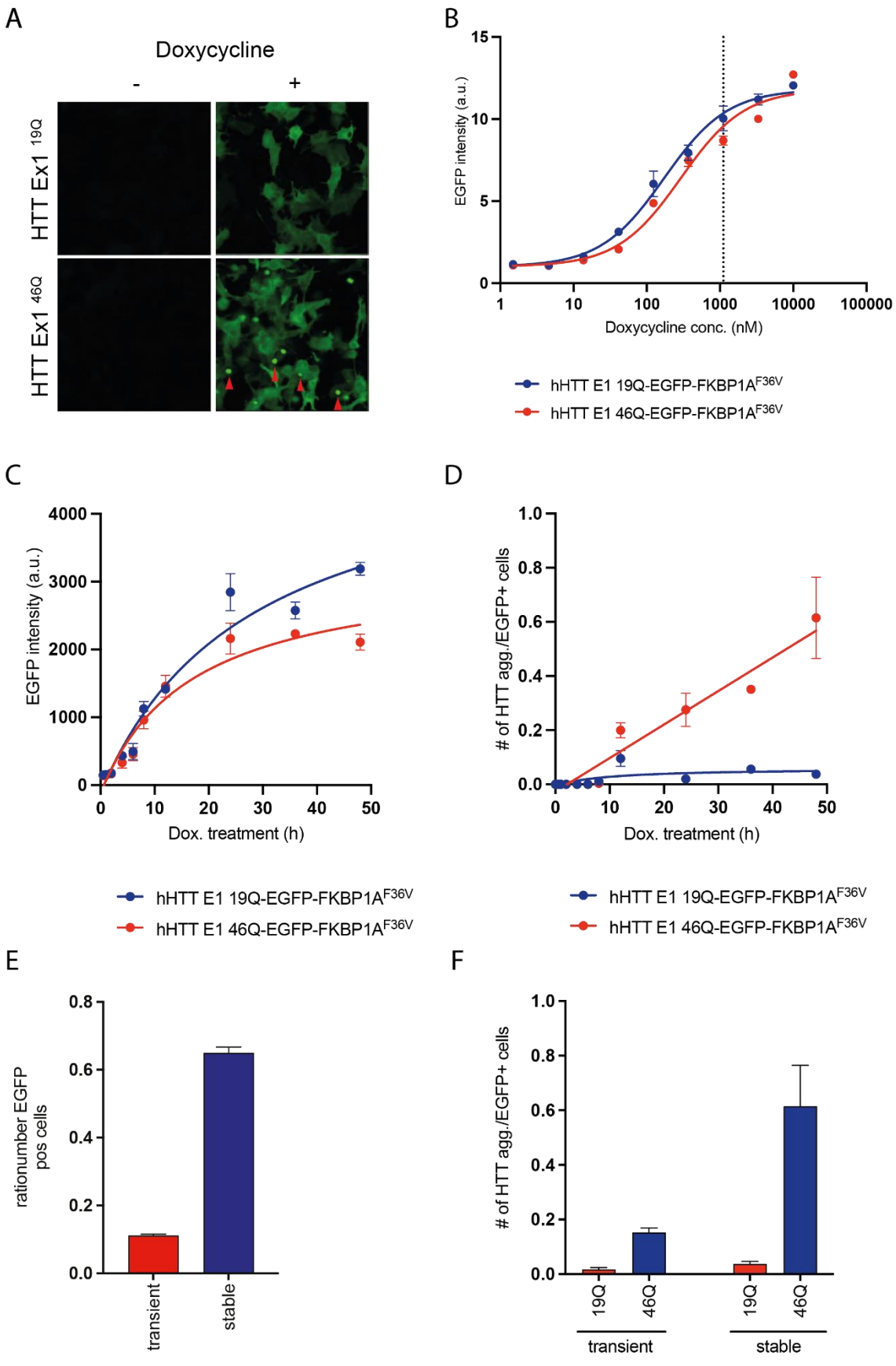
A
Doxycycline
-
+
HTT Ex1 19Q
HTT Ex1 46Q
B
EGFP intensity (a.u.)
Doxycycline conc. (nM)
hHTT E1 19Q-EGFP-FKBP1A F36V
hHTT E1 46Q-EGFP-FKBP1A F36V
C
EGFP intensity (a.u.)
Dox. treatment (h)
hHTT E1 19Q-EGFP-FKBP1A F36V
hHTT E1 46Q-EGFP-FKBP1A F36V
D
# of HTT agg./EGFP+ cells
Dox. treatment (h)
hHTT E1 19Q-EGFP-FKBP1A F36V
hHTT E1 46Q-EGFP-FKBP1A F36V
E
rationumber EGFP pos cells
transient
stable
F
# of HTT agg./EGFP+ cells
19Q
46Q
19Q
46Q
transient
stable

Figure 41 I Validation of the stable HTT expressing cell lines.

(A) Microscopic imaging of HeLa cells stable expressing 19Q and 46Q constructs. Magnification: 40x. **(B)** Image quantification shows same expression for 19Q and 46Q constructs. 1000 nM of Doxycycline (dashed line) has been chosen for further experiments **(C)** Kinetic of Doxycycline treatment shows maximum expression is reached after 24 h of Doxycycline treatment for both HTT cell lines. **(D)** Kinetic of Doxycycline treatment shows continuous increase of aggregate numbers per EGFP positive cell. **(B-D)** Data are means ± SD of six replicate samples. Comparison of transient and stable cell lines show a better transduction efficiency in stable cell lines over the transfection efficiency **(E)**, and a better assay window in stable expressing cells **(F)**.

When using the ICC assay, it can be seen that the Tet-on system works, as both cell lines (19Q and 46Q) only express the HTT fusion proteins when Doxycycline is added to the culture medium (**Figure 41A**). The ICC assay also showed that aggregates are formed in the 46Q expressing cell line, whereas aggregates were not produced for the 19Q expressing cell line (**Figure 41A**). For determination of the optimal Doxycycline concentration to induce HTT protein expression, a titration curve was performed for both cell lines. The quantification of the images in terms of EGFP intensity showed that both cell lines are expressing the fusion constructs (19Q and 46Q) in comparable levels. For further studies a concentration of 1 µM of Doxycycline was used (**Figure 41B**). As a next step the right Doxycycline treatment period was determined by a kinetic. For that purpose, the two stable cell lines were treated with 1 µM of Doxycycline for different periods (2 h - 48 h). The image analysis shows a steep increase of the construct expression and then reaches a plateau after 24 h (**Figure 41C**). In terms of aggregates/ EGFP positive cells, a linear increase of the HTT aggregates can be observed for the 46Q expressing cell line whereas the 19Q cell line does not show an increase of aggregate numbers (**Figure 41D**). As the best assay window was observed at 48 h post Doxycycline treatment, the 48 h has been chosen for further assays. In comparison with the transiently transfected system, it was demonstrated that the transduction efficiency with the lentivirus is about 6x efficient as the plasmid transfection (**Figure 41E**). Comparing the assay window, it can be shown that the stable expressing cell lines show about a 4x increased assay window (**Figure 41F**). With this validation, we demonstrated that the inducible system in stable cell lines is working and that the 46Q cell line can form aggregates as expected.

As a further step before testing kinetics of ATAC mediated HTT degradation, a BRET aggregation assay was performed to determine whether the ATAC compound was working in the stable cell system. For that purpose, the stable HTT Ex1 46Q-EGFP-

FKBP1A^{F36V} expressing cell line was co-transfected with HTT Ex1 46Q-NLuc and Halo-LC3B and treated with the ATAC compound.

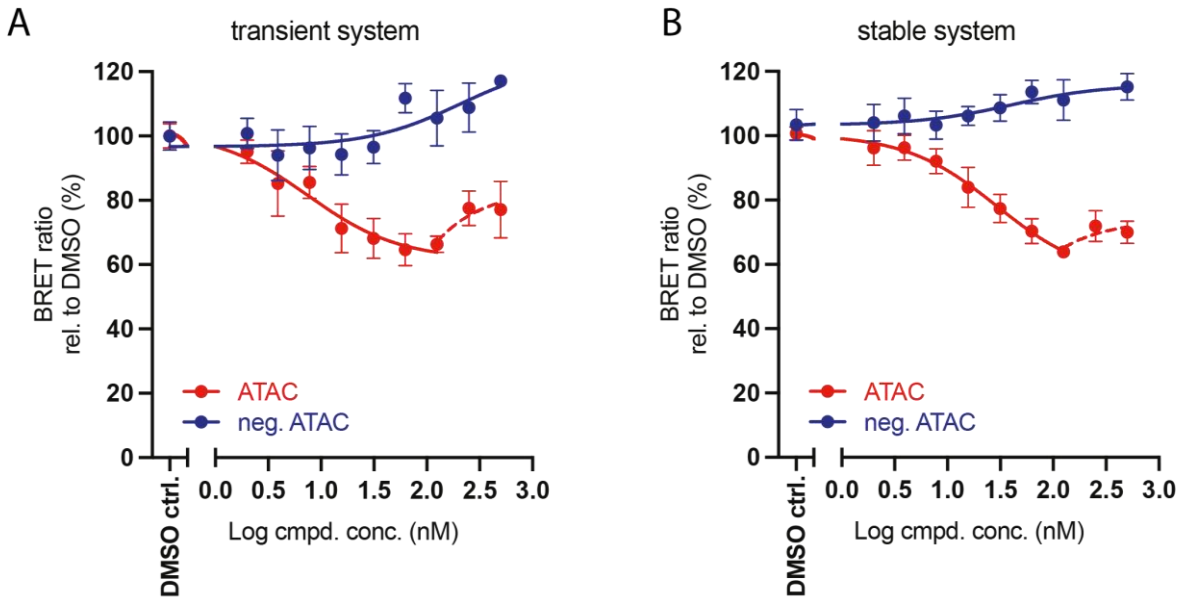

Figure 42 I Comparison of the stable and transient HTT system in BRET assay.
BRET assay shows no difference between **(A)** transient and **(B)** stable HTT aggregation systems. Both conditions showed a max. effect of about 35% with hook effect at 125 nM. HeLa cells were co transfected with **(A)** HTT Ex1 46Q-EGFP-FKBP1A^{F36V}, HTT Ex1 46Q-NLuc and Halo-LC3B or **(B)** HTT Ex1 46Q-NLuc and Halo-LC3B for **(A)** 24 h before 24 h compound treatment and **(B)** 48 h before 24 h compound treatment. Protein expression in the stable cell line was induced by 48 h Doxycycline (1 µM) treatment. Data are presented in percentage relative to the DMSO control condition. Data are means ± SD of quadruplicate samples.

The BRET assay showed that the stable cell line approach works as well as the transient HTT expression approach (**Figure 42**). In both systems, a concentration dependent decrease of the BRET signal can be observed, indicating a degradation of HTT aggregates upon ATAC treatment. The maximum effect of 37% for the transient system and 34% for the stable system is comparable. Both systems showed a hook effect at 125 nM. In order to investigate the kinetics of ATAC mediated degradation of HTT aggregates, a BRET assay over a 50 h period was performed. For that purpose, the NLuc substrate was changed from Furimazine to the expanded live cell substrate Endurazine optimized for the use with NLuc. Endurazine is a commercially available ester conjugated form of Furimazine, requiring ester hydrolysis by cellular esterases to release bioavailable Furimazine[105]. Due to the steady release of Furimazine, experiments of several hours to days can be performed.

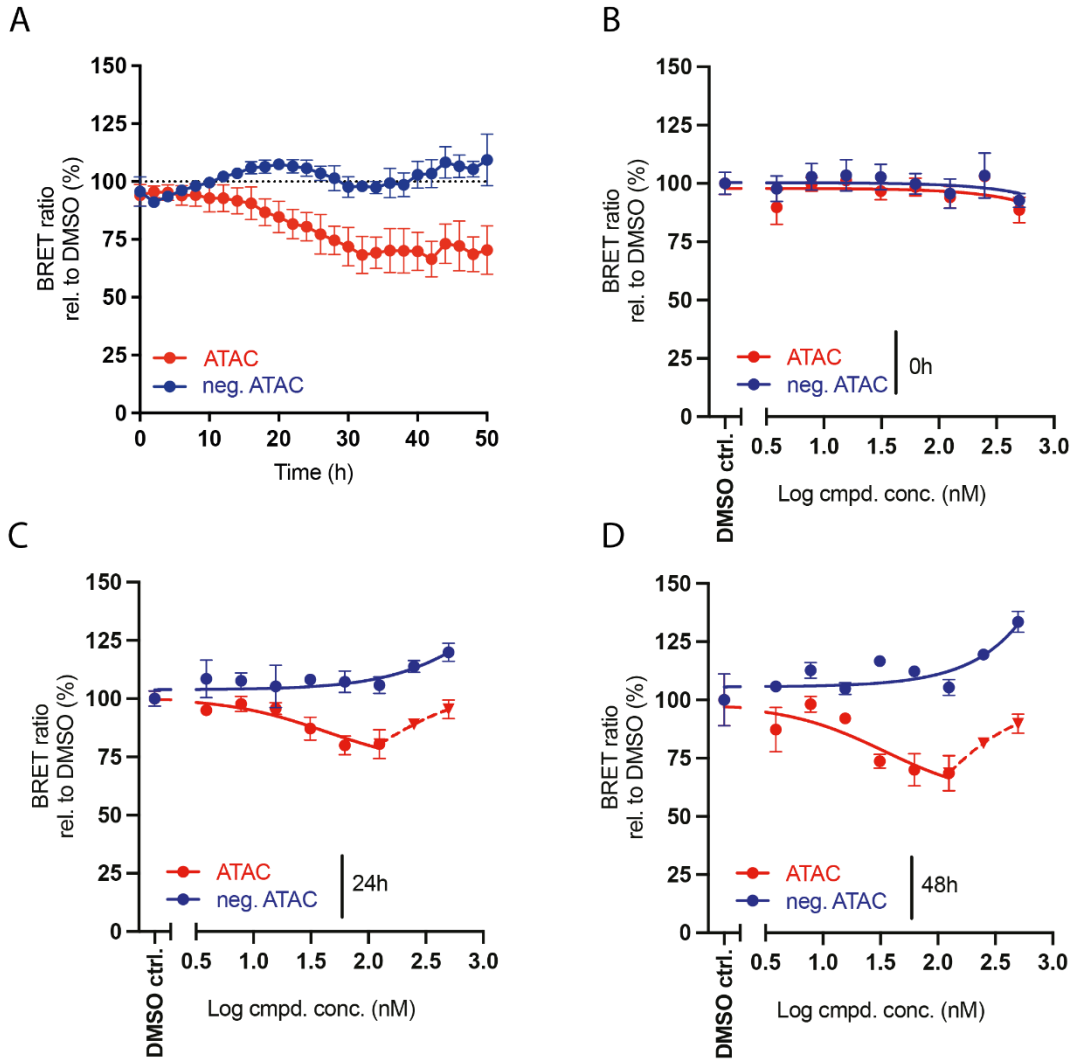

Figure 43 I Kinetic of ATAC mediated HTT degradation in BRET assay.
(A) BRET assay of 125 nM ATAC vs. neg. ATAC compounds in a 50 h kinetic. **(B-D)** Extracted CRCs of **(B)** 0 h, **(C)** 24 h and **(D)** 48 h time points. 24 h and 48 h time points show concentration dependent degrease of BRET signal with hook effect at 125 nM. HeLa cells were co transfected with HTT Ex1 46Q-NLuc and Halo-LC3B for 48 h before 50 h compound treatment. Protein expression in the stable cell line was induced by 48 h Doxycycline (1 µM) treatment. Data are presented in percentage relative to the DMSO control condition. Data are means ± SD of quadruplicate samples.

The kinetic in the BRET aggregation assay showed that that after 33 h of ATAC treatment, the maximum effect of 31% HTT degradation was reached. From this time point no further degradation was observed. When extracting the CRCs of the kinetic, it has been shown that at t=0 h post treatment, no compound effect can be observed as expected. 24 h later, a concentration dependent reduction in BRET signal with a maximum effect of 20% and hook effect at 125 nM was observed. After a further 24 h of compound treatment, a further degradation (maximum effect 31%) was shown, indicating a long-lasting ATAC compound effect.

For future perspective, there is more research necessary, which investigates the kinetics of ATAC mediated degradation of protein aggregates in more detail. Additionally, screening for LC3 binders is needed in order to develop a ATAC which is not dependent on protein tags.

4 Discussion

4.1 Screening for and modulation of autophagy related PPIs

Protein-protein interactions (PPIs) are key for signal transduction and play a crucial role in almost all biological processes[170]. In general, methods for PPI detection can be classified into three categories, *in silico*, *in vitro* and *in vivo* methods[134]. *In silico* methods are based on computer simulations for prediction of PPIs based on protein sequences or structures[134]. *In vitro* PPI assays such as AlphaScreen, TR-FRET or single-molecule fluorescence spectroscopy, using purified proteins or cell lysates, lack the native environment in which the interaction takes place[171]. Due to the fact that PPIs can be highly dynamic, *in vivo* assays using cellular systems for characterization of PPIs have a clear advantage over *in vitro* approaches[172] with regard to studying the modulation of PPIs in dynamic systems such as autophagy. For detection of PPIs *in vivo*, several different techniques have been established[113]. With regard to sensitivity and specificity, each type of method comes with its own strengths and limitations.

The most prominent and applied genetic method for PPI analysis is the Yeast two-hybrid (Y2H) system[173], which was developed in 1989. However, this technique produces a large amount of false-positive hits as a result of auto-activation of reporter genes without the interaction with an interaction partner[174]. Furthermore, the use of yeast as a host may cause interactions of other species not to be detected[175] as the protein of interest needs to be fold correctly and be stable within the yeast cell. This might not be the case when analyzing PPIs of mammalian proteins of interest, where some interactions are dependent on post translational modifications such as glycosylation, phosphorylation or the formation of disulfide bonds[176-177], which may occur inappropriately or not at all in yeast. Another method for the determination of PPIs are spectrometry based approaches such as affinity purification mass spectrometry (AP-MS). After purification, proteins are separated and digested to get protein fragments which can be analyzed in mass spectrometry to identify interacting proteins[178]. However, such mass spectrometry-based approaches just give qualitative information on PPIs[123] and are therefore not suited for investigations of the dynamic processes of autophagy.

Most current PPI detection methods are based on the fusion or interaction of two separate molecules (probes) attached to the proteins of interest[171]. Based on the nature of the assembly or interaction, it can be distinguished between two categories of probes, which are protein-fragment complementation assays (PCA) and two hybrid

assays[113]. PCA assays such as bimolecular fluorescence complementation (BiFC) and bimolecular luminescence complementation (BiLC) assays rely on two non-functional fragments of a reporter protein (fluorescent protein or luciferase)[123]. Once the proteins of interest interact with each other, the two fragments come into close proximity and assemble into the functional reporter emitting measurable fluorescence or luminescence[123]. Based on the fact that in BiFC irreversible protein complexes are formed, it can be used for the detection of weak or transient protein-protein interactions[179]. However, as the protein complex formation of fluorescent protein fragments is irreversible, BiFC cannot be used to study the dissociation of PPIs. Furthermore, the analysis of dynamic systems such as in autophagy which includes formation and dissociation of PPIs might be complicated. A further disadvantage is that many split fluorescence probes tend to self-assemble spontaneously leading to high background[123]. BiLC in turn evades some of the disadvantages of BiFC as the assembly of the luciferase fragments into the functional luciferase is a reversible process, allowing determination of induction as well as dissociation of PPIs. Furthermore, BiLC provides a better signal to background ratio compared to BiFC[123].
The luminescence-based mammalian interactome mapping (LUMIER) also makes use of a luciferase as a reporter[175]. This co-immunoprecipitation-based assay detects PPIs by a luminescence signal upon co-precipitation. However, as LUMIER is dependent on cell lysis, it is not capable to detect the dynamics of an interaction in a live cell and therefore is not suitable for studying autophagy related PPIs[175]. Among the fluorescence or luminescence reporter assays, there are further assays using the expression of a reporter gene to detect a PPI. Approaches such as the mammalian protein–protein interaction trap (MAPPIT), kinase substrate sensor (KISS) and mammalian membrane two hybrid (MaMTH) are based on a bait prey system[175]. However, as MaMTH and MAPPIT are limited to interactions located at the cytosolic submembrane region[175], this assay cannot be used for autophagy related PPIs. As all the reporter gene expression based assays only detect PPIs indirectly[175], we preferred to use a method for direct detection of PPIs. Biosensor based approaches such as FRET and BRET rely on two discrete molecules, each functional in its own. Both techniques use proteins of interest tagged with appropriate donor (fluorophore, luciferase) and acceptor molecules (fluorophore or dark quencher)[171,180-181]. FRET and BRET methods rely on the non-radiative energy transfer from the donor to the acceptor, where through long-range dipole-dipole interaction the acceptor gets excited

and emits light. Using donor saturation assays in FRET and BRET, where cells express constant amounts of donor tagged proteins and increasing amounts of acceptor tagged proteins, quantitative data about a PPI can be obtained [123,180]. By calculating $FRET_{50}$ or $BRET_{50}$ values, the binding strength between two proteins can be estimated.

The fact that FRET assays show a low signal/background ratio impedes the assay performance in high throughput approaches. Furthermore, FRET assays require an artificially strong overexpression of the proteins of interest which might lead to artefacts by affecting its endogenous function. Additionally, photobleaching of the fluorophores, which poses a problem in time lapse experiments, outlines a further limitation of FRET assays[182]. BRET in turn circumvents many issues of FRET as it uses a luciferase instead of a fluorescent protein as a donor. This replacement enables the use of a substrate instead of an external light source for activation and prevents cell auto-fluorescence. The oxidation of the substrate by the luciferase leads to the emission of light which is transferred to the acceptor by a process of dipole-dipole non-radiative energy transfer[114]. Furthermore, the strong light emission of the luciferase allows the use of lower protein expression and leads to a superior signal/background ratio (this can circumvent artefacts due to an artificial, strong overexpression of the proteins of interest)[183].

To date very few autophagy related PPIs such as the mTOR-FKBP12 interaction have been analyzed in a quantitative manner[110]. In order to get new insights into the mode of action of new autophagy modulating compounds, quantitative analysis of PPIs is essential. Moreover, new findings about the modification of autophagy related PPIs by small molecules might facilitate screening for novel autophagy modulators.

Prior work has established that BRET assays are a valuable tool for studying PPIs in living cells as well as in isolation[115,123,127]. In order to validate the BRET assay for our purposes of modulating autophagy related PPIs, donor saturation assays of reference PPIs as well as modulation studies were performed. Previously, the interaction between BAD and BCL-2 has already been described by using various methods. Maiuri *et al.* showed the interaction by using co-precipitation based assays[184], but BRET assays were also already performed to detect the BAD-BCL-2 interaction[185]. With the data obtained from donor saturation assays, we confirmed the data from Pecot *et al.*[185] and Trepte *et al.*[115] who used similar BRET based approaches. With the donor saturation experiment, we validated the BRET assay as a powerful tool to study PPIs and as a suitable technique for investigating PPIs in a quantitative manner.

As this project aims for the modulation of autophagy related PPIs, we have investigated whether the BRET assay is sensitive enough to determine the influence of mutations on PPIs. Pattingre *et al.* have shown that a single point mutation (F123A) in the BH3 domain of BECN1 disrupts its interaction with BCL-2[146]. Maiuri *et al.* showed in a fluorescence polarization assay that BECN1 with a F123A mutation does not bind to BCL-XL[184]. However, in our BRET donor saturation experiment, we were not able to observe a full inhibition of the interaction between mutant BECN1 and BCL-2. The curves remain hyperbolic for BECN1 F123A and the BH3 deletion mutant which indicate a that both interaction partners continue to be in close proximity to each other. The differences between our findings and the results of Maiuri *et al.* might be due to the fact that Maiuri *et al.* analyzed the interaction using purified proteins. It is well established that BECN1 forms homo dimers in its inactive state[186]. This behavior may explain the remaining BRET signal for mutant BECN1 proteins as mutant BECN1 can form heterodimers with endogenous BECN1 proteins. Endogenous BECN1 can bind to BCL-2, which brings BECN1mt-NLuc and mCitrine-BCL-2 in a close vicinity. However, the fact that the BRET max is strongly reduced, suggests that the donor and acceptor are not in direct contact, supporting the heterotrimer hypothesis. Using the BRET assay, we showed the influence of point mutations on PPIs and confirmed the findings of Han *et al.*[130] and Trepte *et al.*[187]. Due to the fact that we detect a remaining affinity of the BECN1 mutation for BCL-2, we additionally validated the BRET assay with a STX1A binding deficient mutant of STXBP1 confirming the results of Trepte *et al.*[115]. Our data shows the sensitivity of the BRET assay to detect point mutation induced effects on PPIs. However, attention should be paid to the possibility of a remaining BRET signal due to the formation of protein complexes. In the case of known protein complex members, an assay under knockdown or knockout conditions could be performed. In that case, silencing the protein bridging the two interaction partners may prevent complex formation and the previously detected PPI cannot be detected. We found that the BRET assay is a sensitive tool for investigating PPIs and its modulation by small molecules as well as on a genetic level.

The molecular function of a protein in cellular processes cannot be fully understood without information on its interaction with other proteins. As many cellular processes are highly dynamic, quantitative analysis of PPIs is essential. Qualitative approaches to determine PPIs only give a yes or no answer about whether two proteins interact with each other but does not give any information to what extent. In order to monitor

binding affinities and lifetimes of PPIs giving information about the dynamic nature of PPIs, quantitative approaches are of high importance[123]. Quantitative analysis of PPIs can detect changes of the binding strength which might be concealed for qualitative approaches. To address the objective of analyzing autophagy related PPIs in a quantitative manner, donor saturation assays were performed for PPIs at different stages of the autophagic pathway. A focused screen for PPIs involved in the autophagic cascade, confirmed most previously published PPIs. 70% of the analyzed PPIs, listed in the HIPPIE database, were confirmed with the BRET assay, demonstrating the validity of the assay. It was shown that the confirmation rate between the interactions at the different stages of the autophagic pathway is consistent, further confirming the validity of the BRET assay for analyzing autophagy related PPIs. As expected, we found a clear correlation between the HIPPIE score and the confirmation rate. Nevertheless, PPIs not in the HIPPIE database which are usually not well characterized were still found at a confirmation rate of 57%.

Among the listed interactions, the BRET assay detected four PPIs, which were so far not listed in the HIPPIE database. Among these are the interactions between LC3A and LC3B with STX17, which are all autophagosomal membrane proteins. This finding is in line with a recent publication by Kumar *et al.* who described the recruitment of STX17 to the autophagosomal membrane. A vital role during this process plays the immunity-related GTPase M (IRGM) which mediates the recruitment of STX17 to the autophagosome as well as its integration into the autophagosomal membrane[135]. IRGM has been shown to interact directly with STX17 and LC3 forming a protein complex called autophagosome recognition particle (ARP) which facilitates the delivery to autophagosomal membranes[135]. Another PPI was found for ATG12 and TRIM50. TRIM50 is an E3-ligase which is involved in the regulation of the initiation phase of starvation induced autophagy by BECN1 polyubiquitination and association to ULK1[188]. ATG12 has been described to be involved in the autophagosome formation by complexing with ATG5 and ATG16[189]. So far, the interaction between ATG12 and TRIM50 has not been reported and needs further investigation. Few autophagic targets of TRIM50 have been identified so far, limiting the understanding of the molecular mechanism of TRIM50 mediated autophagy modulation[190]. New insights into TRIM50-ATG12 PPI could lead to the identification of new targets for drug discovery.

For 20% of the analyzed protein pairs, the BRET assay was not able to confirm the interactions listed in the HIPPIE database. This discrepancy might be due to the nature

of the BRET assay where the proteins of interest are tagged with donor and acceptor molecules. It´s possible that the tag of one or both interaction partners interfere with the PPI due to interferences with the binding domain. In some cases, this issue can be resolved by switching the terminus of the tag, as this might remove the tag from the binding domain and proper binding of the interaction partner can take place. Furthermore, the Luciferase and fluorescent protein tags might also affect the subcellular localization, protein folding and function of the target proteins.

The presented PPI-network is based on interaction data deduced from quantitative analysis with the BRET assay, combined with additional data from the HIPPIE database. One unique feature of this autophagy PPI network is the quantitative information about the binding affinity of the interaction partners. While the results of many conventional PPI assays demonstrate a static map of physical connections between proteins, no information on binding affinities and dynamics in such networks are given[191]. For a better understanding of cellular processes, quantitative information on PPIs is of particular importance in order to detect changes of the affinity of two proteins to each other. As the autophagy cascade is a highly dynamic and complex process, regulated by many PPIs involved in multiple steps, quantitative analysis is necessary for a better understanding of the underlying processes. The BRET assay overcomes the limitation of qualitative methods since the detection of PPIs takes place in a quantitative manner in living cells. This gives information about the binding strengths and affinity as well as the dynamics of PPIs in a living cell environment which cannot be extracted from qualitative data.

The presented network represents a small fraction of all autophagy related PPIs. In order to get a more detailed network of autophagy related PPIs it is necessary to expand the number of PPIs analyzed in a quantitative manner. For a future perspective it would also be interesting to test the behavior of the autophagy related PPIs in response to autophagy stimulating or inhibiting stimuli. This data could give in-depth insights into the dynamics of autophagy related PPIs as well as identifying new potential drug targets. Based on the created network two PPIs (BECN1-BCL-2 as well as STX17-VAMP8), involved in autophagy induction as well as autophagosome lysosome fusion event, were identified as interesting interactions that warrant further investigation.

In the last 30 years, autophagy research was focused on early steps such as induction and autophagosome formation[136]. Later stages like the autophagosome lysosome

fusion event were less studied. Recently, the fusion event of autophagosomes and lysosomes attracted increasing attention[136], resulting in many publications describing the fusion process on a molecular level[68,85,135,192]. From these studies, it becomes apparent that the interaction between STX17 and VAMP8 plays a central role in the fusion event. This interaction may serve as a kind of probe for monitoring the autophagic flux in living cells. Based on the fact that the BECN1-BCL-2 interaction and its inhibition play a key role in autophagy induction[193], modulation studies using BRET assay may give new insights into its eligibility as a new therapeutic target. The BRET assay for the interaction of STX17 and VAMP8 might be a promising tool for monitoring autophagic flux. As the fusion proteins do not require a high expression, the BRET assay can be performed at endogenous like protein levels. Compared to other methods, the BRET assay can give real time information on autophagic flux in living cells and is therefore superior over traditional immunoassays such as TR-FRET or Western Blot. Furthermore, the BRET assay is sensitive to detect fusion blockage as well as induction of autophagic flux without the need of comparing two samples with and without lysosomal inhibition. The good signal to background ratio of the BRET assay makes it superior over the RFP-GFP-LC3 probe approaches which also detect the fusion event in living cells. Furthermore, the BRET assay does not suffer from reabsorption issues such as in RFP-GFP-LC3 probes, also FRET from GFP to RFP can be excluded by using BRET assay.

As a future perspective, the BRET assay for the interaction between STX17 and VAMP8 needs to be validated by autophagy modulating stimuli such as starvation, genetical and pharmacological interventions. Autophagy induction can take place by small molecule treatment with Rapamycin and Torin1. Autophagy inhibition can be achieved by autophagy blockers such as Bafilomycin and Chloroquine or the knockdown of key autophagy genes such as ATG5. After successful validation, the interaction between STX17 and VAMP8 could be used for a novel targeted screen for autophagy modulating compounds. Furthermore, using a stable Cas9, NLuc-STX17 and mCitrine-VAMP8 expressing cell lines could be used for genome wide screens for fusion modulating proteins by CRISPR/Cas9 screen. Therefore, endogenous STX17 and VAMP8 proteins can be tagged by CRISPR Cas9 to work with endogenous protein levels. Proteins of the hit genes of the CRISPR/Cas9 screen can be targets for further drug development of new autophagy modulating compounds. Additionally, hits from

the genetic screen might give new insights into the molecular basis of the fusion event between autophagosome and lysosome.

In 1998, Liang *et al.* described BECN1 as the first discovered mammalian autophagy gene and BCL-2 interacting protein[194]. Further research revealed that BECN1 is not only a positive regulator of autophagy, but also involved in other cellular processes such as apoptosis, cytokinesis and endocytosis[195]. Early studies found the interaction between BECN1 and BCL-2 as autophagy inhibitory. As BECN1 homodimerizes in its inactive state and is stabilized by BCL-2, it cannot promote autophagosome formation[151].

In order to investigate the BECN1-BCL-2 PPI as a possible target for autophagy induction, pharmacological interventions to disrupt the interaction between BECN1 and BCL-2 have been addressed. As BECN1 binds with its BH3 domain to the hydrophobic groove of BCL-2, competitors for this binding site could dissociate BECN1 from BCL-2[196]. Indeed, previous studies have shown that BH3 mimetic small molecules such as Navitoclax can inhibit the interaction between BECN1 and BCL-2[132]. It has been previously described that BH3 mimetics do not only inhibit the interaction between BECN1 and BCL-2 as well as BCL-2L1, but also the interaction between the apoptosis regulator BCL-2 associated X Protein (BAX) and BCL-2 homologous antagonist/killer (BAK) with BCL-2 and BCL-2L1[151]. Once dissociated from BCL-2/-2L1 BAX and BAK induce apoptosis by forming pores in the outer mitochondrial membrane[150]. Due to the fact that the autophagy inducing effect of current BH3 mimetics is inevitably associated with the induction of apoptosis, there is a need for small molecules selectively inducing the dissociation between BECN1 and BCL-2/-2L1 without affecting the interaction of BCL-2/-2L1 with BAX and BAK. In 2018, Chiang *et al.* identified this issue and screened for selective BECN1-BCL-2/-2L1 inhibitors[132]. This led to the identification of SW063058 and SW076956 respectively, with the desired properties. Our attempts to confirm the activity of these compounds demonstrated no disrupting effect on the interaction between BECN1 and BCL-2. Furthermore, assessing autophagic activity in HEK293 and human iPSC-derived neurons indicate that SW063058 does not induce autophagy.

Our data shows the autophagy inducing effect of BH3 mimetic treatment. However, this effect cannot clearly be related to the disruption of the interaction between BECN1 and BCL-2, as BH3 mimetics are also able to influence other PPIs such as the interaction between BECN1 and BAX or BAK. The autophagy inducing effect is

accompanied by toxicity as the BCL-2 and BCL-2L1 are also involved in apoptotic pathways. The exact mode of action of autophagy induction mediated by BH3 mimetics is still controversially discussed. There are two proposed models explaining the autophagy inducing effect of BH3 mimetic mediated BCL-2 inhibition. The conventional model is that BCL-2 and family members bind to BECN1 and inhibit autophagy by preventing the formation of BECN1-Vps34 complexes[132,151]. The alternative model claims that inhibition of BCL-2 releases BAX and BAK which induces autophagy via an unknown mechanism[149]. Reljic *et al.* claim that the induction of autophagy by BCL-2 inhibition takes place indirectly by a BAX and BAK dependent pathway. Using HTC116 cells, they demonstrated that BCL-2 inhibition by overexpression of BH3 only proteins or BH3 mimetic compounds leads to autophagy induction only if BAX and BAK are present. BAX and BAK1 double knockout cells showed no response to compounds in terms of autophagy induction[149]. Furthermore, Reljic *et al.* argue that the concentration of BH3 mimetic compounds required to induce a BAK and BAX independent lipidation is too high to represent on-target activity[149]. In contrast to RelJic *et al.* Fernández *et al.* demonstrated in mutant BECN1 (unable to bind to BCL-2) mice an increased basal autophagy rate which is associated with an increased lifespan[197], implying beneficial effects of disrupting the BECN1-BCL-2 interaction. So far, the role of the interaction between BECN1 and BCL-2 and its eligibility as a drug target remains controversially discussed in the literature.

It has been shown by Liu *et al.,* that the disruption of the BECN1-BCL-2 interaction induces autophagy[145]. However, Reljic *et al.* postulated that the autophagy inducing effect does not depend on the disruption of BECN1 from BCL-2, but on the disruption of the binding of BCL-2 to BAX and BAK[149]. The apoptosis regulator BCL-2 associated X Protein (BAX) and BCL-2 homologous antagonist/killer (BAK) are two BH3 domain containing proteins involved in apoptosis induction[198]. In order to unravel the role of the interaction between BECN1 and BCL-2, further research is required. Apart from its BECN1-BCL-2 disrupting effect, BH3 mimetics have also been shown to activate further pro-autophagic pathways such as mTOR and IKK and AMPK[147], which can also be promising targets for autophagy induction. Using cell lines resistant to the apoptotic effect of the BH3 mimetic ABT737, Malik *et al.* demonstrated that BH3 mimetic has an inhibiting effect on mTOR which in turn induces autophagy[147]. Furthermore, the activation of the IκB kinase (IKK) complex as well as the AMP-activated kinase (AMPK) by ABT737 has been described[147]. IKK is an upstream

regulator of the nuclear factor κB (NF-κB) pathway. AMPK induces autophagy by association and activation of autophagy inducing kinase ULK1, the most upstream component of the autophagy pathway[199].

As a future perspective, the interaction between BECN1 and BCL-2 seems to be a promising target for drug development, but as BH3 mimetic compounds were initially developed for induction of apoptosis in cancer treatment, new compounds need to be developed which selectively activate the autophagy cascade. In order to screen for new compounds, more research on the mode of action of BH3 mimetics in terms of the interplay of autophagy and apoptosis induction is needed.

4.2 Development of autophagy targeting chimera for targeted degradation of protein aggregates

The autophagy system is an efficient, intracellular degradation system for the response to environmental and cellular stresses. Autophagy plays a fundamental role in maintaining tissue homeostasis and is associated with a wide spectrum of human pathophysiological conditions including neurodegenerative diseases[67-68]. In order to exploit the autophagosomal pathway for therapeutic purposes, we developed ATACs to recruit disease associated protein aggregates to phagophores to promote their degradation. Most of the research efforts for targeted degradation of pathogenic proteins was focused on the development of PROTACs. However, PROTACs are dependent on the UPS which makes them inefficient in degrading large assembled pathogenic proteins, which may contribute to the onset of neurodegenerative diseases[53]. An important aspect of ATACs is that in theory they can be applied to large structures such as protein aggregates, microbial pathogens or even whole organelles[38]. This property makes the ATAC approach complementary to the PROTAC approach.

The basis of our approach is a heterobifunctional small molecule that serves as a bridge to link target proteins to the autophagosomal membrane protein LC3B for its subsequent degradation. We hypothesized that the development of ATACs would overcome some of the limitations of PROTACs, namely a limitation to the degradation of soluble intracellular proteins. Additionally, we expected that the linker length would not have a substantial influence on ATAC efficacy, as no modification of the target proteins is required for lysosomal degradation. Furthermore, additionally to the eased linker design, also the identification of a suitable binder for the target protein might be eased as the effect is not dependent on a specific binding site on the target as

observed for PROTACs[200] .

The aim of the current work was to show that ATACs can increase the degradation of given target proteins that play a causal role in neurodegenerative diseases. For that purpose, we chose the microtubule associated protein Tau as well as Huntingtin due to its well-characterized association with Alzheimer's disease and Huntington's disease, respectively[201-202].

Due to the fact that autophagy receptors such as p62, or optineurin contain an ubiquitin binding domain (UBA) and a LC3 interaction region (LIR), these proteins are inborn bifunctional molecules. Autophagy receptors can bind via its UBA to ubiquitinated proteins and connect these proteins to LC3[203]. For our proof-of-concept (PoC) study of tagging an aggregation prone Tau mutant with a LIR tag, first we first confirmed the binding of different LIRs to LC3. PoC experiments using RavZ-LIR tagged Tau40 constructs revealed that a direct connection between Tau40$^{P301S/S320F}$ and LC3 induces the degradation of protein aggregates. The two negative controls (non-tagged mutant Tau40 and LIRmt-tagged mutant Tau40) showed no effect further suggesting that the LIR triggers the degradation of the Tau40 aggregates. LIR induced degradation prefers to target aggregates over soluble proteins. Long time starvation for 24 h even showed a slight reduction in soluble Tau suggesting that ATACs might also induce the degradation of soluble proteins to some extent. The observation that aggregates are more efficiently degraded, might be due to the fact that aggregates are composed of many Tau proteins increasing the avidity as more LIR tags are available which can interact with the LC3B. Furthermore, protein aggregates may act as nucleation sites for emerging phagophores. Itakura *et al.* observed that p62 oligomers provided many LIRs, co-localized with the autophagosome emerging site[204]. This observation further supports the theory that utilizing the autophagic machinery for targeted degradation is preferred in oligomers and aggregates rather than in monomers.

Based on the data of the PoC experiment, a HTT based cellular assay was developed to investigate whether this degradation can be modulated using bifunctional molecules. As there are currently no well-established small molecule ligands for LC3 available, protein tags were used for well described ligands. Therefore, a tagging system using FKBP1A^{F36V} and HaloTag, was set up. Based on the work of Clackson *et al.*, the synthetic ligand of FKBP (SLF) moiety was used to target FKBP1A^{F36V} HTT[205]. The effector protein LC3B was tagged with a HaloTag, which acts as a binding site for chloroalkanes to recruit the target proteins to the phagophore. The results reported

here indicate that ATACs induce the degradation of HTT aggregates in a concentration dependent manner. From the BRET experiments, comparing ternary complex formation between the HTT construct, the ATAC and either Halo-LC3 or SIAH1^{C44S}-Halo (SIAH1^{C44S} is an inactive E3-ligase mutation[164]) it is clear that the reduction in HTT aggregates is not due to the ternary complex formation with Halo-tagged proteins. Rather, it shows that the aggregate degradation is dependent on the ternary complex formation with Halo-LC3B, indicating the autophagy driven MoA of ATACs. For further research, it would be important to test Halo-tagged proteins as negative controls which are not involved in any degradation pathway, as unknown functions of the mutant SIAH1 regarding the UPS pathway cannot be excluded.

During the progress of this project, Li *et al.* published a similar approach harnessing the autophagic pathway for the removal of mutant HTT(mHTT)[49,51]. Here, autophagy tethering compounds (ATTEC) were described as specific molecular glues tethering target proteins to LC3 for its subsequent lysosomal degradation. Their results showed a promising and allele selective lowering of mHTT in cellular and animal models of Huntington's disease[49]. However, in-house experiments could not reproduce the activity of the compounds (internal communication). Furthermore, Li *et al.* demonstrated that the same ATTEC compounds also degrade mutant Ataxin3 which give rise to doubts about its target specificity. The approach of developing or screening for molecular glues tethering target proteins to LC3, is a similar approach to our ATACs. In a follow up publication, Fu *et al.* used this molecular glue as an LC3 binder for the development of bifunctional ATTECs[206]. But as molecular glues are not bifunctional molecules, its adaption to different target proteins is expected to be challenging. However, despite the more drug like properties of molecular glues, screening for small molecules binding to two proteins (target and effector) further complicates drug development. For these reasons, the ATAC approach might be superior to ATTEC.

We hypothesized that the MoA of ATACs is due to induced connection between cargo and phagophores, thus we have addressed the autophagy dependency by different autophagy modulating stimuli. As the PoC experiment already suggested, starvation also enhanced the ATAC mediated degradation, further suggesting that the degradation is autophagy specific and not due to alternative pathways. Autophagy inhibition studies further completed the picture of the autophagy driven MoA of ATAC. We were able to show that inhibition of autophagy, either by genetic or by

pharmacological intervention, decreases ATAC mediated HTT degradation. Taken together, the induction and inhibition of autophagy is able to change the effect of ATACs suggesting that the degradation is autophagy driven. Nevertheless, the autophagy modulation approaches to inhibit the degradation of HTT did not lead to a full inhibition of the ATAC effect. Therefore, it would be interesting to test the effect of impaired autophagic activity in autophagy deficient (ATG5 knockout) cell lines. Knockdown of the key autophagy gene Atg5 is a common method to suppress autophagy and to demonstrate autophagy dependent MoA, as performed by Li *et al.*[49] and Takahashi *et al.*[52]*.*

Due to the fact that the composition of the linker and its length plays a key role in PROTAC design for ideal ubiquitination, the target protein needs to be in the right orientation to the E2-E3-ligase complex. Linkers which are too long or too short in length may affect protein ubiquitination in a negative way, which complicates PROTAC design considerably[48,163]. Therefore, there is no general strategy for the linker design available[163]. Optimization of the bioactivity of a PROTAC via the synthetic alteration of the linker is usually achieved by an iterative trial and error approach. Based on the assumption that for ATAC mediated degradation, the target protein only needs to be connected with the autophagosome and no further processing is required, we hypothesize that the linker length plays a subordinate role. By comparison of ATACs with different linker lengths, we have demonstrated that activity of the analyzed ATACs is indistinguishable, supporting our initial hypothesis. This could be a major advantage over PROTACs, as it eases the design of ATAC compounds substantially.

From kinetic experiments, it was observed that the onset of the degradation is between 10 and 12 h post treatment. As in many publications, the onset of autophagic activity was observed much faster (2-4 h)[94,91]. Using the AuTAC approach harnessing the autophagic machinery, Takahashi *et al.* demonstrated that the onset of the degradation of mitochondria was shown at about 12 h post treatment[52]. However, as the AuTAC approach requires K63 linked ubiquitination which was observed for about 8 h post treatment, the AuTAC mediated degradation might be delayed by this process. Due to the fact, that the kinetic was performed under high overexpression of mHTT, the observation of first compound effects might be delayed. Using lower expression levels of mHTT might lead to an earlier observation of a degradative effect. Furthermore, the experiments have been done under basal autophagic activity, which further explains the late onset of ATAC effect. Using a condition with higher autophagic activity (e.g.,

under starvation) or cells with higher basal autophagic activity might lead to a decreased lag phase between treatment and effect.

Taken together, we have developed a method to degrade protein aggregates via the autophagosomal pathway by targeting protein aggregates to the autophagosome. The degradation process has been shown to be autophagy driven and to be largely independent of the linker length of the ATAC compound. The concept of selective degradation of large structures such as aggregates via the autophagy pathway represents a promising starting point for further expansion to degrade organelles and non proteinous biomolecules such as mitochondria, peroxisomes or lipid droplets.

The degradation of organelles via the autophagic pathway (organellophagy) plays a crucial role in maintaining cellular homeostasis. The accumulation of dysfunctional and damaged mitochondria has been associated with a high variety of human diseases such as cancer, cardio vascular diseases and neurodegeneration[207-208]. The induction of mitophagy has been shown to be cytoprotective by lowering the levels of reactive oxygen species[208]. The selective degradation of dysfunctional or redundant organelles might be a promising target for ATAC development. In 2019, Takahashi *et al.* demonstrated the targeted degradation of Mitochondria using AuTACs targeting the mitochondrial translocator protein (TSPO) which is located on the outer mitochondrial membrane[52]. Also, the targeted degradation of lipid droplets by ATTECs has been addressed by Fu *et al.*[206].

Furthermore, ATAC might also be an interesting approach to promote the process of LC3 associated phagocytosis (LAP). LAP plays a role in immune regulation and inflammatory responses by the degradation of phagocytosed materials such as pathogens, dying cells or protein aggregates[209]. The dysregulation of LAP has been reported to increase with age and to contribute to an increased susceptibility to many infectious diseases[210]. Here, ATAC compounds could support the recruitment of LC3 to the phagosome after internalization of apoptotic cells, protein aggregates or pathogens to restore LAP activity. The ATAC approach opens up a new direction of research in the field of targeted degradation by extending the scope of targets to larger structures such as aggregates or organelles. Compared to the PROTAC approach, ATACs are superior in degrading aggregates, as PROTACs UPS dependency limits the scope of targeted proteins to soluble small proteins. Based on the small diameter of the proteasome, PROTACs cannot induce the degradation of protein aggregates directly, as these cannot be processed by the proteasome[211]. For PROTACs, the scope

of druggable proteins is limited to soluble proteins, whereas ATACs might be capable of targeting oligomers and aggregates as well as non-proteinous structures by supporting LAP processes.

However, despite the advantages of ATACs over PROTACs, there are also some possible limitations of ATACs. PROTACs have the potential to act tissue specific, as the more than 600 human E3-ligases are not equally distributed among different tissues[40]. In terms of the ATAC, there is not such a wide scope of effector proteins available. Furthermore, autophagosomal proteins are ubiquitously expressed, making the ATAC approach less tissue specific[212]. However, there are seven ATG8 family members described[213] which may also contribute to some selectivity as these proteins may not be even distributed among tissues. Another level of selectivity may be achieved by the different basal autophagy activity among tissues[214]. Furthermore, expanding the range of effector proteins from autophagosomal proteins to autophagy receptors, could show some tissue specificity which can positively affect tissue specificity of ATACs. Additionally, ATACs targeting p62 as an effector protein might be beneficial in terms of the compound efficacy. Due to the fact that the autophagy receptor p62 forms homo oligomers[215] including many LC3 binding sites, the affinity between target proteins and the phagophore might be increased. It has been shown that oligomers bound to selective autophagy receptors such as p62, act as a nucleation site for an emerging phagophore[216]. Another minor drawback of ATACs in comparison with PROTACs might be the fact that the compound is assumed to be degraded in the lysosomal environment.However, PROTACs can be recycled and process more than one protein, as PROTACs are not degraded[39]. Due to this recycling mechanism, only low PROTAC concentrations in picomolar concentrations are needed whereas it might be possible that higher concentrations of ATACs are necessary.

During the progress of this project, further research groups developed similar concepts of targeted autophagy inducers such as ATTEC, AuTAC and LYTAC which shows the high interest in targeted degradation harnessing the autophagic pathway. In order to degrade proteasome resistant proteins, Banik *et al.* developed lysosome targeting chimera (LYTAC) targeting extracellular and membrane proteins (**Figure 44A**). LYTACs consist of an antibody against the target protein of interest and a polymer of mannose-6-phosphate (M6P)[217]. After the ternary complex is formed between the target protein, LYTAC and M6P, the target is degraded via the lysosomal pathway which is induced by binding of M6P to the cationic M6P receptor[217]. However, as this

concept is dependent on the outer membrane bound M6P receptor, this concept cannot be applied to intracellular aggregates.

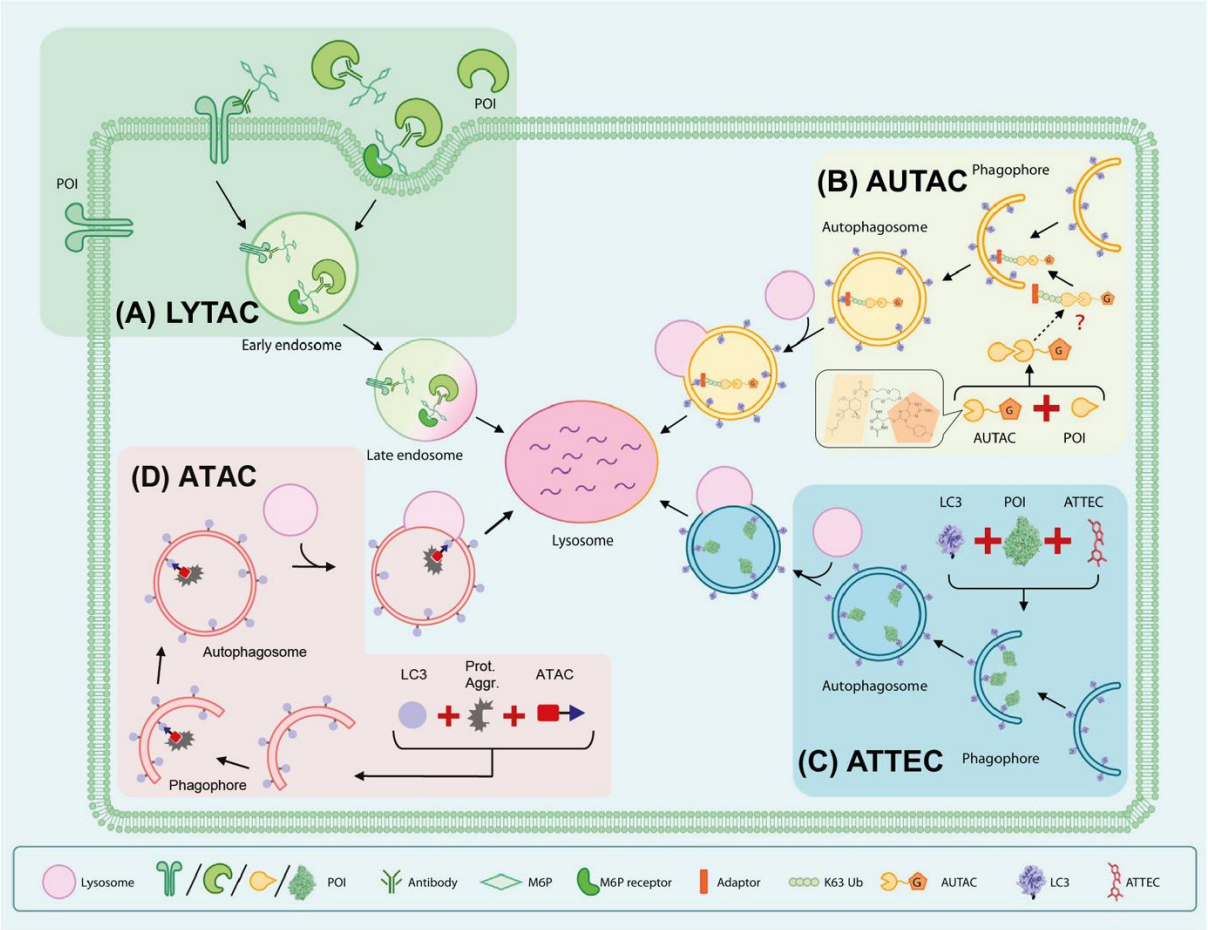

Figure 44 I Comparison of different autophagy utilizing approaches for targeted degradation
(A) LYTACs targeting extracellular proteins of interest. POI are degraded after receptor mediated internalization. **(B)** AUTACs targeting intracellular proteins by K63 ubiquitination and subsequent degradation via the autophagic system. **(C)** ATTECs are molecular glues binding simultaneously to target proteins and LC3. The bound target protein will be degraded via the autophagic system. **(D)** ATACs are bifunctional small molecule compounds connecting protein aggregates to LC3 leading to its subsequent degradation. Figure adapted from Ding *et al.*[38]

In 2019, Takahashi *et al.* developed Autophagy targeting chimera (AuTAC) (**Figure 44B**). The MoA of AuTACs is the K63 linked ubiquitination of target proteins. AuTACs consist of a ligand for the target protein, a p-fluorobenzylguanine (FBnG) moiety and a PEG linker connecting the two moieties[52]. The mechanism of action of the AuTACs is not fully understood, but Takahashi *et al.* have shown that AuTAC treatment leads to the K63 linked ubiquitination of the target protein and its subsequent degradation via the autophagosome pathway[52]. Also in 2019, Li *et al*. developed autophagy tethering compounds (ATTEC) as a more direct way of utilizing autophagy

for targeted degradation (**Figure 44C**). ATTECs are molecular glues inducing the interaction between target proteins and the autophagosomal membrane protein LC3[51]. Li *et al*. demonstrated ATTEC mediated HTT degradation in cellular and animal models[49]. However, as molecular glues are not bifunctional molecules, its adaption to different targets is expected to be challenging. In 2021, Fu *et al.* described the use of bifunctional ATTECs for the selective degradation of lipid droplets and triglycerols. Here, the compound consists of a ligand for LC3 (which is the ATTEC described by Li *et al.*) and a ligand for either Lipid droplets or triglycerols[206]. By using ATTECs, Fu *et al.* showed an autophagy dependent decrease of lipid droplet in cells and mouse models. However, internal experiments using crystallography revealed that the LC3 binding moiety destabilizes the LC3 structure (internal communication).

For the future development of ATACS, it is key to develop specific ligands for LC3. For this purpose, several screening methods might be eligible. For identification of ligands binding to the LIR binding pocket of LC3B, fluorescence polarization or BRET-based competition assays are feasible. In both cases, the possible ligands compete with a LIR peptide probe for the binding site to LC3B. However, competition assays only identify ligands for one specific binding site at the target. Therefore, ligands binding to other sites at the target protein cannot be identified by these methods.

Alternative methods such as DNA encoded library (DEL) screening approaches or surface plasmon resonance (SPR) screens might be more promising in this regard. DEL screens are based on immobilized target proteins, which are incubated with DNA barcode labelled compounds. After washing, only the compounds binding to the target protein will remain, the barcodes are amplified by PCR and readout via sequencing [218]. In SPR screens, direct binding of compounds can be detected by measurement of changes in the refractive index at the surface interface labelled with target proteins[219]. DEL and SPR screens have the advantage that also compounds with binding sites apart from the LIR binding site of LC3B can be identified. After successful identification of a LC3 ligand, ATACs can be developed that engage the inherent autophagy machinery. Furthermore, LC3 ligands may also represent a promising starting point for further research groups developing ATACs for other targets.

Summary

Neurodegenerative diseases are a group of disorders which manifest mainly at higher age and can affect the peripheral nervous system as well as the central nervous system. Hallmark of many neurodegenerative diseases such as Alzheimer's disease, Huntington's disease and Parkinson disease is the presence of disease-specific misfolded and aggregated proteins. Accumulation of aggregation prone proteins such as α-synuclein in Parkinson's disease or Tau in Alzheimer's disease are indicative of an insufficient degradation of these proteins. As so far, all currently approved treatment approaches for neurodegenerative diseases merely alleviate disease-associated symptoms without reversing or slowing down disease progression, there is tremendous need for the development of novel treatment approaches. As autophagy is a highly conserved catabolic mechanism, essential for maintaining cell homeostasis, it represents a promising target for therapeutic interventions aiming for the removal of pathogenic protein aggregates.

In the scope of this thesis, a BRET based cellular assay has been developed to quantitatively analyse autophagy related protein-protein interactions. By running a focused screen of autophagy related protein-protein interactions, several promising interactions for pharmacological intervention have been identified. The interaction between BECN1 and BCL-2 is a valid target for the induction of autophagy. Furthermore, the interaction between SXT17 and VAMP8 has been identified as a novel indicator for monitoring autophagic activity.

Additionally, this work describes the development of autophagy targeting chimera (ATAC), a novel approach for targeted degradation of pathological protein aggregates utilizing the autophagy machinery. Here, we found that ATACs mediate the degradation of protein aggregates such as Tau and HTT aggregates in an autophagy dependent manner.

The results of this work provide new starting points for further drug development by harnessing autophagy for the removal of disease relevant protein aggregates.

Zusammenfassung

Neurodegenerative Erkrankungen ist ein Sammelbegriff für Erkrankungen des peripheren sowie zentralen Nervensystems, welche sich im fortschreitenden Alter manifestieren. Eine Gemeinsamkeit vieler neurodegenerativer Erkrankungen wie Alzheimer, Huntington oder Parkinson sind intrazelluläre Proteinaggregate bestehend aus fehlgefalteten Proteinen. Die Anhäufung von aggregationsanfälligen Proteinen wie α-Synuclein oder Tau deuten auf einen unzureichenden Abbau dieser Proteine hin.

Da die derzeit angewandten Behandlungsoptionen für neurodegenerativen Erkrankungen lediglich die Symptome ohne jedoch deren Ursache sowie Krankheitsverlauf verlangsamen, gelten neurodegenerative Erkrankungen derzeit als unheilbar. Diese Tatsache zeigt einen dringenden Bedarf an der Entwicklung neuer innovativer Behandlungsmethoden auf.

Autophagie beschreibt einen lysosomalen Abbauweg, der für das Überleben und die Homöostase der Zelle essenziell ist. Daher stellt die Autophagie einen vielversprechenden Ansatzpunkt für die Entwicklung von neuen Behandlungsmethoden, mit dem Ziel den Abbau von pathogenen Proteinen zu erhöhen, dar.

Im Rahmen dieser Arbeit wurde ein auf BRET basierender zellulärer Assay zur quantitativen Analyse von Autophagie angehörigen Protein-Protein-Interaktionen entwickelt. In einem ersten Screening für Autophagieinteraktionen, wurden mehrere vielversprechende Interaktionen für eine pharmakologische Intervention identifiziert.

So zeigt sich die Interaktion zwischen BECN1 und BCL-2 als ein vielversrechender Ansatzpunkt zu Autophagieinduktion. Des Weiteren, wurde die Interaktion zwischen STX17 und VAMP8 als ein möglicher Sensor um die Autophagieaktivität beobachten zu können identifiziert.

Zusätzlich beschreibt dies Arbeit die Entwicklung von Autophagy targeting chimera (ATAC), welche einen neuen Ansatz zum gezielten Abbau von Proteinaggregaten über den Autophagie Pathway darstellen. Mit unseren Experimenten konnte gezeigt werden, dass ATAC Compounds den Autophagieabhängigen Abbau von Proteinaggregaten wie Tau und HTT Aggregaten induzieren.

Die Ergebnisse diese Thesis zeigen neue Ansatzpunkte zur Entwicklung neuer Wirkstoffe zur Induktion der Autophagie sowie den gezielten Abbau von Proteinaggregaten auf.

Literature

1. Nations, U., of Economic, D., Affairs, S. & Division, P. *World Population Prospects 2019 Highlights*.
2. Hou, Y. *et al.* Ageing as a risk factor for neurodegenerative disease. *Nature Reviews Neurology* vol. 15 565–581 (2019).
3. Wakabayashi, K., Mori, F., Tanji, K., Orimo, S. & Takahashi, H. Involvement of the peripheral nervous system in synucleinopathies, tauopathies and other neurodegenerative proteinopathies of the brain. *Acta Neuropathologica* vol. 120 1–12 (2010).
4. Kesidou, E., Lagoudaki, R., Touloumi, O., Poulatsidou, K. N. & Simeonidou, C. Autophagy and neurodegenerative disorders. *Neural Regen. Res.* **8**, 2275–2283 (2013).
5. Nixon, R. A. The role of autophagy in neurodegenerative disease. *Nature Medicine* vol. 19 983–997 (2013).
6. Alzheimer's Disease Fact Sheet | National Institute on Aging. https://www.nia.nih.gov/health/alzheimers-disease-fact-sheet.
7. Kumar, V. *et al.* Protein aggregation and neurodegenerative diseases: From theory to therapy. *Eur. J. Med. Chem.* **124**, 1105–1120 (2016).
8. Bhat, A. H. *et al.* Oxidative stress, mitochondrial dysfunction and neurodegenerative diseases; a mechanistic insight. *Biomed. Pharmacother.* **74**, 101–110 (2015).
9. Perry, V. H., Newman, T. A. & Cunningham, C. The impact of systemic infection on the progression of neurodegenerative disease. *Nat. Rev. Neurosci.* **4**, 103–112 (2003).
10. Cummings, J. Disease modification and Neuroprotection in neurodegenerative disorders. *Translational Neurodegeneration* vol. 6 (2017).
11. Ross, C. A. & Poirier, M. A. Protein aggregation and neurodegenerative disease. *Nat. Med.* **10**, S10 (2004).
12. MS, F., JQ, T. & VM, L. Neurodegenerative diseases: a decade of discoveries paves the way for therapeutic breakthroughs. *Nat. Med.* **10**, 1055–1063 (2004).
13. Soto, C. & Pritzkow, S. Protein misfolding, aggregation, and conformational strains in neurodegenerative diseases. *Nat. Neurosci. 2018 2110* **21**, 1332–1340 (2018).
14. Tyedmers, J., Mogk, A. & Bukau, B. Cellular strategies for controlling protein

aggregation. *Nat. Rev. Mol. Cell Biol.* **11**, 777–788 (2010).

15. Zhou, R. & Xu, B. Insight of the Cytotoxicity of the Aggregates of Peptides or Aberrant Proteins: A Meta-Analysis. *PLoS One* **9**, e95759 (2014).
16. Winklhofer, K. F., Tatzelt, J. & Haass, C. The two faces of protein misfolding: gain- and loss-of-function in neurodegenerative diseases. *EMBO J.* **27**, 336 (2008).
17. Ruz, C., Alcantud, J. L., Montero, F. V., Duran, R. & Bandres-Ciga, S. Proteotoxicity and Neurodegenerative Diseases. *Int. J. Mol. Sci.* **21**, 1–25 (2020).
18. Jackrel, M. E. & Shorter, J. Protein-remodeling factors as potential therapeutics for neurodegenerative disease. *Front. Neurosci.* **11**, 99 (2017).
19. Gispert-Sanchez, S. & Auburger, G. *The role of protein aggregates in neuronal pathology: guilty, innocent, or just trying to help? J Neural Transm* vol. 70 (2006).
20. Jucker, M. & Walker, L. C. Pathogenic Protein Seeding in Alzheimer's Disease and Other Neurodegenerative Disorders. *Ann. Neurol.* **70**, 532 (2011).
21. Barbier, P. *et al.* Role of Tau as a Microtubule-Associated Protein: Structural and Functional Aspects. *Front. Aging Neurosci.* **0**, 204 (2019).
22. Guo, J. L. *et al.* The Dynamics and Turnover of Tau Aggregates in Cultured Cells INSIGHTS INTO THERAPIES FOR TAUOPATHIES * □ S. *NUMBER 25 J. Biol. Chem.* **291**, 13175 (2016).
23. Melnikova, I. Therapies for Alzheimer's disease. *Nat. Rev. Drug Discov.* **6**, 341–342 (2007).
24. Nah, J., Yuan, J. & Jung, Y.-K. Autophagy in Neurodegenerative Diseases: From Mechanism to Therapeutic Approach. *Mol. Cells* **38**, 381–389 (2015).
25. Park, H., Kang, J. H. & Lee, S. Autophagy in neurodegenerative diseases: A hunter for aggregates. *International Journal of Molecular Sciences* vol. 21 (2020).
26. Spilman, P. *et al.* Inhibition of mTOR by rapamycin abolishes cognitive deficits and reduces amyloid-β levels in a mouse model of alzheimer's disease. *PLoS One* **5**, (2010).
27. Wang, C., Zhang, X., Teng, Z., Zhang, T. & Li, Y. Downregulation of PI3K/Akt/mTOR signaling pathway in curcumin-induced autophagy in APP/PS1 double transgenic mice. *Eur. J. Pharmacol.* **740**, 312–320 (2014).
28. Shakeri, A., Cicero, A. F. G., Panahi, Y., Mohajeri, M. & Sahebkar, A. Curcumin:

A naturally occurring autophagy modulator. *Journal of Cellular Physiology* vol. 234 5643–5654 (2019).

29. Djajadikerta, A. *et al.* Autophagy Induction as a Therapeutic Strategy for Neurodegenerative Diseases. *J. Mol. Biol.* **432**, 2799–2821 (2020).
30. DeBosch, B. J. *et al.* Trehalose inhibits solute carrier 2A (SLC2A) proteins to induce autophagy and prevent hepatic steatosis. *Sci. Signal.* **9**, ra21 (2016).
31. Rusmini, P. *et al.* Trehalose induces autophagy via lysosomal-mediated TFEB activation in models of motoneuron degeneration. *Autophagy* **15**, 631–651 (2019).
32. Williams, A. *et al.* Novel targets for Huntington's disease in an mTOR-independent autophagy pathway. *Nat. Chem. Biol.* **4**, 295 (2008).
33. Sala, A. J., Bott, L. C. & Morimoto, R. I. Shaping proteostasis at the cellular, tissue, and organismal level. *J. Cell Biol.* **216**, 1231 (2017).
34. Tomoshige, S. & Ishikawa, M. PROTACs and Other Chemical Protein Degradation Technologies for the Treatment of Neurodegenerative Disorders. *Angewandte Chemie - International Edition* vol. 60 3346–3354 (2021).
35. Pujols, J. *et al.* Small molecule inhibits α-synuclein aggregation, disrupts amyloid fibrils, and prevents degeneration of dopaminergic neurons. *Proc. Natl. Acad. Sci.* **115**, 10481–10486 (2018).
36. Dominguez-Meijide, A., Vasili, E. & Outeiro, T. F. Pharmacological Modulators of Tau Aggregation and Spreading. *Brain Sci.* **10**, 1–29 (2020).
37. Medina, M. An Overview on the Clinical Development of Tau-Based Therapeutics. *Int. J. Mol. Sci. 2018, Vol. 19, Page 1160* **19**, 1160 (2018).
38. Ding, Y., Fei, Y. & Lu, B. Emerging New Concepts of Degrader Technologies. *Trends in Pharmacological Sciences* (2020) doi:10.1016/j.tips.2020.04.005.
39. He, Y. *et al.* Proteolysis targeting chimeras (PROTACs) are emerging therapeutics for hematologic malignancies. *J. Hematol. Oncol. 2020 131* **13**, 1–24 (2020).
40. Schapira, M., Calabrese, M. F., Bullock, A. N. & Crews, C. M. Targeted protein degradation: expanding the toolbox. *Nat. Rev. Drug Discov.* **18**, 949–963 (2019).
41. Ito, T. *et al.* Identification of a primary target of thalidomide teratogenicity. *Science (80-.).* **327**, 1345–1350 (2010).
42. Sakamoto, K. M. *et al.* Development of Protacs to target cancer-promoting proteins for ubiquitination and degradation. *Mol. Cell. Proteomics* **2**, 1350–1358

(2003).

43. Chu, T. T. *et al.* Specific Knockdown of Endogenous Tau Protein by Peptide-Directed Ubiquitin-Proteasome Degradation. *Cell Chem. Biol.* **23**, 453–461 (2016).
44. Au, Y. Z., Wang, T., Sigua, L. H. & Qi, J. Peptide-Based PROTAC: The Predator of Pathological Proteins. *Cell Chem. Biol.* **27**, 637–639 (2020).
45. Cacace, A. M. *et al.* A new therapeutic strategy for Tauopathies: Discovery of highly potent brain penetrant PROTAC degrader molecules that target pathologic Tau protein species. *Alzheimer's Dement.* **15**, P1624–P1624 (2019).
46. Wong, E. & Cuervo, A. M. Integration of Clearance Mechanisms: The Proteasome and Autophagy. *Cold Spring Harb. Perspect. Biol.* **2**, (2010).
47. Edmondson, S. D., Yang, B. & Fallan, C. Proteolysis targeting chimeras (PROTACs) in 'beyond rule-of-five' chemical space: Recent progress and future challenges. *Bioorg. Med. Chem. Lett.* **29**, 1555–1564 (2019).
48. Cyrus, K. *et al.* Impact of linker length on the activity of PROTACs. *Mol. Biosyst.* **7**, 359–364 (2011).
49. Li, Z. *et al.* Allele-selective lowering of mutant HTT protein by HTT–LC3 linker compounds. *Nature* **575**, 203–209 (2019).
50. Alabi, S. Novel Mechanisms of Molecular Glue-Induced Protein Degradation. *Biochemistry* **60**, 2371–2373 (2021).
51. Li, Z., Zhu, C., Ding, Y., Fei, Y. & Lu, B. ATTEC: a potential new approach to target proteinopathies. *Autophagy* vol. 16 185–187 (2020).
52. Takahashi, D. *et al.* AUTACs: Cargo-Specific Degraders Using Selective Autophagy. *Mol. Cell* (2019) doi:10.1016/J.MOLCEL.2019.09.009.
53. Clift, D. *et al.* A Method for the Acute and Rapid Degradation of Endogenous Proteins. *Cell* **171**, 1692-1706.e18 (2017).
54. Liu, L. *et al.* Trans-synaptic spread of tau pathology in vivo. *PLoS One* **7**, (2012).
55. Asuni, A. A., Boutajangout, A., Quartermain, D. & Sigurdsson, E. M. Immunotherapy targeting pathological tau conformers in a tangle mouse model reduces brain pathology with associated functional improvements. *J. Neurosci.* **27**, 9115–9129 (2007).
56. Chai, X. *et al.* Passive immunization with anti-tau antibodies in two transgenic models: Reduction of tau pathology and delay of disease progression. *J. Biol. Chem.* **286**, 34457–34467 (2011).

57. Goedert, M., Spillantini, M. G., Del Tredici, K. & Braak, H. 100 years of Lewy pathology. *Nature Reviews Neurology* vol. 9 13–24 (2013).
58. Yu, Y. J. & Watts, R. J. Developing Therapeutic Antibodies for Neurodegenerative Disease. *Neurotherapeutics* vol. 10 459–472 (2013).
59. Gklinos, P., Papadopoulou, M., Stanulovic, V., Mitsikostas, D. D. & Papadopoulos, D. Monoclonal antibodies as neurological therapeutics. *Pharmaceuticals* vol. 14 1–31 (2021).
60. Mahase, E. Aducanumab: European agency rejects Alzheimer's drug over efficacy and safety concerns. *BMJ* **375**, n3127 (2021).
61. Rinaldi, C. & Wood, M. J. A. Antisense oligonucleotides: The next frontier for treatment of neurological disorders. *Nature Reviews Neurology* vol. 14 9–22 (2018).
62. Østergaard, M. E. *et al.* Rational design of antisense oligonucleotides targeting single nucleotide polymorphisms for potent and allele selective suppression of mutant Huntingtin in the CNS. *Nucleic Acids Res.* **41**, 9634–9650 (2013).
63. Kingwell, K. Double setback for ASO trials in Huntington disease. *Nature; News Anal.* **20**, 412–413 (2021).
64. Skotte, N. H. *et al.* Allele-Specific Suppression of Mutant Huntingtin Using Antisense Oligonucleotides: Providing a Therapeutic Option for All Huntington Disease Patients. *PLoS One* **9**, e107434 (2014).
65. Wurster, C. D. & Ludolph, A. C. Antisense oligonucleotides in neurological disorders. *Ther. Adv. Neurol. Disord.* **11**, (2018).
66. Focusing on autophagy. *Nature Cell Biology* vol. 12 813 (2010).
67. Schröder, B. A., Wrocklage, C., Hasilik, A. & Saftig, P. The proteome of lysosomes. *Proteomics* vol. 10 4053–4076 (2010).
68. Huang, L. *et al.* O-GlcNAc-modified SNAP29 inhibits autophagy-mediated degradation via the disturbed SNAP29-STX17-VAMP8 complex and exacerbates myocardial injury in type I diabetic rats. *Int. J. Mol. Med.* **42**, 3278–3290 (2018).
69. Tomaipitinca, L. *et al.* The Role of Autophagy in Liver Epithelial Cells and Its Impact on Systemic Homeostasis. *Nutr. 2019, Vol. 11, Page 827* **11**, 827 (2019).
70. Giampieri, F. *et al.* Autophagy in Human Health and Disease: Novel Therapeutic Opportunities. *Antioxid. Redox Signal.* **30**, 577–634 (2019).
71. Martinez-Vicente, M. Autophagy in neurodegenerative diseases: From

pathogenic dysfunction to therapeutic modulation. *Semin. Cell Dev. Biol.* **40**, 115–126 (2015).

72. Jiang, S. & Bhaskar, K. Degradation and Transmission of Tau by Autophagic-Endolysosomal Networks and Potential Therapeutic Targets for Tauopathy. *Frontiers in Molecular Neuroscience* vol. 13 (2020).
73. Galluzzi, L., Bravo-San Pedro, J. M., Levine, B., Green, D. R. & Kroemer, G. Pharmacological modulation of autophagy: Therapeutic potential and persisting obstacles. *Nature Reviews Drug Discovery* 16 (2017) doi:10.1038/nrd.2017.22.
74. Xie, Z. & Klionsky, D. J. Autophagosome formation: Core machinery and adaptations. *Nature Cell Biology* vol. 9 1102–1109 (2007).
75. Grasso, D., Renna, F. J. & Vaccaro, M. I. Initial steps in Mammalian autophagosome biogenesis. *Frontiers in Cell and Developmental Biology* vol. 6 146 (2018).
76. Zhao, M. & Klionsky, D. J. AMPK-dependent phosphorylation of ULK1 induces autophagy. *Cell Metabolism* vol. 13 119–120 (2011).
77. Hurley, J. H. & Young, L. N. Mechanisms of Autophagy Initiation. *Annu. Rev. Biochem.* **86**, 225 (2017).
78. Yamamoto, Y. & Noda, T. Autophagosome formation in relation to the endoplasmic reticulum. *J. Biomed. Sci. 2020 271* **27**, 1–6 (2020).
79. Alers, S., Löffler, A. S., Wesselborg, S. & Stork, B. Role of AMPK-mTOR-Ulk1/2 in the Regulation of Autophagy: Cross Talk, Shortcuts, and Feedbacks. *Mol. Cell. Biol.* **32**, 2–11 (2012).
80. Nakatogawa, H. Mechanisms governing autophagosome biogenesis. *Nature Reviews Molecular Cell Biology* vol. 21 439–458 (2020).
81. Maruyama, T. & Noda, N. N. Autophagy-regulating protease Atg4: Structure, function, regulation and inhibition. *Journal of Antibiotics* vol. 71 72–78 (2018).
82. He, C. & Klionsky, D. J. Regulation Mechanisms and Signaling Pathways of Autophagy. *Annu. Rev. Genet.* **43**, 67–93 (2009).
83. Mauvezin, C. *et al.* Coordination of autophagosome–lysosome fusion and transport by a Klp98A–Rab14 complex in Drosophila. *J. Cell Sci.* **129**, 971 (2016).
84. Tian, X., Teng, J. & Chen, J. New insights regarding SNARE proteins in autophagosome-lysosome fusion. *Autophagy* (2020) doi:10.1080/15548627.2020.1823124.

85. Mizushima, N., Matsui, T. & Yamamoto, H. YKT6 as a second SNARE protein of mammalian autophagosomes. *Autophagy* **15**, 176–177 (2019).
86. Yim, W. W.-Y. & Mizushima, N. Lysosome biology in autophagy. *Cell Discov. 2020 61* **6**, 1–12 (2020).
87. Xu, H. & Ren, D. Lysosomal physiology. *Annu. Rev. Physiol.* **77**, 57–80 (2015).
88. Klionsky, D. J. *et al.* Guidelines for the use and interpretation of assays for monitoring autophagy (4th edition) 1. *Autophagy* **17**, 1–382 (2021).
89. Yoshii, S. R. & Mizushima, N. Monitoring and Measuring Autophagy. *Int. J. Mol. Sci.* **18**, (2017).
90. Bresciani, A. *et al.* Quantifying autophagy using novel LC3B and p62 TR-FRET assays. *PLoS One* **13**, e0194423 (2018).
91. Farkas, T., Høyer-Hansen, M. & Jäättelä, M. Identification of novel autophagy regulators by a luciferase-based assay for the kinetics of autophagic flux. *Autophagy* **5**, 1018–1025 (2009).
92. Ueno, T. & Komatsu, M. Monitoring Autophagy Flux and Activity: Principles and Applications. *BioEssays* **42**, 2000122 (2020).
93. Kimura, S., Noda, T. & Yoshimori, T. Dissection of the autophagosome maturation process by a novel reporter protein, tandem fluorescent-tagged LC3. *Autophagy* **3**, 452–460 (2007).
94. Kaizuka, T. *et al.* An Autophagic Flux Probe that Releases an Internal Control. *Mol. Cell* **64**, 835–849 (2016).
95. Tan, C.-C. *et al.* Autophagy in aging and neurodegenerative diseases: implications for pathogenesis and therapy. *Neurobiol. Aging* **35**, 941–957 (2014).
96. Hirsch, H. R. The waste-product theory of aging: Waste dilution by cell division. *Mech. Ageing Dev.* **8**, 51–62 (1978).
97. Hara, T. *et al.* Suppression of basal autophagy in neural cells causes neurodegenerative disease in mice. *Nature* **441**, 885–889 (2006).
98. Komatsu, M. *et al.* Loss of autophagy in the central nervous system causes neurodegeneration in mice. *Nature* **441**, 880–884 (2006).
99. Liang, C. C., Wang, C., Peng, X., Gan, B. & Guan, J. L. Neural-specific deletion of FIP200 leads to cerebellar degeneration caused by increased neuronal death and axon degeneration. *J. Biol. Chem.* **285**, 3499–3509 (2010).
100. Ramesh Babu, J. *et al.* Genetic inactivation of p62 leads to accumulation of hyperphosphorylated tau and neurodegeneration. *J. Neurochem.* **106**, 107–120

(2008).

101. Fu, Y. *et al.* A toxic mutant huntingtin species is resistant to selective autophagy. *Nat. Chem. Biol.* **13**, 1152–1154 (2017).
102. Berger, Z. *et al.* Rapamycin alleviates toxicity of different aggregate-prone proteins. *Hum. Mol. Genet.* **15**, 433–442 (2006).
103. Ravikumar, B., Duden, R. & Rubinsztein, D. C. Aggregate-prone proteins with polyglutamine and polyalanine expansions are degraded by autophagy. *Hum. Mol. Genet.* **11**, 1107–1117 (2002).
104. Tsvetkov, A. S. *et al.* Proteostasis of polyglutamine varies among neurons and predicts neurodegeneration. *Nat. Chem. Biol.* **9**, 586–594 (2013).
105. Dale, N. C., Johnstone, E. K. M., White, C. W. & Pfleger, K. D. G. NanoBRET: The Bright Future of Proximity-Based Assays. *Front. Bioeng. Biotechnol.* **7**, 56 (2019).
106. Xu, Y., Piston, D. W. & Johnson, C. H. A bioluminescence resonance energy transfer (BRET) system: Application to interacting circadian clock proteins. *Proc. Natl. Acad. Sci.* **96**, 151–156 (1999).
107. Stoddart, L. A. *et al.* Application of BRET to monitor ligand binding to GPCRs. *Nat. Methods* **12**, 661–663 (2015).
108. Pfleger, K. D. G. & Eidne, K. A. Illuminating insights into protein-protein interactions using bioluminescence resonance energy transfer (BRET). *Nat. Methods* **3**, 165–174 (2006).
109. Bacart, J., Corbel, C., Jockers, R., Bach, S. & Couturier, C. The BRET technology and its application to screening assays. *Biotechnol. J.* **3**, 311–324 (2008).
110. Machleidt, T. *et al.* NanoBRET-A Novel BRET Platform for the Analysis of Protein-Protein Interactions. *ACS Chem. Biol.* **10**, 1797–1804 (2015).
111. Dacres, H., Michie, M., Wang, J., Pfleger, K. D. G. & Trowell, S. C. Effect of enhanced Renilla luciferase and fluorescent protein variants on the Förster distance of Bioluminescence resonance energy transfer (BRET). *Biochem. Biophys. Res. Commun.* **425**, 625–629 (2012).
112. Smirnova, D. V. & Ugarova, N. N. Firefly Luciferase-based Fusion Proteins and their Applications in Bioanalysis. *Photochem. Photobiol.* **93**, 436–447 (2017).
113. Zhou, M., Li, Q. & Wang, P. R. Current Experimental Methods for Characterizing Protein–Protein Interactions. *ChemMedChem* **11**, 738 (2016).

114. Siddiqui, S., Cong, W. N., Daimon, C. M., Martin, B. & Maudsley, S. BRET biosensor analysis of receptor tyrosine kinase functionality. *Front. Endocrinol. (Lausanne).* **4**, 46 (2013).
115. Trepte, P. *et al.* LuTHy: a double-readout bioluminescence-based two-hybrid technology for quantitative mapping of protein-protein interactions in mammalian cells. *Mol Syst Biol* **14**, 1–20 (2018).
116. Nlm Citation: Wade, M., Méndez, J. & Coussens, N. P. Inhibition of Protein-Protein Interactions. *Cell-Based-Assays* (2017).
117. Strang, K. H. *et al.* Distinct differences in prion-like seeding and aggregation between Tau protein variants provide mechanistic insights into tauopathies. *J. Biol. Chem.* **293**, 2408–2421 (2018).
118. Hartley, J. L., Temple, G. F. & Brasch, M. A. DNA Cloning Using In Vitro Site-Specific Recombination. *Genome Res.* **10**, 1788 (2000).
119. Cohen, S. N., Chang, A. C. Y. & Hsu, L. Nonchromosomal Antibiotic Resistance in Bacteria: Genetic Transformation of Escherichia coli by R-Factor DNA* (CaCI2/extrachromosomal DNA/plasmid). **69**, 2110–2114 (1972).
120. Subramani, S. *et al.* Active Interaction Mapping Reveals the Hierarchical Organization of Autophagy. *Mol. Cell* **65**, 761–774 (2017).
121. Lehne, B. & Schlitt, T. Protein-protein interaction databases: Keeping up with growing interactomes.
122. Alanis-Lobato, G., Andrade-Navarro, M. A. & Schaefer, M. H. HIPPIE v2.0: Enhancing meaningfulness and reliability of protein-protein interaction networks. *Nucleic Acids Res.* **45**, D408–D414 (2017).
123. Buntru, A., Trepte, P., Klockmeier, K., Schnoegl, S. & Wanker, E. E. Current approaches toward quantitative mapping of the interactome. *Front. Genet.* **7**, 1–9 (2016).
124. Pfleger, K. D. G., Seeber, R. M. & Eidne, K. A. Bioluminescence resonance energy transfer (BRET) for the real-time detection of protein-protein interactions. *Nat. Protoc.* **1**, 337–345 (2006).
125. Couturier, C. & Deprez, B. Setting up a bioluminescence resonance energy transfer high throughput screening assay to search for protein/protein interaction inhibitors in mammalian cells. *Front. Endocrinol. (Lausanne).* **3**, 1–13 (2012).
126. Szalai, B. *et al.* Improved Methodical Approach for Quantitative BRET Analysis of G Protein Coupled Receptor Dimerization. *PLoS One* **9**, e109503 (2014).

127. Hamdan, F. F., Percherancier, Y., Breton, B. & Bouvier, M. Monitoring Protein-Protein Interactions in Living Cells by Bioluminescence Resonance Energy Transfer (BRET). *Curr. Protoc. Neurosci.* **34**, (2006).
128. Levine, B., Sinha, S. & Kroemer, G. Bcl-2 family members: Dual regulators of apoptosis and autophagy. *Autophagy* **4**, 600–606 (2008).
129. Opydo-Chanek, M., Gonzalo, O. & Marzo, I. Multifaceted anticancer activity of BH3 mimetics: Current evidence and future prospects. *Biochem. Pharmacol.* **136**, 12–23 (2017).
130. Han, G. A., Bin, N.-R., Kang, S.-Y. A., Han, L. & Sugita, S. Domain 3a of Munc18-1 plays a crucial role at the priming stage of exocytosis. *J. Cell Sci.* **126**, 2361–2371 (2013).
131. Banaszynski, L. A., Liu, C. W. & Wandless, T. J. Characterization of the FKBP-rapamycin-FRB ternary complex. *J. Am. Chem. Soc.* **127**, 4715–4721 (2005).
132. Chiang, W. C. *et al.* High Throughput Screens to Identify Autophagy Inducers that Function by Disrupting Beclin 1/Bcl-2 Binding. *ACS Chem. Biol.* **13**, 2247–2260 (2018).
133. Rose, P. W. *et al.* The RCSB protein data bank: Integrative view of protein, gene and 3D structural information. *Nucleic Acids Res.* **45**, D271–D281 (2017).
134. Rao, V. S., Srinivas, K., Sujini, G. N. & Kumar, G. N. S. Protein-Protein Interaction Detection: Methods and Analysis. *Int. J. Proteomics* **2014**, 1–12 (2014).
135. Kumar S *et al.* Mechanism of Stx17 recruitment to autophagosomes via IRGM and mammalian Atg8 proteins. *J. Cell Biol.* **217**, 997–1013 (2018).
136. Lőrincz, P. & Juhász, G. Autophagosome-Lysosome Fusion. *Journal of Molecular Biology* vol. 432 2462–2482 (2020).
137. Fu, R. *et al.* A novel autophagy inhibitor berbamine blocks SNARE-mediated autophagosome-lysosome fusion through upregulation of BNIP3. *Cell Death Dis.* **9**, 1–15 (2018).
138. Itakura, E., Kishi-Itakura, C. & Mizushima, N. The hairpin-type tail-anchored SNARE syntaxin 17 targets to autophagosomes for fusion with endosomes/lysosomes. *Cell* **151**, 1256–1269 (2012).
139. Dodson, M. *et al.* Increased O-GlcNAcylation of SNAP29 drives arsenic-induced autophagic dysfunction. *Mol. Cell. Biol.* **38**, (2018).
140. Chourasia, A. H. & Macleod, K. F. Tumor suppressor functions of BNIP3 and

mitophagy. *Autophagy* **11**, 1937–1938 (2015).

141. An, S. & Fu, L. Small-molecule PROTACs: An emerging and promising approach for the development of targeted therapy drugs. *EBioMedicine* vol. 36 553–562 (2018).
142. Luzio, J. P., Pryor, P. R. & Bright, N. A. Lysosomes: fusion and function. *Nat. Rev. Mol. Cell Biol.* **8**, 622–632 (2007).
143. Corona, A. K., Jackson, W. T. & Jackson, W. T. Finding the Middle Ground for Autophagic Fusion Requirements. *Trends Cell Biol.* **28**, 869–881 (2018).
144. Holt, M. *et al.* Identification of SNAP-47, a novel Qbc-SNARE with ubiquitous expression. *J. Biol. Chem.* **281**, 17076–17083 (2006).
145. Liu, J. *et al.* Piperlongumine restores the balance of autophagy and apoptosis by increasing BCL2 phosphorylation in rotenone-induced Parkinson disease models. *Autophagy* **14**, 1554–8627 (2018).
146. Pattingre, S. *et al.* Bcl-2 antiapoptotic proteins inhibit Beclin 1-dependent autophagy. *Cell* **122**, 927–939 (2005).
147. Malik, S. A. *et al.* BH3 mimetics activate multiple pro-autophagic pathways. *Oncogene 2011 3037* **30**, 3918–3929 (2011).
148. Samra, B., Konopleva, M., Isidori, A., Daver, N. & DiNardo, C. Venetoclax-Based Combinations in Acute Myeloid Leukemia: Current Evidence and Future Directions. *Frontiers in Oncology* vol. 10 (2020).
149. Reljic, B. *et al.* BAX-BAK1-independent LC3B lipidation by BH3 mimetics is unrelated to BH3 mimetic activity and has only minimal effects on autophagic flux. *Autophagy* **12**, 1083–1093 (2016).
150. Ewald, L., Dittmann, J., Vogler, M. & Fulda, S. Side-by-side comparison of BH3-mimetics identifies MCL-1 as a key therapeutic target in AML. *Cell Death Dis.* **10**, (2019).
151. Maejima, Y., Isobe, M. & Sadoshima, J. Regulation of autophagy by Beclin 1 in the heart. *J. Mol. Cell. Cardiol.* **95**, 19–25 (2016).
152. Johansen, T. & Lamark, T. Selective Autophagy: ATG8 Family Proteins, LIR Motifs and Cargo Receptors. *Journal of Molecular Biology* vol. 432 80–103 (2020).
153. Sa, A. ˚, Birgisdottir, B., Lamark, T. & Johansen, T. The LIR motif-crucial for selective autophagy. *J. Cell Sci.* **126**, 3237–3247 (2013).
154. Beale, R. *et al.* A LC3-interacting motif in the influenza A virus M2 protein is

required to subvert autophagy and maintain virion stability. *Cell Host Microbe* **15**, 239–47 (2014).

155. Kwon, D. H. *et al.* A novel conformation of the LC3-interacting region motif revealed by the structure of a complex between LC3B and RavZ. *Biochem. Biophys. Res. Commun.* **490**, 1093–1099 (2017).
156. Wesch, N., Kirkin, V. & Rogov, V. V. Atg8-Family Proteins-Structural Features and Molecular Interactions in Autophagy and Beyond. *Cells* vol. 9 (2020).
157. Shpilka, T., Weidberg, H., Pietrokovski, S. & Elazar, Z. Atg8: an autophagy-related ubiquitin-like protein family. *Genome Biol.* **12**, 226 (2011).
158. Pankiv, S. *et al.* p62/SQSTM1 Binds Directly to Atg8/LC3 to Facilitate Degradation of Ubiquitinated Protein Aggregates by Autophagy. *J. Biol. Chem.* **282**, 24131–24145 (2007).
159. Sugawara, K. *et al.* The crystal structure of microtubule-associated protein light chain 3, a mammalian homologue of Saccharomyces cerevisiae Atg8. *Genes to Cells* **9**, 611–618 (2004).
160. Nabet, B. *et al.* The dTAG system for immediate and target-specific protein degradation. *Nat. Chem. Biol.* **14**, 431–441 (2018).
161. England, C. G., Luo, H. & Cai, W. HaloTag technology: a versatile platform for biomedical applications. *Bioconjug. Chem.* **26**, 975–86 (2015).
162. Buckley, D. L. *et al.* HaloPROTACS: Use of Small Molecule PROTACs to Induce Degradation of HaloTag Fusion Proteins. *ACS Chem. Biol.* **10**, 1831–1837 (2015).
163. Troup, R. I., Fallan, C. & Baud, M. G. J. Current strategies for the design of PROTAC linkers: a critical review. *Explor. Target. Anti-tumor Ther.* **1**, 273–312 (2020).
164. Zhao, J. *et al.* E3 ubiquitin ligase Siah-1 facilitates poly-ubiquitylation and proteasomal degradation of the hepatitis B viral X protein. *FEBS Lett.* **585**, 2943–2950 (2011).
165. Yuan, H. X., Russell, R. C. & Guan, K. L. Regulation of PIK3C3/VPS34 complexes by MTOR in nutrient stress-induced autophagy. *Autophagy* **9**, 1983–1995 (2013).
166. Redmann, M. *et al.* Inhibition of autophagy with bafilomycin and chloroquine decreases mitochondrial quality and bioenergetic function in primary neurons. *Redox Biol.* **11**, 73–81 (2017).

167. Iershov, A. *et al.* The class 3 PI3K coordinates autophagy and mitochondrial lipid catabolism by controlling nuclear receptor PPARα. *Nat. Commun. 2019 101* **10**, 1–18 (2019).
168. Wu, Y.-T. *et al.* Dual Role of 3-Methyladenine in Modulation of Autophagy via Different Temporal Patterns of Inhibition on Class I and III Phosphoinositide 3-Kinase. *J. Biol. Chem.* **285**, 10850 (2010).
169. Fujita, N. *et al.* An Atg4B mutant hampers the lipidation of LC3 paralogues and causes defects in autophagosome closure. *Mol. Biol. Cell* **19**, (2008).
170. Erbil-Bilir, S., Kocaturk, N. M., Yayli, M. & Gozuacik, D. Study of Protein-protein Interactions in Autophagy Research. *J. Vis. Exp.* **2017**, 55881 (2017).
171. Xing, S., Wallmeroth, N., Berendzen, K. W. & Grefen, C. Techniques for the Analysis of Protein-Protein Interactions in Vivo. *Plant Physiol.* **171**, 727–758 (2016).
172. Wade, M. Cell-based assays for protein-protein interactions. *Eur. Pharm. Rev.* **18**, 66–69 (2013).
173. Fields, S. & Song, O. A novel genetic system to detect protein–protein interactions. *Nat. 1989 3406230* **340**, 245–246 (1989).
174. Shivhare, D., Musialak-Lange, M., Julca, I., Gluza, P. & Mutwil, M. Removing auto-activators from yeast-two-hybrid assays by conditional negative selection. *Sci. Reports 2021 111* **11**, 1–9 (2021).
175. Snider, J. *et al.* Fundamentals of protein interaction network mapping. *Mol. Syst. Biol.* **11**, 1–20 (2015).
176. Brückner, A., Polge, C., Lentze, N., Auerbach, D. & Schlattner, U. Yeast Two-Hybrid, a Powerful Tool for Systems Biology. *Int. J. Mol. Sci.* **10**, 2763 (2009).
177. Van Criekinge, W. & Beyaert, R. Yeast Two-Hybrid: State of the Art. *Biol. Proced. Online* **2**, 1 (1999).
178. Arndt, V. & Vorberg, I. Defining the Cellular Interactome of Disease-Linked Proteins in Neurodegeneration. *Protein Interact.* (2012) doi:10.5772/37751.
179. Wong, K. A. & O'Bryan, J. P. Bimolecular fluorescence complementation. *J. Vis. Exp.* (2011) doi:10.3791/2643.
180. Dimri, S., Basu, S. & De, A. Use of BRET to study protein-protein interactions in vitro and in vivo. in *Methods in Molecular Biology* vol. 1443 57–78 (Humana Press Inc., 2016).
181. Holzmeister, P., Wünsch, B., Gietl, A. & Tinnefeld, P. Single-molecule

photophysics of dark quenchers as non-fluorescent FRET acceptors. *Photochem. Photobiol. Sci.* **13**, 853–858 (2014).

182. Zal, T. & Gascoigne, N. R. J. Photobleaching-Corrected FRET Efficiency Imaging of Live Cells. *Biophys. J.* **86**, 3923 (2004).
183. Komatsu, N. *et al.* A platform of BRET-FRET hybrid biosensors for optogenetics, chemical screening, and in vivo imaging. *Sci. Reports 2018 81* **8**, 1–14 (2018).
184. Maiuri, M. C. *et al.* Functional and physical interaction between Bcl-XL and a BH3-like domain in Beclin-1. *EMBO J.* **26**, 2527–2539 (2007).
185. Pécot, J. *et al.* Tight Sequestration of BH3 Proteins by BCL-xL at Subcellular Membranes Contributes to Apoptotic Resistance. *Cell Rep.* **17**, 3347–3358 (2016).
186. Menon, M. B. & Dhamija, S. Beclin 1 Phosphorylation – at the Center of Autophagy Regulation. *Front. Cell Dev. Biol.* **6**, 1–9 (2018).
187. Trepte, P. *et al.* DULIP: A Dual Luminescence-Based Co-Immunoprecipitation Assay for Interactome Mapping in Mammalian Cells. *J. Mol. Biol.* **427**, 3375–3388 (2015).
188. Fusco, C. *et al.* TRIM50 regulates Beclin 1 proautophagic activity. *Biochim. Biophys. Acta - Mol. Cell Res.* **1865**, 908–919 (2018).
189. Walczak, M. & Martens, S. Dissecting the role of the Atg12–Atg5-Atg16 complex during autophagosome formation. *Autophagy* **9**, 424 (2013).
190. Di Rienzo, M., Romagnoli, A., Antonioli, M., Piacentini, M. & Fimia, G. M. TRIM proteins in autophagy: selective sensors in cell damage and innate immune responses. *Cell Death and Differentiation* vol. 27 887–902 (2020).
191. Celaj, A. *et al.* Quantitative analysis of protein interaction network dynamics in yeast. *Mol. Syst. Biol.* **13**, 934 (2017).
192. Liu, R., Zhi, X. & Zhong, Q. ATG14 controls SNARE-mediated autophagosome fusion with a lysosome. *Autophagy* **11**, 847–849 (2015).
193. Lindqvist, L. M. & Vaux, D. L. BCL2 and related prosurvival proteins require BAK1 and BAX to affect autophagy. *Autophagy* **10**, 1474–1475 (2014).
194. Liang, X. H. *et al. Protection against Fatal Sindbis Virus Encephalitis by Beclin, a Novel Bcl-2-Interacting Protein*. *JOURNAL OF VIROLOGY* vol. 72 https://journals.asm.org/journal/jvi (1998).
195. McKnight, N. C. & Yue, Z. Beclin 1, an Essential Component and Master Regulator of PI3K-III in Health and Disease. *Curr. Pathobiol. Rep.* **1**, 231–238

(2013).

196. Decuypere, J.-P., Parys, J. B. & Bultynck, G. Regulation of the Autophagic Bcl-2/Beclin 1 Interaction. *Cells* **1**, 284–312 (2012).
197. Fernández, Á. F. *et al.* Disruption of the beclin 1/Bcl-2 autophagy regulatory complex promotes longevity in mice. *Nature* **558**, 136 (2018).
198. Pedro, J. M. B. S. *et al.* BAX and BAK1 are dispensable for ABT-737- induced dissociation of the BCL2-BECN1 complex and autophagy. *Autophagy* **11**, 452–459 (2015).
199. Jang, M. *et al.* AMPK contributes to autophagosome maturation and lysosomal fusion. *Sci. Reports 2018 81* **8**, 1–10 (2018).
200. Lai, A. C. *et al.* Modular PROTAC Design for the Degradation of Oncogenic BCR-ABL. *Appl. Chem.* **128**, 818–821 (2016).
201. Medeiros, R., Baglietto-Vargas, D. & Laferla, F. M. The role of tau in Alzheimer's disease and related disorders. *CNS Neurosci. Ther.* **17**, 514–524 (2011).
202. Landles, C. & Bates, G. P. Huntingtin and the molecular pathogenesis of Huntington's disease. *EMBO Rep.* **5**, 958 (2004).
203. Birgisdottir, Å. B., Lamark, T. & Johansen, T. The LIR motif – crucial for selective autophagy. *J. Cell Sci.* **126**, 3237–3247 (2013).
204. Itakura, E. & Mizushima, N. p62 targeting to the autophagosome formation site requires self-oligomerization but not LC3 binding. *J. Cell Biol.* **192**, 17 (2011).
205. Clackson, T. *et al.* Redesigning an FKBP-ligand interface to generate chemical dimerizers with novel specificity. **95**, 10437–10442 (1998).
206. Fu, Y. *et al.* Degradation of lipid droplets by chimeric autophagy-tethering compounds. *Cell Res.* **31**, 965–979 (2021).
207. Um, J. H. & Yun, J. Emerging role of mitophagy in human diseases and physiology. *BMB Reports* vol. 50 299–307 (2017).
208. Xiang, Q. *et al.* Gerontoxanthone I and Macluraxanthone Induce Mitophagy and Attenuate Ischemia/Reperfusion Injury. *Front. Pharmacol.* **11**, 452 (2020).
209. Heckmann, B. L. & Green, D. R. LC3-associated phagocytosis at a glance. *J. Cell Sci.* **132**, (2019).
210. Inomata, M. *et al.* Macrophage LC3-associated phagocytosis is an immune defense against Streptococcus pneumoniae that diminishes with host aging. *Proc. Natl. Acad. Sci. U. S. A.* **117**, 33561–33569 (2020).
211. Li, H. *et al.* Protein degradation technology: a strategic paradigm shift in drug

discovery. *J. Hematol. Oncol. 2021 141* **14**, 1–23 (2021).

212. Tanida, I., Ueno, T. & Kominami, E. LC3 and autophagy. *Methods Mol. Biol.* **445**, 77–88 (2008).
213. Sora, V. *et al.* Structure and Dynamics in the ATG8 Family From Experimental to Computational Techniques. *Front. Cell Dev. Biol.* **8**, 420 (2020).
214. Chapin, H. C., Okada, M., Merz, A. J. & Miller, D. L. Tissue-specific autophagy responses to aging and stress in C. elegans. *Aging (Albany. NY).* **7**, 419–434 (2015).
215. Misra, M. & Dikic, I. RNA binding to p62 impacts selective autophagy. *Cell Res. 2019 297* **29**, 512–513 (2019).
216. Kirkin, V. & Rogov, V. V. A Diversity of Selective Autophagy Receptors Determines the Specificity of the Autophagy Pathway. *Mol. Cell* **76**, 268–285 (2019).
217. Banik, S. M. *et al.* Lysosome-targeting chimaeras for degradation of extracellular proteins. *Nature* **584**, 291–297 (2020).
218. Martín, A., Nicolaou, C. A. & Toledo, M. A. Navigating the DNA encoded libraries chemical space. *Commun. Chem. 2020 31* **3**, 1–9 (2020).
219. CA, S., AL, H. & I, N. Fragment screening by SPR and advanced application to GPCRs. *Prog. Biophys. Mol. Biol.* **116**, 113–123 (2014).

List of abbreviations

AB	antibody
ADAS-Cog-13	Alzheimer’s disease assessment scale subscale 13
ALS	amyotrophic lateral sclerosis
AMPK	AMP-activated kinase
ANOVA	analysis of variance
AP-MS	affinity purification mass spectrometry
ARP	autophagosome recognition particle
ASO	antisense oligonucleotides
ATTAC	autophagy tethering compound
ATAC	autophagy targeting chimera
a.u.	arbitrary units
AuTAC	autophagy targeting chimera
ATP	adenosine triphosphate
BAD	BCL-2-antagonist of cell death
BAF	Bafilomycin
BAK	BCL-2 homologous antagonist/killer
BAX	BCL-2 associated X Protein
BBB	blood brain barrier
BCL-2	B-cell lymphoma 2
BCL-2L1	BCL-2-like protein 1
BECN1	beclin1
BioGRID	biological general repository for interaction datasets
BRET	bioluminescence resonance energy transfer
CMA	chaperone mediated autophagy
CNS	central nervous system
CQ	Chloroquine
CTG	CellTiter-Glo®
DIP	database of interacting proteins
DMEM	Dulbecco's modified Eagle's medium
DTT	dithiothreitol
EDTA	ethylene diamine tetra acetate
EPG5	pic P-granules autophagy protein 5 homolog
ER	endoplasmic reticulum

FBnG	p-fluorobenzylguanine
FBS	fetal bovine serum
FDA	U.S. food and drug administration
FIP200	focal adhesion kinase family interacting protein of 200 kDa
FKBP	12-kDA FK506 binding protein
FPZ	Fluphenazine
FRB	FKBP-rapamycin binding domain
FRET	fluorescence resonance energy transfer
HBSS	Hanks' balanced salt solution
HEK	human embryonic kidney
HIPPIE	human integrated protein-protein interaction reference
HOPS	homotypic fusion and protein sorting
HPRD	human protein reference database
HSP70	heat shock cognate protein 70
HTT	huntingtin
IAM	inner autophagosomal membrane
IKK	IκB kinase
IntAct	IntAct molecular interaction database
IP3	inositol phosphate 3
IRGM	immunity-related GTPase M
KISS	kinase substrate sensor
LAP	LC3 associated phagocytosis
LAMP2A	lysosomal receptor lysosome associated membrane protein 2A
LIR	LC3 interaction region
LUMIER	luminescence-based mammalian interactome mapping
LYTAC	lysosome targeting chimera
MAPPIT	mammalian protein–protein interaction trap
MEM	minimum essential medium
mRNA	messenger ribonucleic acid
mTOR	mammalian target of Rapamycin
mTORC1	mTOR complex 1
$MgCl_2$	magnesium chloride
MINT	molecular interaction database
MoA	mode of action

MOI	multiplicity of infection
NaF	sodium fluoride
NaCl	sodium chloride
NF-κB	nuclear factor κB
NLuc	nano luciferase
mTOR	mammalian/mechanistic target of Rapamycin
ND	neurodegenerative diseases
NEAA	non-essential amino acid solution
PE	phosphatidylethanolamine
PBS	phosphate buffered saline
PCA	protein-fragment complementation assays
PEG	polyethylene glycol
PFA	paraformaldehyde
PI3P	phosphatidylinositol 3 phosphate
PKA	protein kinase-A
PLEKHM1	pleckstrin homology and RUN domain containing M1
PMSF	phenylmethanesulphonyl fluoride
PPI	protein-protein interaction
PROTAC	proteolysis targeting chimera
RLuc	renilla luciferase
SDS-PAGE	sodium dodecyl sulfate polyacrylamide gel electrophoresis
SNARE	soluble N-ethylmaleimide-sensitive factor attachment protein receptor
SLF	synthetic ligand of FKBP12
TMR	tetramethylrhodamine
TSPO	mitochondrial translocator protein
UBA	ubiquitin associated domain
ULK1	Unc-51- like kinase 1
UPS	ubiquitin proteasomal system
VPS15	vacuolar protein sorting 15
VPS34	vacuolar protein sorting 34
WB	western blot
WFI	water for injection
YFP	yellow fluorescent protein

Y2H	yeast two-hybrid

Acknowledgements

This thesis would not have been possible without the support and input of a lot of people. First of all, I want to thank my Evotec supervisor Dr. Alexander Buntru for his continued guidance, patience and endless supply of knowledge in many fascinating projects. His revision of my written work helped enormously to bring structure and sense to my diffused thoughts. I would also like to thank Dr. Hyoungseok Ju for his supervision in the last few years and his revision of this thesis.

A special thanks also goes to Dr. Andreas Weiss for giving me the opportunity to start my PhD project in his department, and I highly appreciate his scientific input during the course of this project. I would also like to thank Dr. Susan Boyce for releasing me from her department, even in times of high workload.

I would like to express my gratitude to my doctoral advisor Prof. Dr. Manuel A. Friese for accepting me as PhD student without hesitation. Thank you for the warm welcome into your group and the guidance offered during the past years. Also, thanks to my thesis committee members Prof. Dr. Markus Glatzel and Prof. Dr. Thomas Eschenhagen, I greatly enjoyed our thesis committee meetings.

A big thank you goes to Dr. Heinz von der Kammer who pushed me out of my comfort zone which fostered my scientific development. I thank the whole translational biology team, especially Zoe Fuller and Dr. Pascale Eede for proofreading this thesis. Thanks, Soumya Katamani for pushing me to bring cake for any reason. Special thanks also goes to Christina Schmidt and her team for cloning so many plasmids. Furthermore, I want to thank Dr. Carina Wollnik and Dr. Christina Thiede for image quantifications. A special thanks goes to Anne Willing for guiding me through the jungle of UKE regulations. Thanks to Dr. Marina Keul for your help with molecular modelling.

Lastly, my family deserves endless gratitude. Thanks to Anja, Paul, Willi and Fritz who endured this long period of time with me, offering plenty of unconditional love even during difficult times. Without your support, this thesis would not have been possible. I love you all!

Curriculum vitae

Lebenslauf wurde aus datenschutzrechtlichen Gründen entfernt

Eidesstattliche Versicherung

Ich versichere ausdrücklich, dass ich die Arbeit selbständig und ohne fremde Hilfe verfasst, andere als die von mir angegebenen Quellen und Hilfsmittel nicht benutzt und die aus den benutzten Werken wörtlich oder inhaltlich entnommenen Stellen einzeln nach Ausgabe (Auflage und Jahr des Erscheinens), Band und Seite des benutzten Werkes kenntlich gemacht habe.
Ferner versichere ich, dass ich die Dissertation bisher nicht einem Fachvertreter an einer anderen Hochschule zur Überprüfung vorgelegt oder mich anderweitig um Zulassung zur Promotion beworben habe.
Ich erkläre mich einverstanden, dass meine Dissertation vom Dekanat der Medizinischen Fakultät mit einer gängigen Software zur Erkennung von Plagiaten überprüft werden kann.

Unterschrift: .....
Daniel Küver